Marlene Knausz

Dissertation

Influence of polymeric encapsulation materials on quality and reliability of PV modules

May 2015

Submitted to

Institute of Materials Science and Testing of Polymers

Department Polymer Engineering and Science

Montanuniversitaet Leoben

Leoben, Austria

Conducted at

PCCL Polymer Competence Center Leoben GmbH

Leoben, Austria

Academic Supervisor

Univ.-Prof. Dr. Gerald Pinter

Institute of Materials Science and Testing of Polymers

Montanuniversitaet Leoben

Supervisor

Dr. Gernot Oreśki

PCCL Polymer Competence Center Leoben GmbH

AFFIDAVIT

I declare in lieu of oath, that I wrote this thesis and performed the associated research myself, using only the support indicated in the literature cited.

Leoben, May 2015 Dipl.-Ing. Marlene Knausz

ACKNOWLEDGMENTS

I would like to thank **Univ.-Prof. Dr. Gerald Pinter**, Head of the Institute of Materials Science and Testing of Polymers for his cooperative discussions about the work. His positive attitude and believe in trying new and different approaches were always an encouragement to give the best.

I would like to express my deeply gratitude to **Dr. Gernot Oreški** for giving the opportunity to contribute to this interesting project. His way to let me try different approaches, while giving always the knowledge of his trust in that, was in my opinion a good support. He also contributed considerably to the scientific quality of this work.

Furthermore I want to thank my office colleagues and friends **DI Bettina Hirschmann** and **Astrid Rauschenbach** for many conversations with content related inputs as well as diverting topics which eased me off from work when it was necessary.

I also want to express my gratitude to **BSc. Markus Schmidt**, who performed his Bachelor thesis on thermal expansion properties of polymeric encapsulants under the supervision of Dr. Gernot Oreški and me. I am also grateful to **Dr. Gabriele Eder** for arranging the permeation measurements at OFI Austrian Research Institute for Chemistry and Technology in chapter 4 and for her support in discussions about the scientific work in this thesis. Also, thanks to **DI Karl Berger**, **DI Yuliya Voronko** and **Dr. Thomas Koch** for contributions in discussions about results presented in this work. Thanks going to **Dipl.-Chem. Amal Ballion** and **Dipl.-Chem. Andreas Piekarczyk** for the extensive and elaborate permeation measurements described in chapter 4 and performed at Fraunhofer ISE. Gratitude is also owed to **Univ.Ass. Dr.techn. Bernadette Duscher** for conducting the rheological measurements in chapter 3 and **DI Martin Tscherner** for discussion about permeation related subjects.

Most of all I thank my **family** for their support and giving me the knowledge to be here for me whenever I need them.

Finally I would like to thank my boyfriend **Christian Novak** for his unlimited patience, support and always positive attitude giving me strength whenever I needed.

FUNDING

This research work was performed at the Polymer Competence Center Leoben (PCCL) within the project **“Analysis of PV Aging” (FFG Nr. 829918, 4. Call “Neue Energien 2020”, Klima- und Energiefonds)** in cooperation with the Institute of Materials Science and Testing of Polymers at the Montanuniversitaet Leoben. The PCCL is funded by the Austrian Government and the State Governments of Styria and Upper Austria.

Leoben, April 2015

ABSTRACT

As solar PV is starting to play a substantial role in electricity generation worldwide, further research is important to improve the energy output and reliability of PV systems. Thus, the work presented here aimed at improvements in the reliability of PV modules. The focus was on characterizing polymeric materials in photovoltaic modules with analytical techniques in order to examine the chemical and physical aging processes which allow for increased quality and an early prediction of the potential life time of modules. To achieve these goals, investigations in the short-term behavior, the long-term behavior and permeation properties of several polymeric materials used in PV modules were carried out.

To examine the short-term behavior of polymeric encapsulation materials, systematic investigations in the thermal expansion behavior of various encapsulants were made. To date, nearly no data on the thermal expansion behavior and material anisotropy of solar cell encapsulants have been published in scientific literature. Therefore, in this work, an overview of the thermal expansion behavior for nine different encapsulants is presented. To determine the thermal expansions, Thermo-Mechanical Analysis (TMA) was used with parameters chosen in accordance to application, respectively lamination procedure. It revealed highly relevant influences of the thermal expansion behavior of polymeric encapsulants on PV module lamination processes. Thermo-Mechanical Analysis proved to be a suitable method for applicability but also for quality control of solar cell encapsulation films.

Additionally the influence of lamination process and accelerated aging conditions on a polyamide-based backsheet was investigated. The results indicated no significant chemical aging processes in the backsheet. Only a physical change in the polyamide, which can be attributed to a partial re-crystallization process, was detected. This process was found to be temperature and time dependent. It was confirmed that the re-crystallization process influences the elongation at break significantly and is more pronounced for samples measured in the transversal (TD) direction of the film. Considering thermal loads of the lamination process and of hot climate zones, only

limited influence of weathering-induced re-crystallization on the mechanical stability of the backsheet, and consequently the PV module reliability, can be expected.

A comprehensive understanding of chemical and physical aging mechanisms of polymeric backsheets is necessary to give conclusions about their long-term behavior. A remaining question in reliability testing of components for PV modules is about material (in)compatibilities and synergistic effects and thus, how the results of singly tested materials correlate with materials aged within PV modules, two accelerated aging methods were used on single and module samples. Therefore, test modules (module samples) using the same components (glass, encapsulant, solar cells etc.), varying only in the backsheet used, were produced. Two accelerated aging conditions were chosen: the DH (85°C/ 85 % RH) aging according to the standard IEC 61215, but with extended exposure time up to 2000 h, and the simultaneously impact load of enhanced temperature (50°C), humidity (80 %) and irradiation (300-2800 nm metal halide lamp, 1000 W/m²) (climate) for 1000 h. The results indicated post-crystallization (physical aging) and hydrolytic degradation (chemical aging) of PET under DH conditions. It was also detected for the climate-aged samples but to a smaller extent, with initiation of chemical aging for the outer/inner layers. From the results it can be stated that for reliability testing of PET based backsheets under DH conditions, investigations (aging characterization) on single sheets yield meaningful results which can be directly correlated to the behavior of the backsheets laminated within a module. Exceptions are backsheets with barrier layers. This allows simplified sample preparation, lower costs and offers more testing options for the characterization of the aging induced changes of the polymeric materials. For reliability testing of backsheets under climate conditions, the interpretation is more difficult than for DH aging. Irradiation warming induced a different microclimate on modules (higher temperature) compared to the single sheets which went along with enhanced extents in detected aging mechanisms.

In c-Si PV modules permeation of water vapor and oxygen play a major role on reliability. Thus, the knowledge of the permeation rates through the backsheets and their sensitivity to the aging behavior of the materials involved is of prime importance.

Hence, the water vapor (WVTR) and oxygen transmission rates (OTR) of six backsheets were investigated in their initial and accelerated aged states. Also, different measurement techniques for determination of OTR and WVTR were compared. It clearly pointed out the difficulties when permeation results of different techniques are compared. The results of OTR and WVTR gave an overview on the general permeation properties of the investigated backsheets. Changes in the course of aging are not negligible and revealed increases in OTR.

As PV modules operate at different temperatures due to diurnal and seasonal cycles, but also to operation in different climate zones, special emphasis was given to the temperature dependence of OTR and WVTR of four backsheets. It was seen that temperature dependency significantly influences the resulting transmission rate and followed the Arrhenius approach. The evaluations allow for the calculation of activation energies at required temperatures. The results revealed generally lower energies necessary for inducing oxygen permeation. Changes of the temperature dependencies in the course of aging are significant. The influence of the humidity level on oxygen permeation of a polyamide-based backsheet was found to have a significant role on resulting OTR values.

KURZFASSUNG

Die maßgebliche Rolle von solaren PV Anlagen an der Elektrizitätsgewinnung nimmt weltweit zu. Weitere Untersuchungen in der Forschung sind daher wichtig um einerseits die Zuverlässigkeit von PV Systemen und damit andererseits die Stromgewinnung zu erhöhen. Folglich zielte die präsentierte Arbeit auf Verbesserungen in der Zuverlässigkeit von PV Systemen ab. Der Fokus wurde auf die Charakterisierung polymerer Materialien für Photovoltaikmodulanwendungen gerichtet. Es wurde mit diversen analytischen Methoden gearbeitet um Einsicht in chemische und physikalische Alterungsprozesse zu erhalten, die wiederum eine Erhöhung der Qualität sowie eine frühe Vorhersage der möglichen Lebensdauer von Modulen erlauben. Dabei wurden das Kurz- und Langzeitverhalten sowie die Permeationseigenschaften polymerer Materialien von PV Modulen untersucht.

Um Aufschluss über das Kurzzeitverhalten von polymeren Materialien zu bekommen wurden systematische Untersuchungen des thermischen Ausdehnungsverhaltens verschiedener Einkapselungsmaterialien durchgeführt. Bisher wurden noch keine Daten zum Ausdehnungsverhalten und der Materialanisotropie solarer Einkapselungsmaterialien in wissenschaftlicher Literatur veröffentlicht. Daher wurde in dieser Arbeit das erste Mal ein Überblick über das thermische Ausdehnungsverhalten von neun verschiedenen Einkapselungsmaterialien gegeben. Um die thermischen Ausdehnungen zu ermitteln wurden Messungen mittels Thermo-Mechanischer Analyse (TMA) unter anwendungsrelevanten Parametern, beziehungsweise in Bezug auf den Laminationsvorgang, gewählt. Der Einfluss des thermischen Ausdehnungsverhaltens wurde als hoch relevant für den PV Modullaminationsprozess und damit dem Endprodukt identifiziert. Ebenso erwies sich die TMA als geeignete Methode für die Prüfung der Anwendbarkeit als auch Qualitätskontrolle von Einkapselungsmaterialien.

Zusätzlich wurden der Einfluss des Laminationsprozesses und beschleunigter Alterungsverfahren auf eine Polyamid-basierte Rückseitenfolie untersucht. Die Ergebnisse zeigten keine signifikanten chemischen Alterungsprozesse. Eine

physikalische Änderung im Polyamid, die einer Rekristallisation zugeordnet werden kann, wurde detektiert und als temperatur- und zeitabhängig nachgewiesen. Die Bruchdehnungswerte der Folie zeigten sich signifikant davon abhängig und waren in Querrichtung der Rückseitenfolie ausgeprägter. Der Rekristallisationsprozess mit seinem negativen Einfluss auf das mechanische Verhalten kann in Bezug auf thermische Belastungen des Laminationsprozesses oder Anwendungen in heißen Klimazonen in Hinblick auf die Zuverlässigkeit von PV Modulen vernachlässigt werden.

Ein umfassendes Verständnis von chemischen und physikalischen Alterungsmechanismen von polymeren Rückseitenfolien ist notwendig um Rückschlüsse über deren Langzeitverhalten schließen zu können. Da eine immer wiederkehrende Frage in der Zuverlässigkeitsprüfung von PV Modulkomponenten sich über Materialunverträglichkeiten und synergistischen Effekten ergibt, wurden verschiedene beschleunigte Alterungsverfahren an einzelne und im Modul verbaute Folien getestet. Als beschleunigte Alterungsverfahren wurde einerseits die „damp heat" (DH: 85°C/ 85 % RH) Alterung in Anlehnung an die Norm IEC 61215, aber mit erweiterter Auslagerungszeit bis auf 2000 h, gewählt. Andererseits wurde die simultane Bewitterung mit erhöhter Temperatur (50°C), Feuchtigkeit (80 %) und Bestrahlung (300-2800 nm Metallhalogenidlampe, 1000 W/m²) (Climate) für 1000 h gewählt. Die Ergebnisse zeigten Nachkristallisation (physikalische Alterung) und Hydrolyse (chemische Alterung) unter DH Bedingungen. Dasselbe wurde auch für die Climate gelagerten Proben detektiert, jedoch in einem kleineren Ausmaß und zusätzlicher Initiierung chemischer Alterung der Außen- und Innenschichten der Rückseitenfolien. Aus den Ergebnisse kann rückgeschlossen werden, dass für die Zuverlässigkeitsprüfung unter DH Bedingungen die Auslagerungen an den Einzelmaterialien Ergebnisse liefern, die direkt mit denen im PV Module verbauten Materialien zusammenhängen. Die einzige Ausnahme war eine Rückseitenfolie mit Barriereschicht. Das ermöglicht vereinfachte Probenpräparation, geringere Kosten und bietet mehr Testmöglichkeiten für die Charakterisierung von alterungsinduzierten Veränderungen in den polymeren Materialien. Für die Zuverlässigkeitsprüfung von

Rückseitenfolien unter zusätzlicher Bestrahlung ist die Interpretation schwieriger als für die DH Alterung, da die Strahlungserwärmung ein anderes Mikroklima an den Modulen und damit höhere Temperatur im Vergleich zu den Einzelfolien induzierte. Dies ging einher mit erhöhten Ausmaßen der detektierten Alterungsmechanismen.

In Bezug auf die Zuverlässigkeit von c-Si PV Modulen spielt Permeation von Wasserdampf und Sauerstoff eine maßgebliche Rolle. Daher ist die Kenntnis von Permeationsraten der Rückseitenfolien und deren Veränderung während ihrer Alterung von vorrangiger Bedeutung. In dieser Arbeit wurde die Wasserdampf- (WVTR) und Sauerstofftransmissionsraten (OTR) von sechs verschiedenen Rückseitenfolien im ungealterten und gealterten Zustand untersucht. Ebenso wurden Ergebnisse verschiedener Messmethoden zur Erfassung der WVTR und OTR gegenübergestellt, die Schwierigkeiten bei den Vergleichbarkeiten aufzeigten. Die Ergebnisse gaben einen Überblick über das generelle Permeationsverhalten der untersuchten Folien. Veränderungen im Zuge der Alterung sind nicht vernachlässigbar und zeigten Zunahmen der OTR.

PV Module sind aufgrund täglicher und auch saisonaler Zyklen, sowie Anwendung in verschiedenen Klimazonen verschiedenen Temperaturen ausgesetzt. Daher wurde besonderer Wert auf die Temperaturabhängigkeit der WVTR und OTR Werte von vier verschiedenen Rückseitenfolien gelegt. Die Temperaturabhängigkeit beeinflusste maßgeblich die resultierenden Transmissionsraten, die dem Arrheniusansatz folgten. Die Ergebnisse zeigten generell niedrigere Aktivierungsenergien für die Indizierung von Sauerstofftransmission. Die gezeigten Auswertungen ermöglichen die Kalkulation der Transmissionsraten bei anderen geforderten Temperaturen. Veränderungen der Temperaturabhängigkeit im Zuge der Alterung sind nicht vernachlässigbar. Der signifikante Einfluss von verschiedenen relativen Luftfeuchten während der Messungen auf das Sauerstofftransmissionsverhalten einer Polyamid-basierten Rückseitenfolie wurde nachgewiesen.

TABLE OF CONTENT

CHAPTER I:

INTRODUCTION AND OBJECTIVES

1.1 Worldwide energy usage

In the end of the year 2014 a world population of 7.284.283.000 people was predicted [1]. Further estimations for the expected increase in world population are shown in Figure 1 [2]. Besides a lot of problems which are going along with the population increase e.g. urbanization, feeding etc. also the supply of energy has to be solved.

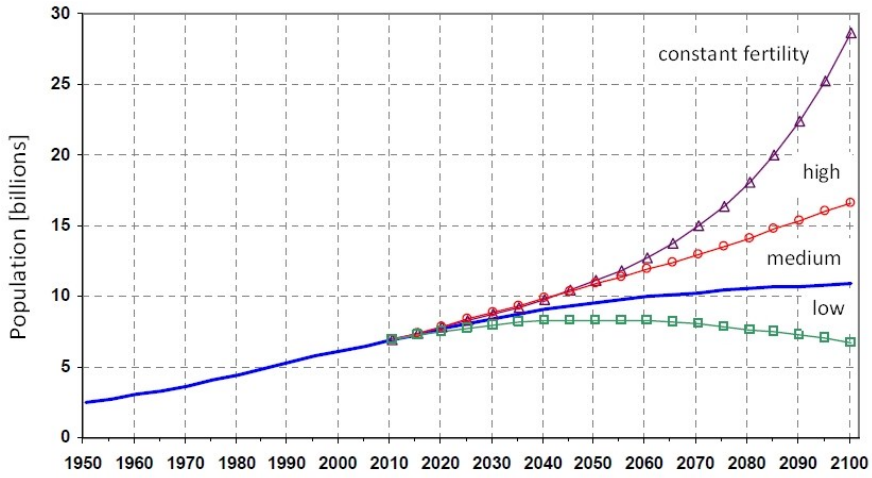

Figure 1: Population of the world, 1950-2100, according to different projections and variants [2]

The world total primary energy supply from 1971 to 2012 is shown in Figure 2 [3]. In this figure the part of renewable energies like geothermal, solar, wind, photovoltaics etc. are barely visible (category Other). When looking on the proportionately energy share of renewable energy sources on the global electricity production it is higher than those on the primary energy supply, as shown in Figure 3 [4]. Nonetheless the global electricity production is with a far higher percentage of 77.9 % from fossil fuels and nuclear and just 22.1 % from renewable sources. The growing demand on energy supply due to population increase, future estimations of the foreseeable run out of fossil fuels and the important fact that the use of fossil fuels leads to unwanted CO_2 emissions gives a necessity in the promotion of renewable energy. Indisputable the promotion has to be done for different technologies of renewable energy sources, as each one has its advantages and drawbacks. Besides the political changes and

orientations which must be done, also further investigation in research is important to improve the energy output and reliability of the alternative technologies.

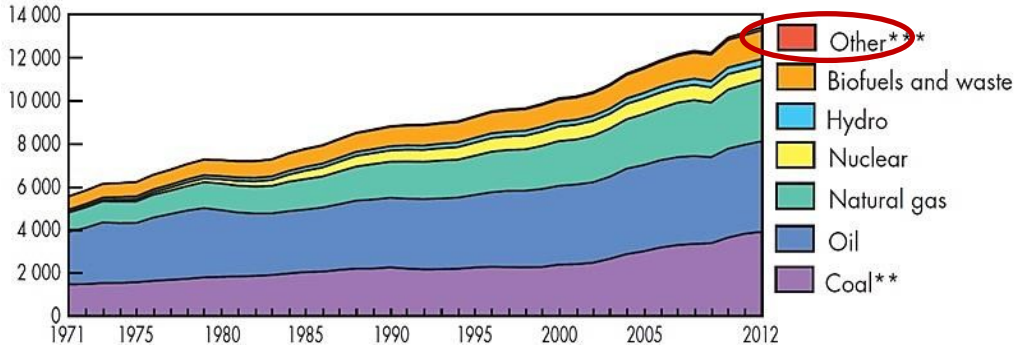

Figure 2: World total primary energy supply from 1971 to 2012 by fuel (Mtoe) [3] **In these graphs, peat and oil shale are aggregated with coal ***Includes geothermal, solar, wind, heat, etc.

Figure 3 shows the share of renewable energy sources, which reflects this mix of different kinds of techniques. In this work further discussions will be focused on PV technologies. The proportionately share of PV on the electricity generation worldwide is about 0.7 %, while in Europe its share is about 3 % [4] [5]. It seems that solar PV is starting to play a substantial role in electricity generation in some countries, particularly in Europe, while lower prices are opening new markets from Africa and the Middle East to Asia and Latin America [4]. Prices for PV modules dropped about 75 % from 2009 to 2014 [6]! Nowadays in middle Europe the utility scale costs of PV electricity is about 8.2 c€/kWh with an energy pay-back time of 1.4 years. With additional consideration of environmental aspects PV technologies are competitive e.g. with electricity generation by hard coal (7.1 c€/kWh) [7].

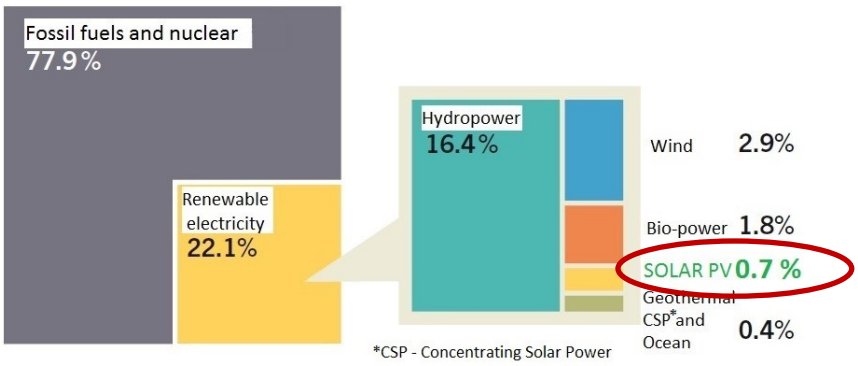

Figure 3: Estimated renewable energy share of global electricity production for end of 2013 [4]

The solar PV market had a record year 2013, adding more than 39 GW for a total exceeding 139 GW [4]. The cumulative capacities installed in the end of 2013 are shown in Figure 4 [8]. Germany (25 %) followed by China (14 %) and Italy (13 %) had the most installed cumulative capacities. The center of gravity in installed PV capacity will change in future e.g. China accounted nearly one-third (12.92 GW) of global capacity added in 2013, followed by Japan and the United States [8] [4].

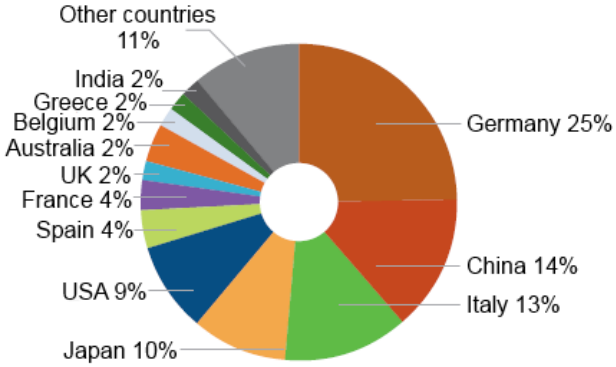

Figure 4: Cumulative capacities of PV module installations at the end of 2013 [8]

In the end of 2013 the proportionately share of PV on the electricity generation in Austria was for first time above 1 %. It was an increase of about 81 % in comparison to the year 2012 (0.61 %). The cumulative capacity for Austria in the end of 2013 was 626 MW. The general trend of increasing installations in the last years in combination with the low module prices may have led to a cumulative capacity of 1 GW in the end of 2014 [9].

1.2 State of the art PV module technologies

At the time of birth of the terrestrial PV industry (developed from space solar cells in 1955) in the mid-1970s, the conventional wisdom was that crystalline silicon (c-Si) solar cells, were hopelessly too expensive as a terrestrial energy source, and that some new, breakthrough technology would quickly emerge and dominate [10]. Perhaps the biggest surprise today is that crystalline silicon still dominates, being responsible for 91 % of the power module market (see Figure 5) [11].

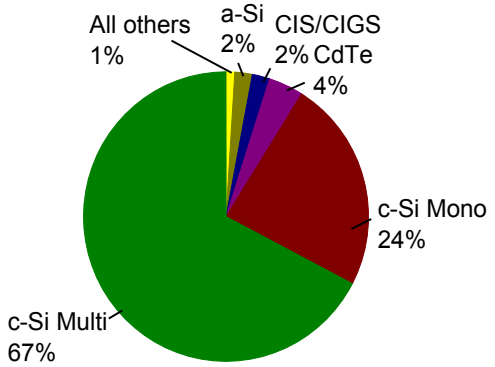

Figure 5: Solar PV module production by Technology 2014 [11]

Although cell efficiencies on research level reached values of 25 % for mono- and just 20.4 % for multi-crystalline cells the market share of PV modules with multi-crystalline cells is bigger [12]. This can be attributed to the simpler production process of multi-crystalline cells. Overall module efficiencies can vary due to different module sizes, cell distances etc. In 2011 the PV module efficiencies using mono-crystalline Si cells ranged between 13- 19 % and multi-crystalline Si cells between 11- 15 %. Converted into a surface area needed for the generation of 1 kWp this means about 5- 8 m^2 for mono-crystalline and 7- 9 m^2 for multi-crystalline Si PV modules [13]. However, while in research activities many different technologies (20 different approaches besides c-Si technologies) are still under investigation (for further details have a look on the well-known NREL chart of Research Cell Efficiency Records depicted in Figure 6 [12]), just three other PV technologies reaching shares of ≥2 % in the terrestrial solar PV module production (see Figure 5). C-Si based PV modules are thus still the dominating module type and in this work the investigations are limited to polymers used in this kind of modules. The operating principles and/or photovoltaic conversion of sunlight

as well as information on different cell technologies are outside the scope of this work. The reader is referred to standard text books as [14] [15].

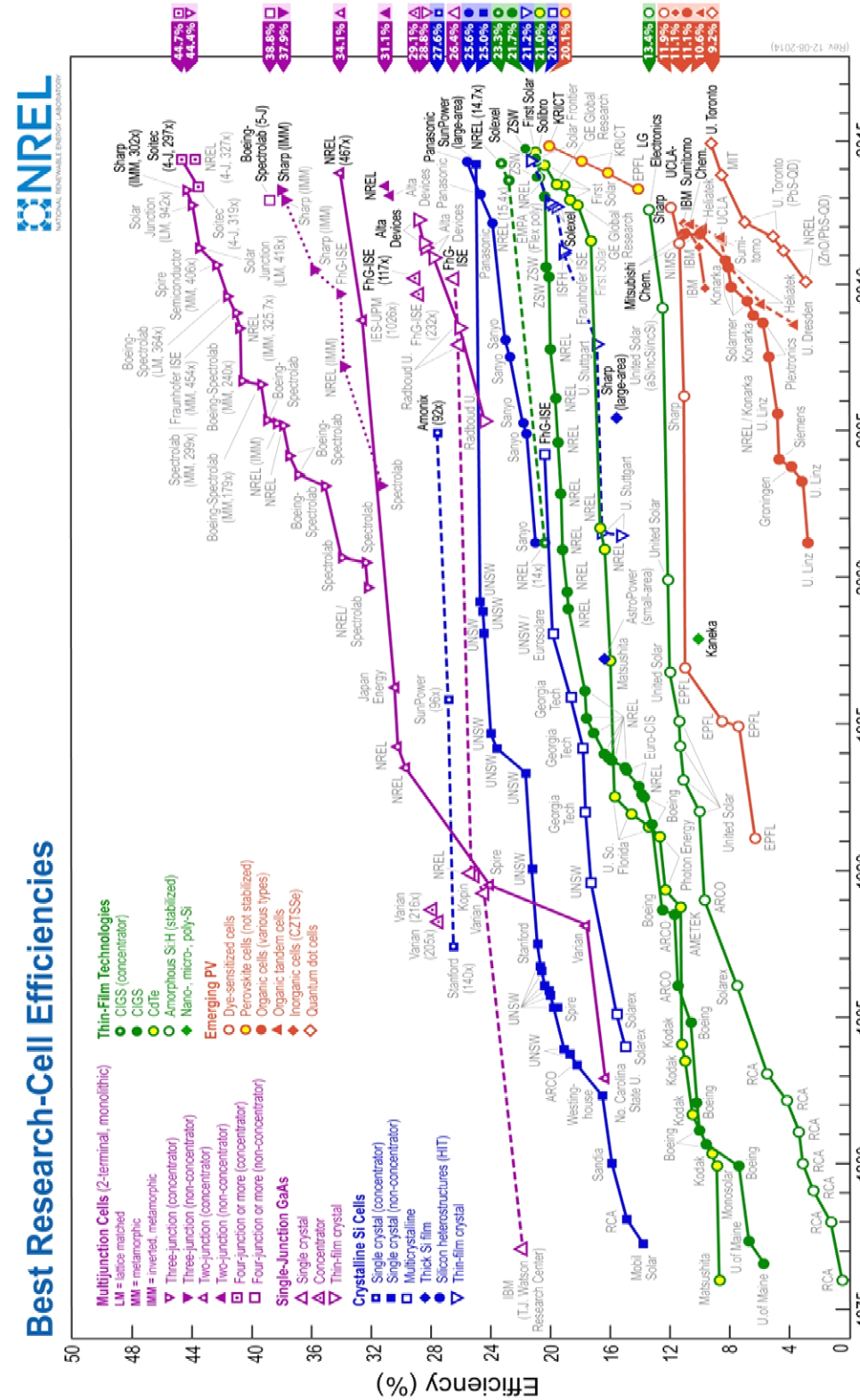

Figure 6: NREL chart of Best Research-Cell Efficiencies [11]

1.3 C-Si module technologies

1.3.1 PV module composition

The general module constitution for c-Si, as shown in Figure 7, has been developed in the Flat-Plate Solar Array Project in the 1970s and 1980s and has not significantly changed since then [16]. The most important parts in a PV module are, for sure, the cells. All other components are just needed for the transport of the produced electricity, to protect the cell from environmental influences and to give electrical insulation due to safety issues. Nevertheless the operational reliability of a PV module depends strongly on the additional components.

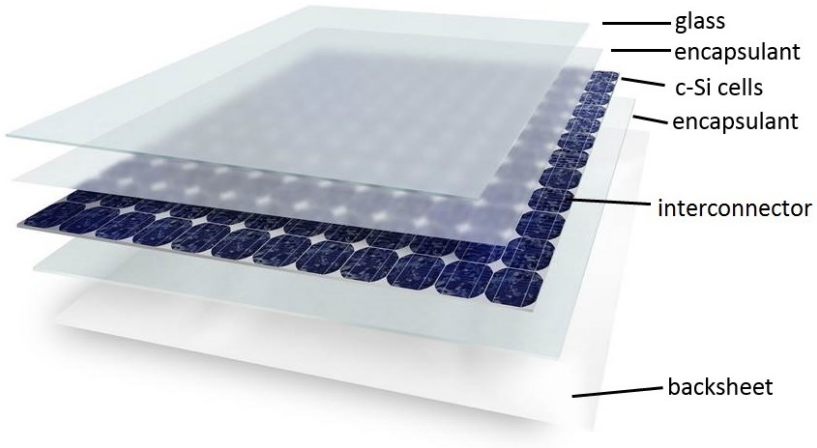

Figure 7: Schematic PV module constitution of standard c-Si modules

The most common used material for front protection is glass. The glass used for PV modules is typically tempered and has a low iron content. Standard thicknesses are about 3.2 mm. This cover glass provides mechanical rigidity, impact resistance, optical transparency, electrical insulation of the solar cell circuit and outdoor weatherability [17]. The low iron content is used for a higher solar transmittance. As the polymeric materials in a PV module typically degrade under extended exposure to UV light (<400 nm), a small amount of the element cerium (Ce) is added to absorb the short wavelengths [17]. Typical resulting UV cut-offs are ~320 nm [18]. Also very common is the addition of an antireflection coating to enhance the transmission of light [19]. In some cases the glass on the front side can also be replaced by a transparent polymer film, mainly fluoropolymers like ethylene-tetrafluoroethylene (ETFE- DuPont),

tetrafluoroethylen/ hexafluoro-propylencopolymer (FEP- Saint Gobain), fully fluorinated fluoropolymer (PFA, MFA– Solvay Solexis), polycarbonate (PC- Bayer Materials Science AG) or ethylene-chlorotrifluoroethylene (ECTFE- Solvay Solexis, CPP SOLAR) to get flexibility and reduced weight [20]. These films are more often used in thin film modules, where the enhanced flexibility and the reduced weight compensate the higher prices.

In Figure 8 a schematic c-Si cell surface with its metallization is shown. Nowadays typical thicknesses of c-Si cells are about 140 to 200 µm [21]. On all types of c-Si cells a SiN antireflection coating (ARC) is deposited on the front [22]. To transport the electricity from the solar cells, interconnectors (respectively busbars) are needed. Busbars are copper ribbons that are completely covered with solder material. The solder material is typical a lead (Pb)-free or Pb containing tin [23]. Copper is chosen because of its excellent electrical conductivity which is, after silver, the best of all metals [21]. The solder material is necessary to contact the busbars under heat to the metallization surface of the solar cells (via soldering). Since 2006 a lead ban from nearly all electric and electronic is restricted, whereas the photovoltaic industry is still excluded [24]. Therefore Pb-free solder materials came up as well as one relative new approach where the solder material is replaced with an electrical conductive adhesive.

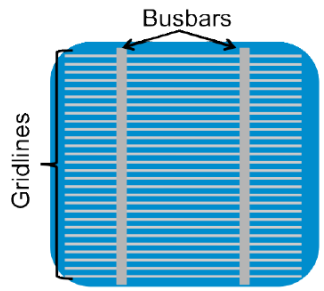

Figure 8: Metallization on a silicon cell consists of gridlines and busbars [25]

This adhesive is in most cases an epoxy-matrix with conductive particles of e.g. silver [26] [27]. The busbars collecting the electrical current from the cell gridlines to transport it on the back of the neighboring solar cell [21]. All the produced electricity is transferred via these paths to the junction box (J-box) on the upper back of the PV module.

The primary purpose of the encapsulant is to bond the multiple components of a module together. Especially the surrounding of the brittle solar cells with its electrical connections is very important to give also the required protection. Once the PV module compound is build the encapsulant has to provide structural support via a good adhesion to different materials. The provision of structural support requires the use of a polymeric material with a low modulus and viscoelastic behavior to compensate the different thermal expansion coefficients of materials, i.e. glass, solar cells, interconnects and polymers, in a PV module [16] [28]. Of primary purpose is also the optical coupling with a high optical transmittance of incident light between 290 and 1100 nm (useable wavelengths of solar spectrum for c-Si) [28]. The refractive index of air is 1, for glass of PV application it is 1.5 and for the ARC of the solar cell (SiN) it is 2.05 [29]. To ensure high light transmission the encapsulant has to have a refractive index in between the values of glass and the ARC. Furthermore electrical insulation (operational voltage of ≤1 kV), physical isolation/protection and thermal conduction for the module are requirements [28]. Not at least also a low price and easy processability are reasons for the use of some encapsulants. These properties have to be stable from the initial to end of lifetime of a module. Therefore also a high resistance against incoming UV light and thermal oxidation during application should be achieved.

The role of the backsheet is to give structural support via mechanical strength, to be a barrier against humidity and oxygen, to provide electrical insulation and weathering protection. Furthermore also a high resistance against incoming UV light, thermal oxidation and a good adhesion to the encapsulation material during application should be achieved [30]. Due to the low costs and the good processability the use of polymeric backsheets is the most common used material on the backside of a PV module. In some cases instead of a backsheet on the back side, also glass can be used to derive a so called glass/glass module. Glass/glass constructions were often found to trap harmful compounds that catalyzed moisture-driven corrosion and may induce additional stresses in the module enhancing delamination and/or glass breakage [31]

[25]. Therefore it is mainly used for building integrated PV modules, where the enhanced stiffness of the module is required.

1.3.2 Processing of PV modules

The production of c-Si modules includes several processing steps: cell control and sorting by efficiencies, glass cleaning, stringing, lamination, framing, J-box mounting, module power inspection and packing [21] [32]. The two critical steps are the soldering and the lamination. The soldering process is typically automated. Therein the cells get coupled to the interconnectors (busbars) at elevated temperatures, which depends on the soldering material (183°C for lead solder, 221°C for lead free solder material and <150°C for electrical conductive adhesives) [21] [33]. The critical aspect during this process is the discrepancy of the thermal expansion coefficients for the different materials, which therefore inducing different stresses [21]. It can lead to inhomogeneous contacts to the cells and/or arising cracks. Electrical conductive adhesives can significantly reduce the cracks due to the required lower temperatures at soldering [34] [33] [26] [27]. In the next step all materials are put together and given in a so called flat-bed laminator (see Figure 9). Evaluating the production process of PV modules, the most time consuming step is the lamination of the modules. It is needed to bond all components together to get a PV module compound. This is done by melting of the encapsulant to guarantee a full flow around and further bonding to all components, and in case of EVA (ethylene vinyl acetate) also to ensure the required crosslinking density. It is highly relevant for quality and long term stability of a PV module [35]. Variables in the lamination process are the temperature, time and pressure [32]. All of them depend on the chosen encapsulant and its thickness, glass thickness and the principal construction (glass/backsheet or glass/glass module).

An example for a typical temperature profile during PV module lamination for a glass/backsheet (with EVA as encapsulant) construction is shown in Figure 10. The first step is the insertion of the cold PV module lay-up into the laminator. Then Evacuation

1 phase starts with evacuation of the vacuum chamber which shifts the module to the heating plate (see Figure 9 and Figure 10).

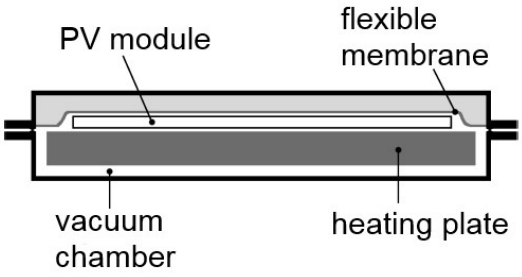

Figure 9: Schematic configuration of a flat-bed laminator for PV module production [21]

In the Evacuation 2 phase the pressure around the module will be reduced (~0.6 mbar). In the third step pressures of ~850 mbar via the upper chamber (above the flexible membrane) is applied. At this point also the EVA crosslinking phase is initiated [35]. Then the PV module will be vented (cooled down to room temperature). After lamination the most PV modules get an aluminum frame on the outside which is bonded with an edge sealant to the PV module compound. This makes the installation of PV module systems easier and supports the whole module mechanical.

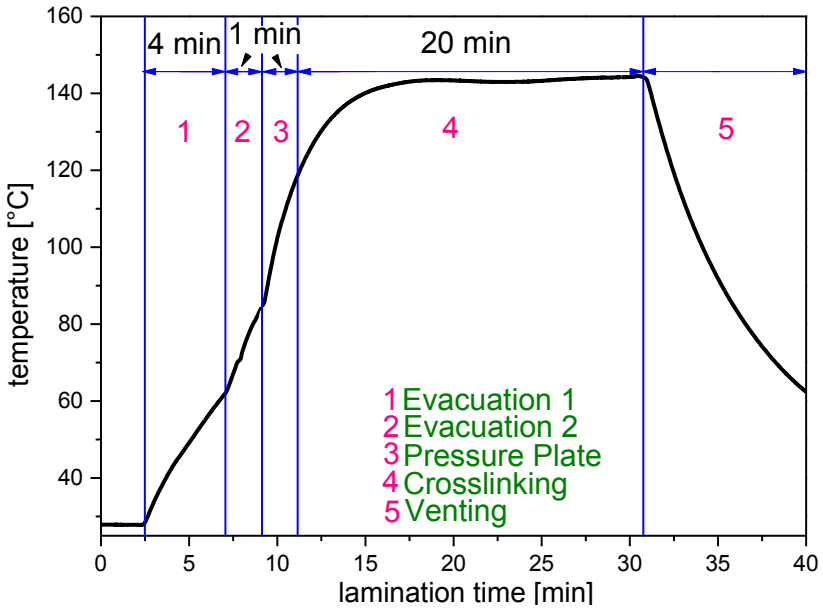

Figure 10: Example for a temperature profile during PV module lamination [35]

1.3.3 Polymeric materials in PV modules

1.3.3.1 Encapsulants

The first silicon module designed for outdoor use was fabricated in 1955 at Bell laboratories, with an encapsulation of the cells in silicone oil in a plastic case [36]. This module was removed 5 months after installation in 1956. With some following modules without encapsulation the Solar Power Corporation, established in 1973, was the first which used a silicone rubber as top cover. The first entire encapsulation was done also with silicone rubbers (polydimethyl siloxane– PDMS) at 1976 [36]. They were chosen because of their exceptional stability against thermal- and ultraviolet (UV) light induced stresses [16] [37]. A further advantage of silicones is their high transmission at wavelengths below 380 nm (typical UV cut-off for most EVAs) [38] [39]. It results in an increase in transmission, in the for the solar cell usable solar spectrum (c-Si <1100 nm), of about 3 % [38]. The principal molecular structure consists of a backbone with alternating Si and O atoms. The silicon atom is much larger than oxygen or carbon and so there is a greater freedom of motion for rotation and bending of Si-C side-group and Si-O backbone bonds compared to hydrocarbon based polymers [40]. It results in a polymer with extremely low glass transition temperatures (~-120- -45°C) and high temperature stability until ~250°C [41]. This attributes, as well as the resulting modulus, can be controlled via its crosslinking density [39]. Silicone rubbers for PV modules require completely different processing equipment compared to EVA, as the encapsulant is liquid when it is applied on the module [38]. These Silicone rubbers are typically a two component liquid system where one part being the Si polymer (SiVinyl) and Pt catalyst (to start of the curing reaction) and the second part being the SiH oligomer (for more detailed information have a look on [42], [43] and [40]). The curing process proceeds at room temperature and will be significantly accelerated at enhanced temperatures [40] [39]. The higher prices for silicones and the need for other processing equipment let them play an inferior role as encapsulant. For curing conditions, time and more the reader is

referred to supplier homepages of for example Dow Corning (USA), Momentive (USA) and Wacker Chemie AG (Germany).

Following approaches were, besides the use of silicone rubbers, the replacement via polyvinyl butyral (PVB) in 1976 and the replacement of PVB via ethylene vinyl acetate (EVA) in 1980. PVB is a random terpolymer made from vinyl acetate (VA), vinyl alcohol (VOH) and vinyl butyrale (VB) (see Figure 11). The most common application for this polymer is the use in safety glass [44]. For PV applications it is mostly used for building integrated PV (BIPV) and therefore glass/glass PV modules. Furthermore thin-film modules (e.g. in a-Si and µc-Si) are often built with PVB [45]. Dependent on the cell type and constitution of the PV module with PVB different processing types can be used. For first the common vacuum lamination process and for second a two-step process, which is e.g. always used for glass/glass modules. In the two-step process a vacuum- or rolled pre-compound is built with a subsequent autoclave processing [46]. PVB is an amorphous polymer and due to the lack of elasticity a brittle and glassy thermoplast. With the addition of plasticizers the elastic modulus is lowered and its phase transition temperatures tailored [40]. Physical crosslinks in this polymer are provided from the hydrogen bonds on the polymer chain. PVB used for photovoltaic modules has a T_g of ~15°C [40]. Three main aging mechanisms for PVB can be declared. At elevated temperature the hydroxyl groups getting segregated and long chain segments with double bonds are built. They cause yellowing. Furthermore a volatilization of low molecular components as e.g. plasticizers can happen under elevated temperatures [44]. PVB also shows a high water uptake and susceptibility to hydrolysis [47] [48]. Therefore PVB requires stabilizers e.g. antioxidants and UV stabilizers to be durable during application. More information about that can be found in [49]. Suppliers for PVB are e.g. Kuraray Europe GmbH (Germany), Eastman Chemical Company (USA).

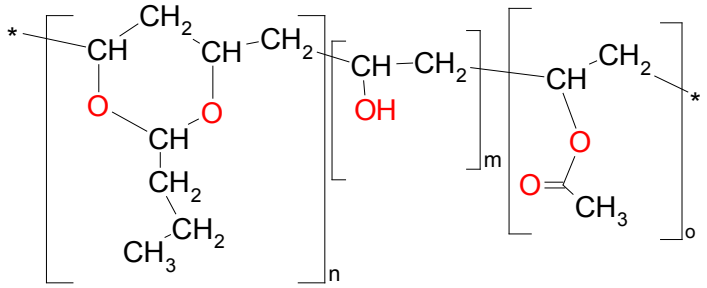

Figure 11: Molecular structure of PVB with n=~76 %, m=~22 % and 0=~2 %

EVAs advantages like e.g. the lower cost (most important factor), better clarity and dimensional stability made it to be the still dominating material on the market [16]. EVA is a random copolymer consisting of ethylene (E) and vinyl acetate (VA). In the PV industry, the copolymer consists of ethylene and about 28-33 wt% vinyl acetate (see Figure 12) [50]. Polyethylene is a very simple and inexpensive polymer, but if used alone, it is typically an opaque or translucent (depending on polymerization conditions) semi-crystalline polymer with a modulus too high (≥ 200 MPa) to mechanically protect a PV device [51] [52]. Poly vinyl acetate is a transparent, amorphous polymer, but with a glass transition temperature (T_g) of about 35°C which makes it too brittle under typical environmental exposure [51]. Therefore a copolymerization of both polymers breaks up the crystallites of polyethylene, making it a semi-crystalline, highly transparent material with a low T_g [51] [52]. The resulting thermoplastic polymer has melting temperatures between 60- 70°C with a T_g around -30°C and is mildly opaque, which would therefore neither fulfill the mechanical nor the optical requirements [53].

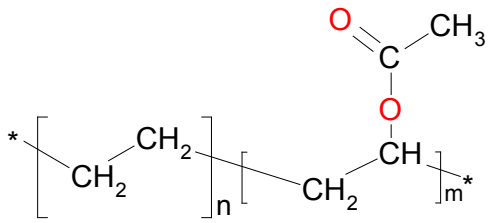

Figure 12: Molecular structure of EVA with n=~67- 72 and m=~28- 33 for PV module applications

However, by crosslinking the copolymer chains (VA) during PV module lamination, the EVA sheet is transformed into a transparent, dimensional stable encapsulation

material. This crosslinking is initiated via a radical reaction, using an organic peroxide or peroxycarboxylic acid as radical initiator (“crosslinker”) [28] [52]. The initial degree of crosslinking (after lamination) is very important as it strongly influences the long-term characteristics of the material and is therefore highly relevant for quality and long term stability of the produced PV module [28] [35]. It is controlled by lamination temperature (affecting the amount of crosslinker activated per time unit), the lamination time and the initial crosslinker concentration [53]. After crosslinking EVA has a melting range between 30 and 70°C with calculated crystallinities of approximately 7- 9 % [53]. The resulting solar transmittance of EVA is between 88 to 90 %, dependent on the type of UV absorber [54]. One new approach is an EVA with a lower UV-cut off than ~340- 410 nm. The UV-cut off of this new formulation at 305 nm is claimed to gain an increase of 1 % in the module power output in respective to an EVA formulation with an UV-cut off at 360 nm [55]. Offered EVA products differing in the VA contents and additive formulations (undisclosed) e.g. crosslinking agents (also amount), UV absorber, hindered amine light stabilizers and antioxidants [49]. General recommended curing times ranging from 7 to 25 min with temperatures in between 145 to 155°C. Suppliers on the market are e.g. Arkema (France), Bridgestone (Japan), Evasa (Spain), Hangzhou First (China), Mitsui (Japan), SKC (Korea), STR (USA). However, as EVA films have also some disadvantages, there are still silicones and PVB commercial available. The disadvantages of these encapsulants have not been solved completely up to now. The fast-paced PV market aims for an encapsulation material with a lower price, a better stability (no formation of acetic acid) with absence of PID and better properties like e.g. optical transmission. Additional, it should enable a faster processing during PV module production. Recently, new materials have been introduced to the PV market. These “alternative” encapsulants are ionomers, polyolefines, thermoplastic polyurethanes and thermoplastic silicone elastomers.

Thermoplastic polyurethanes were offered by Bayer Material Science AG (Germany) and Stevens Urethane (USA). They disappeared from the market because of a low temperature stability and high susceptibility to yellowing under environmental conditions.

Ionomers are produced by copolymerization of ethylene with carboxylic acid (e.g. methacrylic acid). The acid introduces anionic groups to the polymeric backbone. Ion salts (cations) are used to neutralize the carboxylic acid side chains of the ethylene backbone (see Figure 13). As cations zinc or sodium are used [41]. With ion contents of ≤10 %, in the otherwise nonpolar polymer, the designation ionomer is used [52]. In contrast to common thermoplastic polymers, where intermolecular forces are only built from Van der Waals forces, also ionic forces occurring between the polymer chains of ionomers. This ionic forces result in physical crosslinks in between the chains. The T_g of ionomers for PV applications is around 30°C and its melting temperatures ~70°C. Ionomers under elevated temperature and humidity tend to show a strong stiffening which is assumed to occur due to recrystallization effects [56]. The solar transmittance for Ionomers is between 84- 87 % [54].

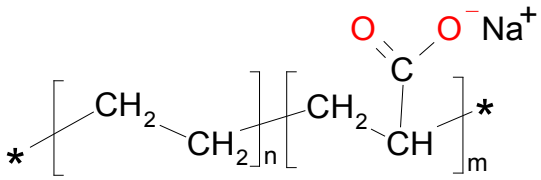

Figure 13: Molecular structure of ionomers

In comparison to EVA or PVB they have a higher stiffness and a lower lamination cycle time is required [57] [58]. Its main disadvantage of a high price in respect to EVA made it to play an inferior role as encapsulant. Suppliers for ionomers are e.g. DuPont (USA) and Juraplast (Germany).

In the PV industry the designation polyolefin for encapsulants refers to the polyethylene backbone. Therefore they consist in principal from an ethylene backbone but with introduced side chains (R1; see Figure 14). The side chains can be for example $(CH_2)_nCH_3$ or more complex like e.g. a Methylacrylat-group (C(=O)OCH3) [40] [59]. If there are side chains with acrylates or acrylic acids the exact designation is ethylene copolymer. These materials provide similar or better mechanical and optical properties before and after weathering. An advantage which they have is no formation of acetic acid during aging [59]. The introduced side chain is needed for lowering the crystallinity to increase the transmission, decrease the modulus of

ethylene and to provide a physical crosslinking (via its polar character) between the polymer chains. The overall solar transmittance of one found value in literature with 82.7 % and from own investigations (83- 88 %) was lower than this of EVA (88- 90 %) [54]. The exact formulation of this material was not given in [54]. However as the exact molecular structure is under nondisclosure of the producer and will be different for every material, further information in literature is hardly to find. Suppliers like DNP (Japan), Dow (USA) and Juraplast (Germany) serve their products since 2006 [60]. A new introduced (2013) polyolefin based encapsulant is offered from the company Isovoltaic (Austria). This product can be used with the same standard vacuum lamination technology (like EVA) and has a lower UV cut-off (290- 320 nm) in comparison to EVA (fast cure EVA: ~340- 410 nm) and therefore a higher transmission of for the solar cell usable solar spectrum. It is claimed to give an increase in power output of about 0.5 % [61].

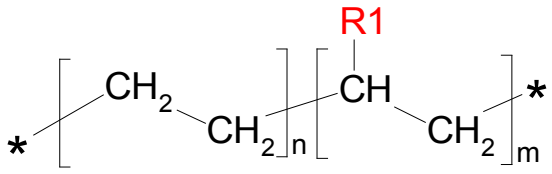

Figure 14: Principal molecular structure of ethylene based polyolefines for PV applications

Another new released product, which is comparable to EVA is from STR (USA) and a polyolefin elastomer. For this material the vinyl acetate group is replaced. Therefore no acetic acid will be built during aging, but a peroxide crosslinking is still necessary [62] [54].

In 2009 a new encapsulant with a completely different approach in the molecular constitution was developed by Wacker Chemie AG (Germany). This polymeric encapsulant is a thermoplastic silicone elastomer (TPSE) which means it is a non-crosslinking silicone with thermoplastic polymer chain parts in between. It consists in principal of PDMS with NH_2 end-groups and diisocyanates (see Figure 15). The silicone chains therein are the “soft” segments giving elasticity. The thermoplastic polymer chains are the hard segments leading to a physically bonded network (between the NH and CO groups). Furthermore the resulting block-copolymer is processable like a

thermoplast and has all advantages of silicones like e.g. the UV-stability, transparency [63]. By variation of the amount of PDMS backbone (n) and diisocyanate (m) the attributes of the polymer can be tailored. Its T_g was detected to be in a very broad range of -115- -90°C with a maximum of a softening region (corresponds to the thermoplast chain parts) at ~155°C [64]. TPSE provides a very good adhesion to glass and backsheets, with only a slight temperature dependence [65]. The solar transmittance of this encapsulant is, like for EVA, between 88- 90 % [54]. For this material a quite good UV-stability was reported, but humidity was assumed to play a more critical factor [63]. Due to the higher price and no corrosive by-products during application it was mainly used for thin-film production. As the market pressure on prices of encapsulants was too high, Wacker discontinued the production in end of 2013.

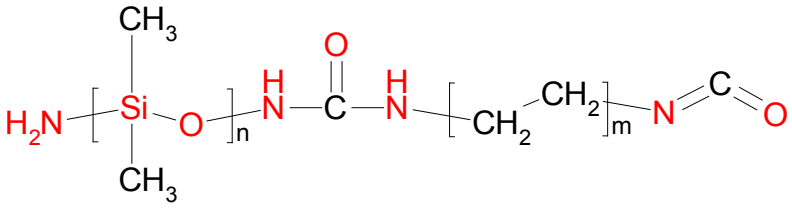

Figure 15: Molecular structure of thermoplastic silicone elastomers for PV applications

In Figure 16 an overview an all commercial available polymeric encapsulants is given. Silicones, EVA and polyolefin elastomers have to be cured to form a chemical crosslinking between the polymer chains. In contrast, all others are thermoplastic polymers with physical crosslinks in between the polymer chains to give the required strength and creep resistance [66]. Where the chemical crosslinking means irreversible covalent bonding the physically crosslinking results in thermo-reversible bonding provided from ionic or hydrogen bonds in between the polymer chains.

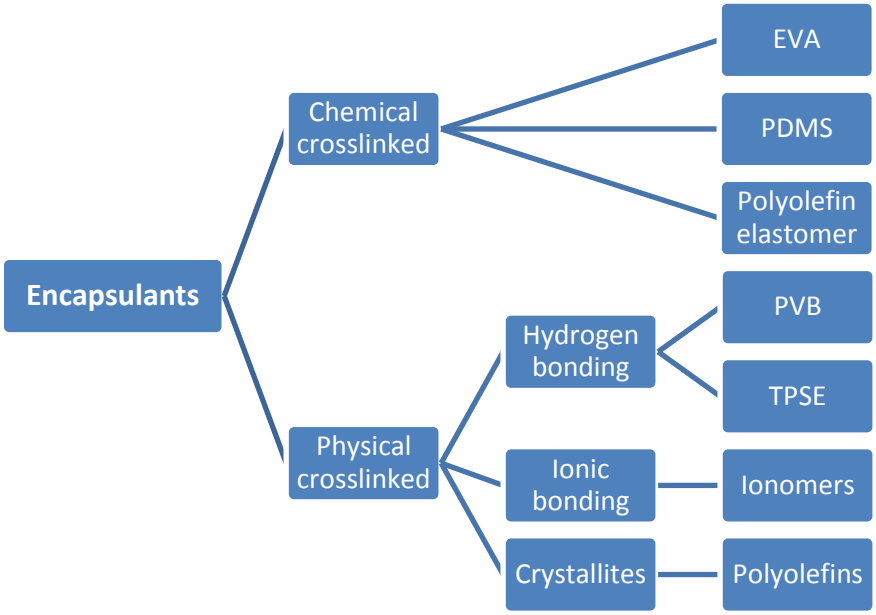

Figure 16: Overview of commercial available polymeric encapsulants

About 6 to 7 % of module costs are attributed to the encapsulants. But to reduce module costs also the total cost of life has to be considered to ensure a reliable long-time stable PV module [58]. This gives more possibilities for alternative encapsulants, although EVA is still the cheapest material. However in [60] it is said, that from 2009 to 2010 there were 14 up to 20 encapsulation foil suppliers on the market with EVA being still by far the dominating material.

1.3.3.2 Backsheets

Since the beginning of PV module encapsulation with polymeric materials multilayer films were used as backsheets. The most common used materials were polyvinyl fluoride (PVF) on the outsides (inner and outer layer) with polyethylene terephthalate (PET) as middle layer. The so derived “first generation” backsheet is called in the industry TPT for Tedlar®/PET/Tedlar® (Trade name of PVF from DuPont). PVF for PV applications has only one supplier (DuPont) and its price is, in comparison to alternative polymer films, very high. PVF was/is taken because of its excellent weathering stability and due to its proven performance also in other outdoor applications [67] [68]. PVF (Tedlar®, DuPont) is still by far the most common used fluoropolymer for outer protection of the middle layers. PVF is made from polymerization of vinyl fluoride, the resulting molecular structure is given in Figure 17.

PVF films are manufactured using a plasticized melt extrusion method [69]. It is a semi-crystalline polymer with cristallinities of ~40 % [69]. Its melting temperatures are given in between 190-200°C and its Tg at ~-20°C [41] [69]. Results from PVF films for solar applications revealed a broad range of T_g for this material as therein the T_g for PVF was between 50- 60°C. This can be attributed to the the lower crystallinities of 26 % for this films. The melting temperature therein was ~194°C [70].

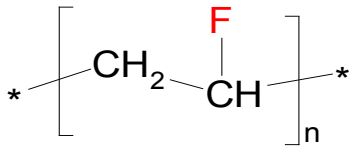

Figure 17: Molecular structure of PVF

PET was/is used mainly for its mechanical stability, high electrical insulation properties and low costs [68]. PET is produced via polycondensation of terephthalic acid with ethylene glycol; the resulting molecular structure is shown in Figure 18. The polymer is in general a semi-crystalline thermoplast with crystallinities between 30 to 40 %. The melting temperatures of semi-crystalline PET are between 250- 260°C and its T_g at ~80°C [52] [41]. Polycondensation polymers have a low resistance against hydrolysis, which makes a predrying prior to extrusion of films necessary and can also induce problems in outdoor applications [41]. PET was used for years as an electrical insulation material, which makes it an ideal material for backsheets in respect to the required electrical insulation for operating voltages <1 kV (dielectrical strength of PET 60 kV/mm) [41]. The extraordinary required weatherability (>20 years) for application in a PV module requires an adequate stabilization against thermo-oxidation, photo-oxidation (PET absorbs UV light between 290 and 330 nm) and hydrolysis [48].

For enhancing the barrier properties within PET containing backsheets may an aluminum barrier as interlayer is used. With this aluminum layer the water vapor transmission of the backsheet is reduced almost to 0 [68]. In c-Si modules with EVA as encapsulant a high barrier can be unwanted as degradation products from EVA like acetic acid will not be able to escape and therefore lead to corrosion of metallic components [31]. For the encapsulation with PVB the low WVTR can be wanted, as

PVB shows a high water uptake and susceptibility to hydrolysis [47]. But any small breach in electrical insulation over the entire surface of the foil will result in the entire foil being charged at system voltage, when an aluminum barrier layer is used. Therefore it requires a more robust electrical insulation layer in between the cells and the metal foil. Furthermore, a metal foil will act as a high voltage capacitor with the cells serving as one of the electrodes [25]. Therefore they are more often used for thin-film modules as they are much more sensitive against moisture. On the other hand also layers with silicon oxide (SiO_x) deposited on PET are used to enhance barrier properties (lower water vapor transmission) [68]. These layers reduce the water vapor transmission by a factor of 10 [71].

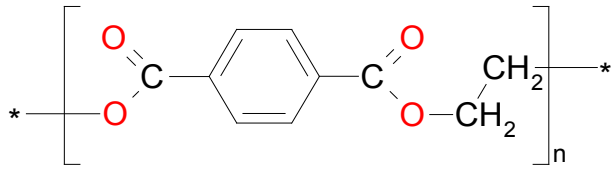

Figure 18: Molecular structure of PET

There are many producers of TPT, e.g. Dunmore Corp. (USA, Germany), Flexcon (USA), Isovoltaic (Austria), Krempel Group (Germany), SFC (South Korea), Taiflex Scientific Co. Ltd. (Taiwan), on the market. An offered alternative is the replacement of PVF with PVDF. Compared to PVF, PVDF has one more fluorine atom on the same carbon in its molecular structure (see Figure 19). The polymerization of vinylidene fluoride results in a semi-crystalline polymer. PVDF is a polymer with four main crystalline forms depending on the processing conditions [72] [69]. The crystal forms α, γ, β and δ differ in their conformation [68]. Where the α and δ-PVDF reveals a trans-Gauche conformation (δ is the polar version of α-PVDF), the β-form reveals a all trans structure [72] [73]. The γ-PVDF reveals an intermediate conformation, consisting in sequences of three trans bonds separated by a Gauche bond [73]. The melting temperature for PVDF in literature is given at 165- 180°C and the Tg -40°C [52] [69]. Its crystallinities can reach values up to 65 % [69]. Results from PVDF films for solar applications revealed a T_g between 55- 65°C. The melting temperature was ~158°C and the calculated crystallinities 13 %. These PVDF films had a β-crystal form in its

initial state, which was attributed to a stretching of the polymer film after extrusion as the α-crystal form is kinetically favored [70]. Its dielectrical strength is given with 63-67 kV/mm in [69] and with 40 kV/mm in [52]. In the wavelength region of 200-400 nm a gradually decomposition of PVDF happens [52]. Below the wavelengths of 295 nm the terrestrial solar spectrum has no radiation. Above this wavelength, the PVDF layer will be to some part protected from the UV cut-off of glass at 320 nm and possibly from the encapsulant, e.g. EVA absorbs most of the UV light below 350 nm [21] [74]. Nevertheless, the outer layer side is directly and/or due to ground reflection indirectly exposed to these wavelengths. PVDF for PV applications are sold from Arkema (Trade name Kynar®) and Solvay Solexis (Trade name Solef®). Suppliers for the in the industry often called KPK- Kynar®/PET/Kynar® (Trade name of PVDF from Arkema) backsheets are e.g. Krempel Group (Germany) and Flexcon (USA). Further combinations with PVF or PVDF include multilayers with PET as middle layer and a modified EVA or a primer as inner layer to give adhesion to the EVA encapsulant.

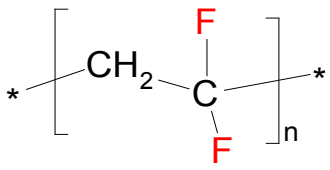

Figure 19: Molecular structure of PVDF

Since 2005 a variety of different polymer materials for backsheets were developed and introduced into the market, some of them without long-term experience or a clear indication of the service life of the backsheet [67]. 2006 was a market boom for PV and simultaneously a material shortage of Tedlar®, PVF films from DuPont. Backsheet manufacturers were forced to seek alternatives [75]. In [76] it is said, that from 2008 to 2009 there were eight up to ten backsheet suppliers on the market. In [60] it is said, that the market grew to 17 backsheet manufacturer until 2010. In 2010 still 49 Tedlar- and 46 non-Tedlar-based backsheets were offered [60]. Backsheets with Tedlar are still dominating the market, but there are alternatives. Especially as there is the need for cheaper materials as backsheet prices dropped by >50 % in 5 years (until 2014) and module prices declining by around 75 % between the end of

2009 and the end of 2014 [77] [6]. So the market moved on from the first generation backsheet structure (TPT) initially due to the limited availability of fluoropolymers and more recently due to cost.

An often used approach since then is the replacement of PVF with PET. These PET layers have a different additive formulation as the incoming of UV light has to be taken into account. The mostly used combination is PET (outer side)/PET/PE or instead of PE the use of EVA. This backsheets are offered from companies like e.g. Coveme Spa (Italy), Dunmore Corp. (USA, Germany), Skultuna Flexible (Sweden), Toppan Printing Co. Ltd. (Japan) and DNP (Japan).

There are also several approaches with unique selling points and completely different polymeric materials. In fluoropolymers the hydrogen-atoms (H) of the main carbon-chains are replaced in whole or partly with fluor-atoms (F). The F-atoms are larger in volume as H-atoms and so they build a compact and protecting envelope around the main carbon-chains. Additionally the F-C-bonds are very stable, which results in a very good chemical inertness also at enhanced temperatures. They are weatherable without stabilizers [52]. Therefore there are also approaches with other fluoropolymers than PVF or PVDF. The company 3M (Germany) introduced from 2006 to 2010 multilayer backsheets with the terpolymer tetrafluoroethylene, hexafluoropropylene and vinylidene fluoride (THV) used as outer layers with PET as middle layer and EVA for adhesion as inner layer (product names are Scotchshield™ Film) [60]. THV is a semi-crystalline copolymer of tetrafluoro ethylene, hexafluoro propylene and vinylidene fluoride (molecular structure is shown in Figure 20 a). The extrusion of this film can be done with general processing equipment. The melting temperature is given between 145- 155°C [69]. THV in general has a low crystallinity, which is caused by the fact that the vinylidene fluoride in combination with other monomers disrupts the high crystallinity typical of the polyvinylidene fluoride (PVDF) homopolymer [78]. In investigations of a THV film for solar thermal application a melting temperature of 162°C and a T_g of 34°C was revealed [79]. The weatherability of this fluoropolymer is claimed to be 10- 15 years which implies an adequate stabilization for longer stabilities [52].

In 2008 DNP (Japan) and Honeywell (Germany) came up with the substitution of PVF with ethylene chlorotrifluoroethylene (ECTFE) [60]. ECTFE is comprised of alternating ethylene and chlorotrifluoro ethylene units in the polymer chain (see Figure 20 b). The copolymerization process leads to a semi-crystalline polymer with crystallinities of 50-60 % [69]. In the literature given melting temperatures are between 210 and 245°C [69] [52]. The single largest use of ECTFE is the flame-resistant insulation for wire and cable applications [69]. The properties of the films for PV application will be for sure dependend on the processing conditions during extrusion and the comonomer content. Due to the ehtylene comonomer content additives against photodegradation are necessary for this fluoropolymer [41].

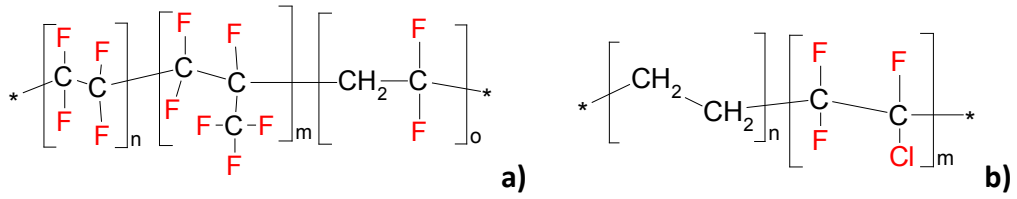

Figure 20: Molecular structure of **a)** THV, **b)** ECTFE

Another example is offered by Isovoltaic (Austria), which made a market introduction in 2009 with several polyamide based backsheets. These products are available with 1) all three layers consisting mainly of polyamide, which is then coextruded and not laminated (AAA for PA/PA/PA) 2) or in combination with PET in the middle (APA for PA/PET/PA) 3), or with PET in the middle and PVF as outer layer (TPA for Tedlar®/PET/PA) [60]. The used polyamide is an aliphatic polyamide 12 (PA 12; see Figure 21). It is produced from laurolactam, which is cyclic in its initial state. With a ring-opening and further polymerization the semi-crystalline polyamide 12 is made. The intermolecular forces (hydrogen bonds) are strongly dependent on the distance between the carbonamide groups (CONH). It therefore has an influence on its melting temperature and crystallinity. The melting temperature given in literature for PA 12 is between 175-180°C, the T_g between 27- 49°C and the crystallinity ~18 % [52] [80] [41]. However the crystallinity depends strongly on the processing conditions. PA 12, as well as polyamides in general, have a high leakage current resistivity and dielectric strength. These attributes and the low oxygen transmission rates for PA 12 are

possibly the reason for the use of this specific polymer [41]. For the coextruded AAA backsheet the inner layer is equipped with TiO_2 to enhance reflection of light back into the module [81]. TiO_2 in polyamides can also be used as nucleating agent [41]. The middle layer is equipped with inorganic additives embedded in a polypropylene to increase the dielectric strength, lower the thermal expansion and water vapor transmission rate and enhance heat conductivity (details are described in [81]).

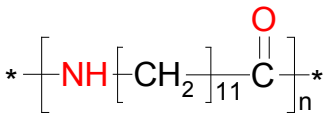

Figure 21: Molecular structure of polyamide 12

Approaches also with unique selling points are the produkt Makrofol® from Bayer (market introduction 2010), which is a polycarbonate blend based backsheet and a PP based backsheet from Renolit [60] [82]. However for the PP based backsheet only the patent (publication date in 2011) was found without any proof of its availability on the market. Polycarbonate based backsheets are offered from Bayer MaterialScience AG (Germany) with the trade name Makrofol®. It seems to be rarely used as no literature could be found on investigations in this material. Makrofol® for PV applications is an extruded film based on a polycarbonate blend [83] [84]. From the use of polycarbonate in glass/glass modules a combination with PVB as encapsulant should be avoided. The plasticizer in the PVB appears to be critical for the long-term stability of the polycarbonate [85].

In 2012 a new backsheet, based on cost effective crosslinked polyolefines was developed for solar modules by 3M™ (Germany) [67]. The coextruded PE based backsheet of 3M™ (Germany) consists of three polyethylene (PE) layers with different additive contents (Scotchshield® Film 800). At least the middle layer is a silane-crosslinked PE (see Figure 22). The crosslinks are built with Si-O-Si bridges with ~5 crosslinks per 1000 C-atoms [52] [41]. It results in a higher thermal stability (120°C for long-term loads) [52]. Results from artificial weathering on this backsheets revealed a good performance [67] [86] [87] [88].

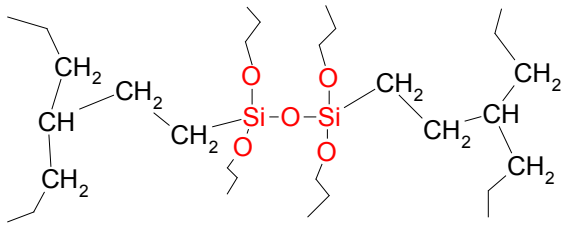

Figure 22: Molecular structure of silane crosslinked polyethylene

In Figure 23 an overview on all commercial available polymeric backsheets is shown with a classification by the used polymeric materials. To build a multilayered backsheet on the one hand the sheets get laminated together or on the other hand a coextrusion process is used.

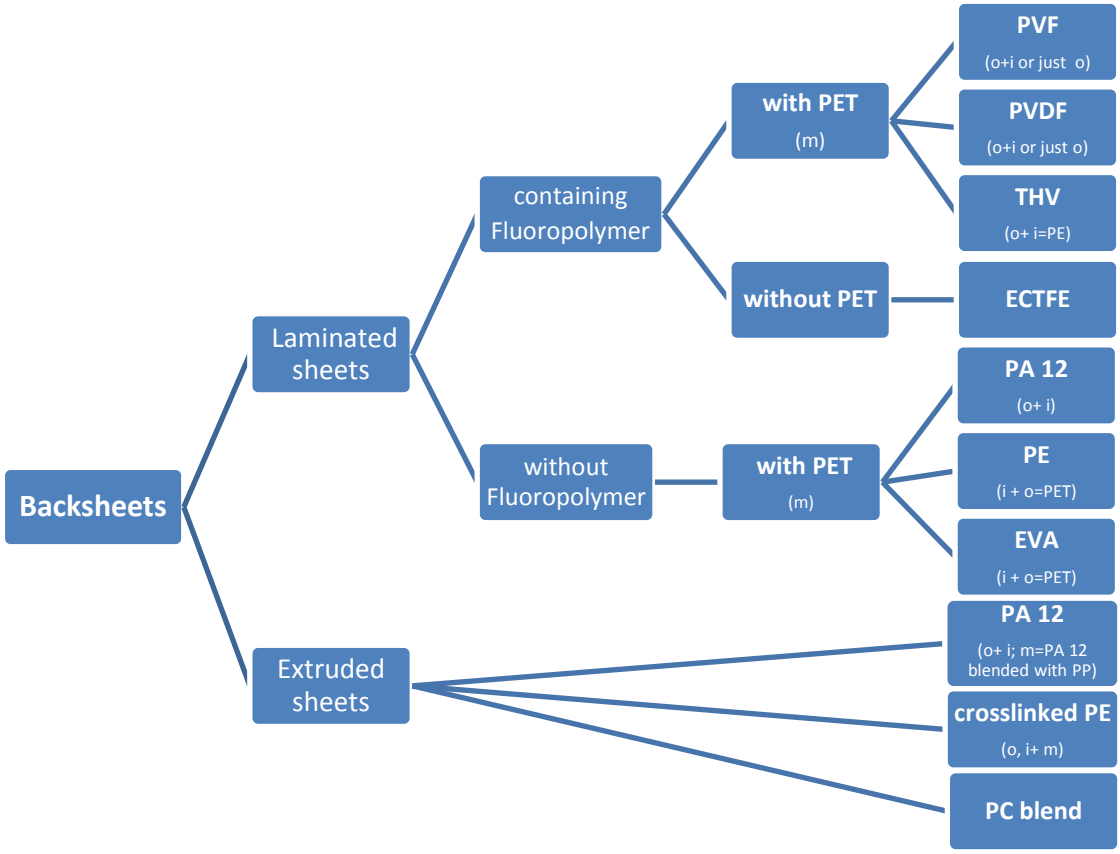

Figure 23: Overview on commercial available backsheets classified by polymeric components; o=outer layer (air side), i=inner layer (encapsulant side), m=middle layer

1.4 Quality and reliability of c-Si PV modules

The first terrestrial PV module from 1955 built at Bell laboratories was removed from service just 5 months after outdoor installation [36]. After that the next big step in module development started in the mid-1970s with large government programs in the USA (initiator power crisis in the early 70s) and the growing interest in the use of PV by large professional bodies for remote area telecommunications, particularly in Australia. It resulted in the development of much more reliable modules. Life targets of already 15 years were for example claimed from Philips in 1976 for their module BPX 47A, but still until the mid-1990s 10 years warranties were the standard [36].

Nowadays, about 60 years later, PV module manufacturer warrant operational lifetimes of at least 20 years over which the total yield loss may not exceed 20 % [53] [89]. Otherwise they wouldn`t be competitive on the market [53]. PV Modules have to withstand many environmental influences during their (expected) lifetime. All these factors like for example the temperature cycles between day and night, incoming irradiance with its warm-up of the modules or the UV-light harming the polymers inside etc. will have to more or less extent an influence on the PV module performance and reliability (all impacts are listed in Figure 24).

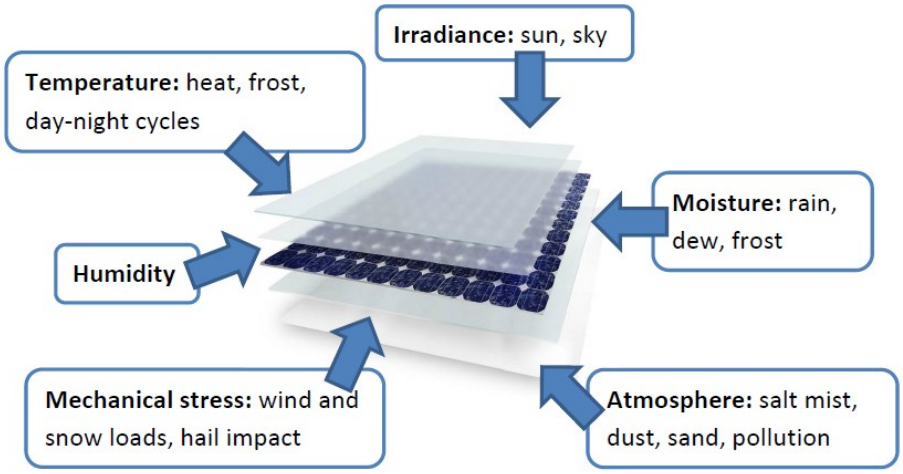

Figure 24: Various environmental impacts on a PV module during application

Jordan et al. gave a review in 2013 on a large number of reports on degradation rates (yield losses) of PV modules. For c-Si technology the average degradation was

0.7 %/year with a median of 0.5 %/year (for 1751 tested modules) [89]. Nevertheless to reduce the costs and enhance the competitiveness of photovoltaic technologies, the reliability and service life time of PV modules has to be improved. The improvements can only be done if there is knowledge of occurring failures in field operation to initiate subsequent, meaningful PV module optimization. In the following a short overview about detected failure mechanisms will be given. Therein a failure by definition is an effect that degrades the module power or creates a safety issue for a PV module.

1.4.1 PV module failure mechanisms in the field

Typically failures of PV modules are divided into the following three categories: infant-failures, midlife-failures and wear-out-failures. The failure rate over time is given in Figure 25. Most failures occur in the beginning life of a module (infant mortality). Midlife failures are catastrophic failures due external impacts like e.g. hail-storms. Most of the PV modules go through the wear out scenario. The failures therein can be attributed to the degradation of the used materials. Typical examples for all three categories are given in the following.

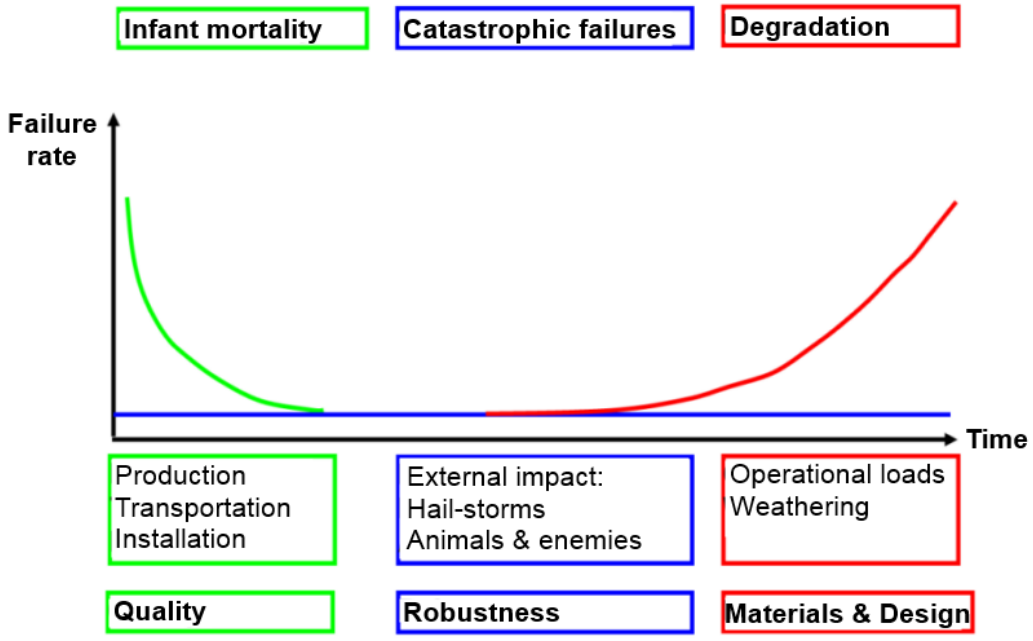

Figure 25: Failure rate over the life-time of a PV module [90].

Flawed PV modules fail quickly in the beginning of their working life. They dramatically impact the costs of the module manufacturer and the installer because they are responsible for these failures [25]. The biggest failure rates therein are attributed to optical losses (20 %), power loss and failures within the J-box and cables with 19 % (see Figure 28 a)). While most failures can be attributed to the manufacturer, failures like glass breakage and/or transport damage can be related to an incorrect handling of the installer [25] [91] (see also Figure 26). However, for the initial failure mechanisms some parts in optical failures (20 %), delamination (5 %) and maybe of the unknown defects (6 %) can be attributed to failures due to polymeric materials.

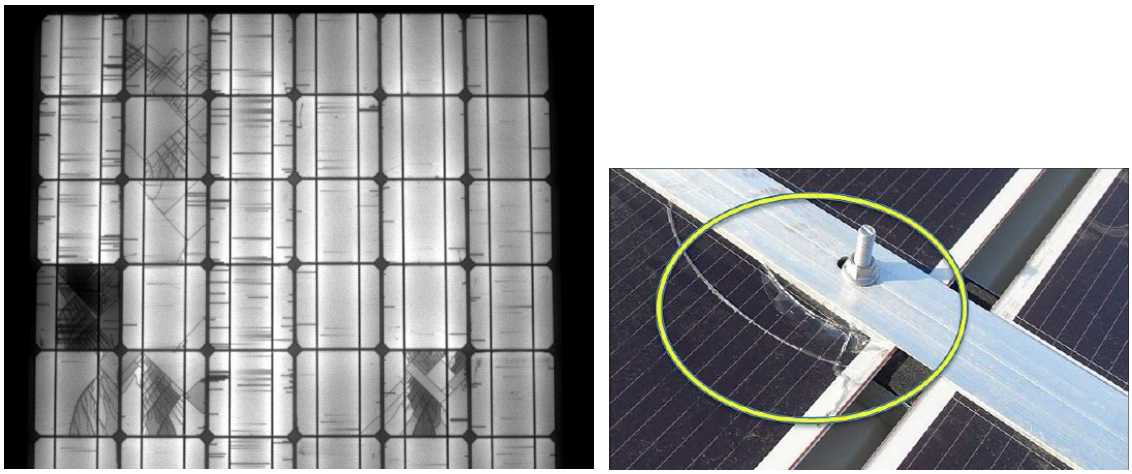

Figure 26: Electroluminescence image of cells with microcracks within a PV module due to inadequate handling during transport [91] (left side); Glass breakage caused by to tight screws [25] (right side)

Failures occurring in the midlife of PV modules (about 8 years of application) are described e.g. in a study of DeGraaff [92] and, in relation to backsheets, from Gambogi [93] [94]. In DeGraaffs study two percent of the PV modules do not meet the manufacturer's warranty after 8 years of operation. For these two percent the study shows a quite high rate of defect interconnections in the module (36 %) and failures due to glass breakage (33 %) (see Figure 28 b) and Figure 27). The failure rate attributed to the encapsulation and backsheet with 9 % is the lowest [92]. Gambogi reported from multiple problems exhibited with backsheets including cracking, delamination and yellowing [93] [94].

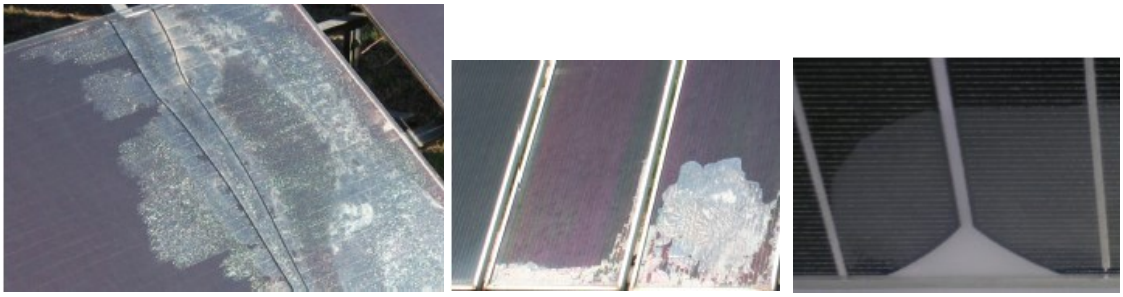

Figure 27: Examples for glass breakage and delaminations in PV modules [95]

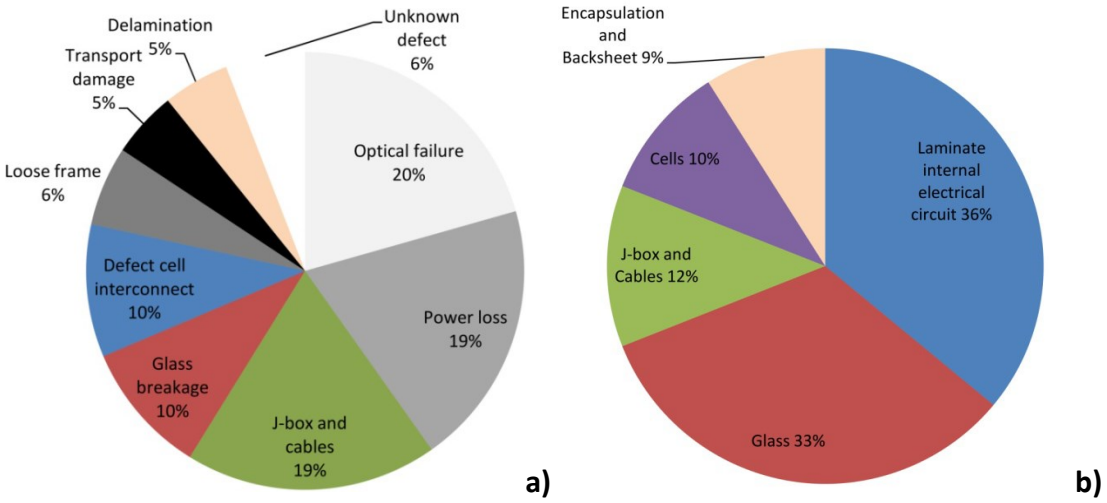

Figure 28: **a)** Failure rates due to customer complaints in the first two years after delivery. The rate is given relative to the total number of failures. The PV modules are delivered by a German distributor in the years 2006-2010 [96] [25]. The statistic is based on a total volume of approximately 2 million delivered PV modules.

b) Field study of PV module failures found for various PV modules of 21 manufacturers installed in the field for 8 years [92] [25]. The rate is given relative to the total number of failures. Approximately 2% of the entire fleet failed after 8 years (do not meet the manufacturer's warranty).

Most of the PV modules go through the wear out scenario [25] [89]. This scenario is the base for the best case yield analysis and determines therewith the cost efficiency of a well operating PV module. Wear out failures occur at the end of the working lifetime of PV modules. The working life of a PV module ends if a safety problem occurs or the PV module power drops under a certain level, which is typically defined between 80 % and 70 % of the initial power rating [25]. Failure mechanisms which are reported from PV modules after 15 years or more at the end of their working life are accorded to discoloration, delamination and cell part isolation due to cell cracks [25]. The reported failure mechanisms from the first grid connected PV system in Europe

(start 13 march 1982, Switzerland) for example are yellowing of encapsulant, backsheet delamination, broken cells, J-box oxidation and cable failures, hot spots, edge sealant penetration, delamination within the module and grid oxidation (see also Figure 29) [97]. Therefore most wear out failures, like yellowing of encapsulant and delamination of backsheet, can be attributed to polymers. One fact should be kept in mind, that the components changed since then. For examples the cell thicknesses changed from about 700 µm to 200 µm and lower, other additive formulations for encapsulants are used, backsheet configurations changed etc. This will also influence the wear out failures of today produced PV modules in future and suitable testing methods have to be improved, which will be discussed in the section Objectives.

Figure 29: Modules from the first grid connected PV system in Europe which show yellowing (left side) and grid oxidation (right side) [97]

1.4.2 Aging mechanisms of polymeric components in PV modules

Aging of polymers stands for changes in the mechanical and physical structure under time, which results in a shortened life-time during application. There are several classifications used, but in this work they will be separated in physical and chemical aging mechanisms.

Typical physical aging mechanisms are changes in the morphology like post-crystallization, re-crystallization, re-orientation and reduction of residual stresses or free volume. Also the outgassing or migration of volatile compounds as well as water absorption or swelling can induce physical aging [98]. Physical aging mechanisms are always a result of thermodynamic unstable states from too high cooling rates during

processing of polymers. The changes in physical structure are often in relation with changes in dimensions like shrinkage or expansion [48]. They have influence on the mechanical, thermo-mechanical and thermal properties of polymers.

Chemical aging mechanisms of polymers are related to changes on the molecular level. They can be classified in three principal groups: 1) changes of the molecular structure: decomposition of molecular weight, changes in the molecular weight distribution, generation of branching and crosslinking 2) generation of functional groups 3) split-off of low-molecular products: de-polymerization, split-off of side groups. Chemical aging mechanisms are a result of thermal decomposition, oxidation, photolysis, ozonolysis and hydrolysis. Besides the direct influence of temperature on aging it significantly enhances chemical reaction processes e.g. thermo-oxidation, hydrolysis [48]. Photolysis occurs always in combination with oxidation (photo-oxidation). Changes in the molecular structure often induce changes in the mechanical properties like e.g. the tensile strength or in optical properties like e.g. yellowing [48].

Factors that can induce aging of polymeric materials in a PV module includes the lamination parameters (temperature loads) and the parameters from outdoor application like temperature (general enhanced as well as the diurnal cycles), humidity, irradiance (especially UV light) and atmospheric gases like e.g. NH_3, SO_2, H_2S, NO_x, Cl_2, O_2 and O_3 (see exemplarily also Figure 24).

1.4.3 Influence of polymeric materials on PV module failure mechanisms

The above mentioned failure categories infant, midlife and wear out failures were discussed in relation to all kinds of occurring failures in field. Now the failures which are related to polymeric encapsulants will be summarized and discussed in detail.

Initial failures can be attributed to problems during production of the polymeric encapsulants and/or backsheets before PV module lamination or to wrong processing conditions during lamination. Results can be for example bubbles in the PV module, wrinkles in modules due to thermal expansion mismatches or delamination due to wrong temperatures at lamination [99] [100]. Hence, they will be seen right after

lamination, and so the concerned modules can be sorted out and the search for the failure source can begin.

For midlife and wear-out failures several failure mechanisms are reported. One of the most overt degradation mechanisms for PV modules is the discoloration of EVA or other encapsulants as well as those of the backsheets. Reported examples for yellowing of backsheets in PV modules from outdoor operation can be found in [101] [102] [94] [93] and for encapsulants in [92] [97] [28] [25] [103] [19]. Discoloration may become apparent to an observer before module current (therefore power production) can be confirmed to decrease [25]. Yellowing of backsheets, however, is reported to have no influence on the electrical performance of the modules, although it obviously indicates polymer degradation [103]. Hence this type of degradation is predominantly considered to be an aesthetic issue. However discoloration of EVA is expected to contribute <0.5 %/year of the ~0.8 %/year power loss that is commonly seen for Si modules [25] [89]. Investigations in the explanations for the yellowing of EVA in literature are predominant related to the additive formulation [25] [50] [104] [105] [106] [107] [108] [109]. EVA is usually formulated with i.e. UV absorber, hindered amine light stabilizer (HALS), antioxidants and crosslinking agents. Interactions between incompatible additives in the field may produce discoloring chromophore species or the depletion of additives (such as UV absorber) over time [25]. Klemchuk et al. found that discoloration is due to interactions between the peroxide curing agent and the UV absorbers or phosphite (antioxidant) compounds [50]. Peike et al. investigated in which way different additive formulations enhance the degradation of EVA under accelerated aging conditions [104] [109]. Therein the highly stabilized EVA films showed higher discoloration rates. It is claimed that the stabilizers resulted in lumophore and chromophore formation and not the EVA itself [104]. An antagonized effect to the discoloration due to the chromophores is the photobleaching (photo-oxidation) reaction in presence of air (oxygen) [107]. An example for yellowing in combination with photobleaching is shown in Figure 30. However due to the complexity of the system and permanent advancement of the additive formulations, a complete understanding of the degradation mechanisms of EVA in a PV module has

not been gained yet [47]. Investigations in the yellowing of other encapsulants are rare [47] [61]. This can maybe attributed to their low market share, but also to a less tendency to build chromophores. Newer approaches correlate the permeation properties of backsheets with the yellowing of EVA or other encapsulants. In [47] the influence of the laminate combination of encapsulant/backsheet was investigated under different accelerated aging conditions. The permeation properties, the water vapor transmission rate (WVTR) and oxygen transmission rate (OTR), were on average higher for the encapsulants than for backsheets. Therefore it is highly relevant to choose the right combination of e.g. a backsheet with high OTR with an encapsulant which tends to discoloration under UV irradiation and a backsheet with low WVTR with an encapsulant susceptible to hydrolysis [47].

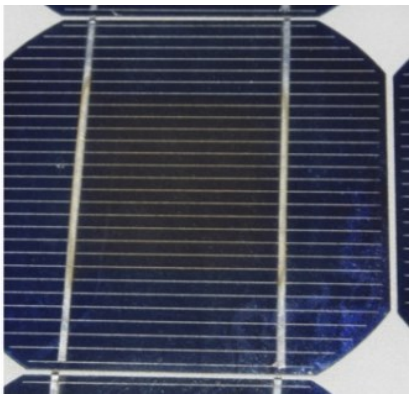

Figure 30: Slightly browned EVA in the center of a multicrystalline Si-cell, with photo-bleaching at the edges of the cell due to presence of oxygen [25]

Delamination can occur between the boundary surfaces of glass to encapsulant, encapsulant to solar cell, encapsulant to backsheet and within the layers of the backsheet (see e.g. Figure 31) [97] [103] [110] [111] [25] [19]. There are several issues that have to be taken into account. When delamination occurs between the encapsulant and the glass or cell surface an optical decoupling decreases the power output, because light will be reflected on the boundaries and therefore not able to reach the solar cell. Another issue is the disclosure for new pathways of water vapor and oxygen, which can lead to corrosion of the solar cell surface (ARC) and interconnectors as well as to degradation mechanisms in the polymers like hydrolysis or photo-oxidation [31] [112]. Delamination on the boundaries of encapsulant to the

backsheet may enable the possibility of exposure to active electrical components [25]. In a central, open area of the back, it will not present an immediate safety issue. An example is shown in Figure 31. That area would likely operate slightly hotter, but as long as the bubble isn't further disturbed and broken or expanded, the performance and safety concerns are minimal. However, if delamination of the backsheet occurs near a junction box or the edges of a module it may provide a direct pathway for liquid water to enter the module during rainfall or in presence of dew and cause a direct electrical pathway to ground [25] [110]. The adhesion between inorganic surfaces (like the ARC of the cell or glass) to the encapsulant is usually done with organic functional silanes [113]. Adhesion properties of the backsheets to the encapsulant are enhanced by various surface treatments [31]. Investigations about the adhesion properties under accelerated aging conditions of several backsheets to EVA can be found in [68] [70] [31]. Investigations about the temperature dependent adhesion of several encapsulants to backsheets or glass can be found in [65]. Delaminations within the layers of the backsheets are caused by adhesive (e.g. polyester-urethane compounds) degradation via hydrolysis [114] [115]. Delamination within backsheets seems to be enhanced if an aluminum barrier layer in between the polymeric materials is used [97].

Figure 31: Delamination of backsheet [25]

Reports about cracks in the backsheets of PV modules can be found in [103] [102] [94] [93]. This type of degradation is predominantly an aesthetic issue (see for example Figure 32). This degradation mechanism in the outdoor environment is related to photo-oxidation of the materials and not due to hydrolysis damage in [102]. However cracks in outer layers of backsheets results in a direct exposure of the inner layer to

the outdoor environment and can therefore enhance further degradation mechanism in the backsheets concerning the reliability of the module.

Figure 32: Module with cracking of the outer polyester layer [102]

Some failure and/or degradation mechanisms in modules are partly supported or enhanced due to the used polymeric materials. For example, as mentioned above, delamination within the polymeric layers can give new pathways for water vapor and so enhance corrosion processes on metallic or cell surfaces within the module. Another issue is the often discussed production of acetic acid via polymeric degradation of EVA. Acetic acid formation in EVA as a product of thermal or photo-thermal degradation has been described in [116] [28] [51] [104] [23]. The schematic reaction mechanism is shown in Figure 33. The EVA formulation plays a major role in the amount of acetic acid produced. Since acetic acid is a common agent in polymer processing it may also be found in acetic acid free encapsulants [23]. The acid has corrosive effects on interconnectors and cell metallization, especially copper (used in interconnectors) is very sensitive towards corrosion. Usually the solder material should protect the copper core of the interconnector, but it is may not compact enough. The metallization corrosion leads to an increased series resistance and therefore losses in module performance [47]. A “breathable” backsheet will not support the out-diffusion through the module as the acetic acid diffusion within EVA is by far too slow [23].

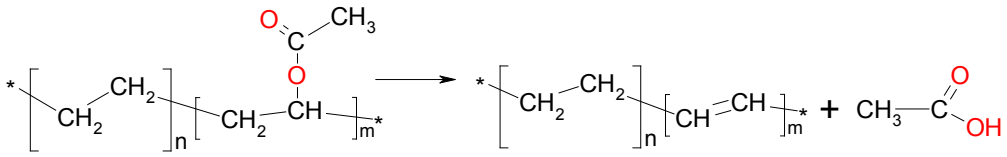

Figure 33: Schematic reaction mechanism of deacetylation of EVA

Another failure cause in c-Si PV modules is the potential induced degradation (PID) effect, which was first reported in 2007 [117] [25]. Therein high system voltages cause leakage currents through the glass cover and the encapsulation material (see also Figure 34) [22]. The resulting electrical potential between frame and cells causes a detrimental effect on power output [117]. There are several contributing factors identified in literature [117] [118] [22] [119] [120]. For example the movement of positive ions (Na^+) from glass to the ARC (SiN) of the cells (modules with cells without ARC show no PID degradation) causing the leakage current. Another example concerns the encapsulant. As the sodium from the glass has to move through the encapsulant it was shown that there is definitive an influence and with the choice of a suitable material the leakage current can be minimized or even inhibited. EVAs with high volume resistivity guarantee strong PID resistance [121]. The volume resistivity can be enhanced via a lower VA ratio and special coagent loadings [122]. High temperatures reduce the resistivity of EVA and seem therefore to be a critical factor [121]. Other encapsulants based upon ethylene copolymers with high volume resistivity and lower water vapor transmission rates (WVTR) show further improvements of resistance to PID effects [120].

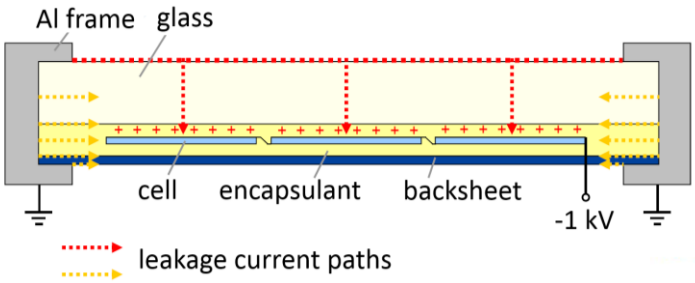

Figure 34: Schematic representation of PID of modules. High system voltages cause leakage currents through the glass cover and the encapsulation material [22]

A new polyolefin based encapsulant, introduced 2013 from the Austrian company Isovoltaic, is claimed to inhibit PID effects in modules. It was assumed that it is due to

no production of acetic acid, in respect to EVA, which may not ease the transport of Na^+ to the cells [61]. Ionomers were also identified to suppress the PID effect, but the required thickness seems not to be cost-efficient [123]. Another approach is the use of a thin ionomer layer (100 µm) between the front glass and EVA [123] [124]. It is claimed to fully suppress the PID effect by capturing the ions [124].

Snail Tracks are a visible effect and it is a discoloration of the silver paste of the front metallization of solar cells (see also Figure 35). In a PV module the effect looks like a Snail Track and it occurs at the edge of the solar cell and along usually invisible small cell cracks. The discoloration itself is reported to have no influence on the performance of the PV module. But the visualized cell cracks can reduce the PV module power. In concern of the polymeric materials the choice of EVA and backsheet type seems to be important for the Snail Track occurrence [25] [125]. In Meyer et al. water vapor coming through the backsheet is claimed to dissolve silver particles which migrate into the encapsulation on top of the grid finger, where a chemical reaction within the encapsulation foil results in the typical observed coloring [126].

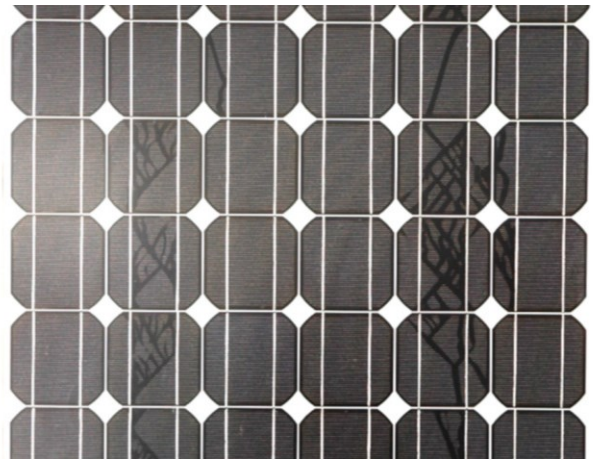

Figure 35: Module with Snail Tracks [125]

1.5 Structure and objectives of this work

The work presented in this dissertation was performed within the project *"Analysis of PV aging" (FFG Nr. 829918, 4.Call "Neue Energien 2020", Klima- und Energiefonds)* in cooperation with OFI Technology and Innovation GmbH (Vienna) and AIT Austrian Institute of Technology GmbH (Vienna). The main objectives of the dissertation can be derived from project aims and summarized as follows:

The fast-paced photovoltaic market development requires frequently adapted production processes to enable mass production and innovative, cost-efficient materials as well as shorter product development times. Thus, the proposed project aimed at characterizing materials in photovoltaic modules with analytical techniques in order to enlighten the chemical and physical aging processes which allowed for an early prediction of the potential life time of modules.

Under operation photovoltaic modules are exposed to various impact/climatic factors (like temperature, humidity, UV radiation, wind and snow....). Thus, another priority of the project was to analyze the (accelerated) aging behavior of polymeric materials used in PV modules. Therein, the accelerated aging was applied with a combination of various environmental impact factors. Innovative analytical methods were used to characterize the materials before, during and after the run of the aging tests. Special emphasis was put on detecting correlations between chemical and physical changes in the material/material combinations. The direct comparison of the aging of isolated materials and of materials incorporated in modules allowed for drawing essential conclusions on material incompatibilities.

Additional within the project "*Analysis of PV aging*" the impact of water vapor and oxygen on the modules was analyzed and evaluated. Especially the influence of external factors like temperature, UV-radiation and humidity on the permeation behavior of oxygen and water vapor through the polymeric materials was in the focus of interest.

In agreement with the general objectives, this dissertation is divided into the following main chapters with its respective objectives:

Chapter II concerns about influences of processing parameters on the material behavior of polymers in PV modules. Special emphasis was given on two aspects. On the one hand the influence of processing conditions of several encapsulant films on PV module lamination was investigated. On the other hand changes in the mechanical behavior of a backsheet, induced by PV module lamination, were investigated. The results of this chapter can be addressed to investigations in short-term reliability of PV modules.

Chapter III focuses on the accelerated aging behavior of backsheets. Therein two kinds of accelerated aging methods were used. For both methods a direct comparison of single and module laminated backsheets was carried out. It allowed for essential conclusions on material interactions and the influence of PV module microclimate on it. The two applied accelerated aging conditions were enhanced temperature and humidity (DH; 85°C/ 85 % RH; 2000 h) or additional irradiation (Climate; 50°C, 80 % RH and 1000 W/m²; 1000 h). The results of this chapter can be addressed to investigations in long-term reliability of PV modules.

Chapter IV concerns about the permeation behavior of backsheets. The oxygen transmission rates (OTR) and water vapor transmission rates (WVTR) of five different backsheets were investigated in their initial and accelerated aged state. Additional, the temperature dependent permeation behavior was evaluated.

1.6 References

[1] http://www.weltbevoelkerung.de/start.html, World Population End of 2014; access 26.12.2014.

[2] United Nations, World Population Prospects: The 2012 Revision, Key Findings and Advance Tables: Working Paper No. ESA/P/WP.227, United Nations, Department of Economic and Social Affairs, Population Division, 2013.

[3] IEA, International Energy Agency, Key World Energy Statistics 2014.

[4] REN21. 2014, Renewables 2014 Global Status Report (Paris: REN21 Secretariat).

[5] H. Fechner, Photovoltaik International, 12. Österreichische PV-Tagung, Linz.

[6] International Renewable Energy Agency, Renewable Power Generation Costs in 2014 (2015).

[7] G. Razongles, Photovoltaic Key Figures, IEA Task 13 Meeting, Leoben, 2015.

[8] IEA International Energy Agency, TRENDS 2014 IN PHOTOVOLTAIC APPLICATIONS; Report IEA-PVPS T1-25:2014.

[9] P. Biermayr, M. Eberl, M. Enigl, H. Fechner, C. Kristöfel, K. Leonhartsberger, F. Maringer, S. Moidl, C. Strasser, W. Weiss, M. Wörgetter, Innovative Energietechnologien in Österreich Marktentwicklung 2013, Bundesministerium für Verkehr, Innovation und Technologie, 2014.

[10] R.M. Swanson, A vision for crystalline silicon photovoltaics, Progress in Photovoltaics: Research and Applications 14 (2006) 443–453.

[11] Solarbuzz, Solarbuzz Quarterly - Current status of global supply/demand balance of solar industry, download 27.12.2014.

[12] NREL National Renewable Energy Laboratory, Best Research-Cell Efficiencies 2014. free download: http://www.nrel.gov/ncpv/.

[13] Solarpraxis AG, Technology: Striving for increased efficiency, in: RENI, PV Power Plants 2011, Industry Guide.

[14] K. Mertens, Photovoltaik: Lehrbuch zu Grundlagen, Technologie und Praxis, Hanser, München, 2011.

[15] A. Goetzberger, B. Voß, J. Knobloch, Sonnenenergie: Photovoltaik, 2nd ed., Teubner Verlag, 1997.

[16] E. Cuddihy, C. Coulbert, A. Gupta, R. Liang, Flat-Plate Solar Array Project Final Report: Volume VII: Module Encapsulation, JPL Publication (1986).

[17] D.L. King, M.A. Quintana, J.A. Kratochvil, D.E. Ellibee, B.R. Hansen, Photovoltaic Module Performance and Durability Following Long-term Field Exposure, Progress in Photovoltaics: Research and Applications 8 (2000) 241–256.

[18] N. Lenck, Polymere Materialien im Modul, in: 12. Österreichische PV-Tagung, Linz, Austria, 2014.

[19] K.-A. Weiß, Neuartige Polymertechnologien für die Photovoltaik, Linz, Austria, 2014.

[20] G. Stollwerck, H. Ehbing, A. Hoffmann, H. Peerlings, Kunststoff-Verkapselungen für Solarmodule, Kunststoffe (2004).

[21] U. Eitner, Thermomechanics of photovoltaic modules. Doctor thesis, Martin-Luther-Universitaet Halle-Wittenberg, 2011.

[22] H. Nagel, Possible cause for PID of crystalline silicon solar cells, in: PV Module Reliability Workshop, Lugano, Switzerland, 2012.

[23] U. Weber, R. Eiden, C. Strubel, T. Soegding, M. Heiss, P. Zachmann, K. Nattermann, H. Engelmann, A. Dethlefsen, N. Lenck, Acetic Acid Production, Migration and Corrosion Effects in Ethylene-Vinyl-Acetate- (EVA-) Based PV Modules, 2012.

[24] S. Nieland, C. Loebner, K.-P. Goerbing, A. Lawerenz, Using microelectronic know-how for solar cell interconnection by adhesive bonding, in: 27th European Photovoltaic Solar Energy Conference and Exhibition, Frankfurt, Germany, 2012.

[25] IEA Task 13, Review on Failures of PV Modules: Report IEA-PVPS T13-01:2013, 2013.

[26] I. Hinz, S.-H. Schulze, F. Barche, M. Schak, F. Wenger, Characterization of electrical conductive adhesives (ECA) for the photovoltaic-industry, in: 27th European Photovoltaic Solar Energy Conference and Exhibition, Frankfurt, Germany, 2012.

[27] M. Daichi, A. Higuchi, A new interconnecting material for Solar Cells with high-potential on busbar-less solar cells, in: 28th European Photovoltaic Solar Energy Conference and Exhibition, Paris, France, 2013.

[28] A.W. Czanderna, F.J. Pern, Encapsulation of PV modules using ethylene vinyl acetate copolymer as a pottant: A critical review, Solar Energy Materials and Solar Cells (1996) 101–181.

[29] W. Mühleisen, L. Neumaier, A. Kogler, A. Plösch, M. Pedevilla, J. Scheurer, R. Messmer, C. Hirschl, Systematic Experimental Evaluation of Encapsulation Loss and Gain in PV Modules, in: 28th European Photovoltaic Solar Energy Conference and Exhibition, Paris, France, 2013.

[30] G. Oreski, G.M. Wallner, R.W. Lang, Ageing characterization of commercial ethylene copolymer greenhouse films by analytical and mechanical methods, Biosystems Engineering 103 (2009) 489–496.

[31] G.J. Jorgensen, K. M. Terwilliger, J. A. DelCueto, S. H. Glick, M. D. Kempe, J. W. Pankow, F. J. Pern, T. J. McMahon, Moisture transport, adhesion, and corrosion protection of PV module packaging materials, Solar Energy Materials & Solar Cells 90 (2006) 2739–2775.

[32] R.F.M. Lange, Y. Luo, R. Polo, J. Zahnd, The lamination of (multi)crystalline and thin film based photovoltaic modules, Progress in Photovoltaics: Research and Applications 19 (2011) 127–133.

[33] M. Pander, S.-H. Schulze, M. Ebert, Mechanical modeling of electrically conductive adhesives for photovoltaic applications, in: 29th European Photovoltaic Solar Energy Conference and Exhibition, Amsterdam, Netherlands, 2014.

[34] R. Ebner, M. Schwark, B. Kubicek, G. Ùjvàri, W. Mühleisen, C. Hirschl, L. Neumaier, M. Pedevilla, J. Scheurer, A. Plösch, A. Kogler, W. Krumlacher, H. Muckenhuber, Increased power output of crystalline silicon PV modules by alternative interconnection applications, in: 28th European Photovoltaic Solar Energy Conference and Exhibition, Paris, France, 2013.

[35] C. Hirschl, L. Neumaier, W. Mühleisen, M. DeBiasio, G. Oreski, A. Rauschenbach, G.C. Eder, B.S. Chernev, M. Kraft, Post-Crosslinking in photovoltaic modules under different conditions, in: 29th European Photovoltaic Solar Energy Conference and Exhibition, Amsterdam, Netherlands, 2014.

[36] M.A. Green, Silicon Photovoltaic Modules: A Brief History of the First 50 Years, Progress in Photovoltaics: Research and Applications 13 (2005) 447–455.

[37] I. Yilgor, E. Yilgor, Thermal stabilities of end groups in hydroxyalkyl terminated polydimethylsiloxane oligomers, Polymer Bulletin 40 (1998) 525–532.

[38] B.M. Ketola, C. Shirk, P. Griffith, G. Bunea, Demonstration of the benefits of silicone encapsulation of PV modules in a large scale outdoor arry, in: 25th European Photovoltaic Solar Energy Conference and Exhibition, Valencia, Spain, 2010.

[39] S. Ohl, G. Hahn, Increased Internal Quantum Efficiency of encapsulated solar cells by using two-component silicone as encapsulant material, 23rd European Photovoltaic Solar Energy Conference and Exhibition, Valencia, Spain, 2008.

[40] M.D. Kempe, Overview of Scientific Issues Involved in Selection of Polymers for PV Applications: Preprint, in: 37th IEEE Photovoltaic Specialists Conference, Seattle, USA, 2011.

[41] H. Dominginhaus, P. Eyerer, P. Elsner, T. Hirth, Kunststoffe: Eigenschaften und Anwendungen, Springer, Berlin Heidelberg, 2007.

[42] F. de Buyl, Silicone sealants and structural adhesives, International Journal of Adhesion and Adhesives 21 (2001) 411–422.

[43] B. Ketola, K. McIntosh, A. Norris, M. Tomalia, Silicones for Photovoltaic Encapsulation, in: 23rd European Photovoltaic Solar Energy Conference and Exhibtion, Valencia, Spain, 2008.

[44] F. Ensslen, Zum Tragverhalten von Verbund-Sicherheitsglas unter Berücksichtigung der Alterung der Polyvinylbutyral-Folie. Doctor Thesis, Bochum, 2005.

[45] S. Muguruma, T. Mukose, H. Yasuda, A. Masuda, H. Shibata, S. Niki, Newly Developed PVB for High Durability and Low Cost Thin Film PV Modules, in: 28th

European Photovoltaic Solar Energy Conference and Exhibition, Paris, France, 2013.

[46] Kuraray Europe GmbH, Solar: Modul-Optimierung mit PVB Folie - Solartechnik in Perfektion, 2012.

[47] C. Peike, P. Hülsmann, M. Blüml, P. Schmid, K.-A. Weiß, M. Köhl, Impact of Permeation Properties and Backsheet-Encapsulant Interactions on the Reliability of PV Modules, ISRN Renewable Energy 2012 (2012) 1–5.

[48] G.W. Ehrenstein, S. Pongratz, Beständigkeit von Kunststoffen, 1st ed., Carl Hanser Verlag, Munich, 2007.

[49] I. Hintersteiner, L. Sternbauer, S. Beissmann, W.W. Buchberger, G.M. Wallner, Determination of stabilisers in polymeric materials used as encapsulants in photovoltaic modules, Polymer Testing 33 (2014) 172–178.

[50] P. Klemchuk, E. Ezrin, G. Lavigne, W. Holley, J. Galica, S. Agro, Investigation of the degradation and stabilization of EVA-based encapsulant in field-aged solar energy modules, Polymer Degradation and Stability (1997) 347–365.

[51] M.D. Kempe, G.J. Jorgensen, K.M. Terwilliger, T.J. McMahon, C.E. Kennedy, T.T. Borek, Acetic acid production and glass transition concerns with ethylene-vinyl acetate used in photovoltaic devices, Solar Energy Materials and Solar Cells 91 (2007) 315–329.

[52] E. Baur, J.G. Brinkman, T.A. Osswald, E. Schmachtenberg, Saechtling Kunststoff Taschenbuch, 30th ed., Carl Hanser, Munich, 2007.

[53] C. Hirschl, M. Biebl–Rydlo, M. DeBiasio, W. Mühleisen, L. Neumaier, W. Scherf, G. Oreski, G. Eder, B. Chernev, W. Schwab, M. Kraft, Determining the degree of crosslinking of ethylene vinyl acetate photovoltaic module encapsulants—A comparative study, Solar Energy Materials and Solar Cells 116 (2013) 203–218.

[54] G. Oreski, Encapsulant materials and degradation effects-Requirements for new materials and research trends, in: IEA PVPS Task 13 Workshop at 29th PVSEC, Amsterdam, Netherlands, 2014.

[55] C. Schmid, J. Chapon, G. Kinsey, J. Bokria, J. Woods, Impact of high light transmission EVA-based encapsulant on the performance of PV modules, in: 27th

European Photovoltaic Solar Energy Conference and Exhibition, Frankfurt, Germany, 2012.

[56] G. Oreski, G.M. Wallner, Damp Heat induced physical ageing of PV encapsulation materials, in: 12th Intersociety Conference on Thermal and Thermomechanical Phenomena in Electronic Systems, Las Vegas, USA, 2010.

[57] K. Nakata, New Modified Ionomer Encapsulant Developments Offer Potential Benefits to Module Makers, in: 26th European Photovoltaic Solar Energy Conference and Exhibition, Hamburg, Germany, 2011.

[58] A. Bennett, S.J. Bennison, A.H. C.H. Butler1, T.L. Nutter, C.A. Smith, S. Schleidt, Next generation ionomer encapsulants for low cost processing in glass—glass photovoltaic modules, in: 26th European Photovoltaic Solar Energy Conference and Exhibtion, Hamburg, Germany, 2011.

[59] G. Oreski, Polar Ethylene Copolymer Films for Solar Applications - Optical Properties and Aging Behavior. Doctor thesis, Leoben, 2008.

[60] D. Richard, EVA and Tedlar still dominate: Market survey on encapsulation materials, Photon International, August 2010, 236–259.

[61] A.-J. Steiner, W. Krumlacher, H. Muckenhuber, M. Plank, K. Sundl, E. Ziegler, New Thermoplastic, Non-Curing Encapsulation Material for PV Module Applications, in: 28th European Photovoltaic Solar Energy Conference and Exhibition, Paris, France, 2013.

[62] I.F. Martínez, New encapsulant options for MWT PV cells, in: 5th Workshop on MWT solar cell and module technology, Freiburg, Germany, 2013.

[63] G. Oreski, G.M. Wallner, P. Randel, Characterization of silicon based thermoplastic elastomer for PV encapsulation, in: 23rd European Photovoltaic Solar Energy Conference and Exhibition, Valencia, Spain, 2008.

[64] S.-H. Schulze, M. Ehrich, M. Ebert, J. Bagdahn, Mechanical behavior and lamination issues of solar modules containing elastomeric and amorphous encapsulates, in: 25th European Photovoltaic Solar Energy Conference and Exhibition, Valencia, Spain, 2010.

[65] G. Oreski, G. Pinter, Comparative study of the temperature dependent delamination behavior of four solar cell encapsulants to glass and backsheet-laminate, in: 26th European Photovoltaic Solar Energy Conference and Exhibition, Hamburg, Germany, 2011.

[66] M.D. Kempe, D.C. Miller, J.H. Wohlgemuth, S.R. Kurtz, J.M. Moseley, A Field Evaluation of the Potential for Creep in Thermoplastic Encapsulant Materials, in: 38th IEEE Photovoltaic Specialists Conference, Austin, USA, 2012.

[67] G. Stollwerck, W. Schoeppel, A. Graichen, C. Jaeger, Polyolefin Backsheet and New Encapsulant Supress Cell Degradation in the Module, in: 28th European Photovoltaic Solar Energy Conference and Exhibition, Paris, France, 2013.

[68] G. Oreski, Untersuchung des Delaminationsverhaltens von Folienverbunden für die Einkapselung von PV-Modulen. Master thesis, Montanuniversitaet Leoben, 2004.

[69] H. Teng, Overview of the Development of the Fluoropolymer Industry, applied sciences 2 (2012) 496–512.

[70] G. Oreski, G.M. Wallner, Delamination behaviour of multi-layer films for PV encapsulation, Solar Energy Materials and Solar Cells 89 (2005) 139–151.

[71] G.D. Barber, G.J. Jorgensen, K. Terwilliger, S.H. Glick, J. Pern, T.J. McMahon, New Barrier Coating Materials for PV Module Backsheets: Preprint, in: 29th IEEE Photovoltaic Specialists Conference, New Orleans, USA, 2002.

[72] Y. Bormashenko, R. Pogreb, O. Stanevsky, E. Bormashenko, Vibrational spectrum of PVDF and its interpretation, Polymer Testing 23 (2004) 791–796.

[73] T. Boccaccio, A. Bottino, G. Capannelli, P. Piaggio, Characterization of PVDF membranes by vibrational spectroscopy, Journal of Membrane Science 210 (2002) 315–329.

[74] G. Stollwerck, W. Schoeppel, A. Graichen, C. Jaeger, M. Kollesch, Polyolefin Backsheet Protects Solar Modules for a Life Time, in: 28th European Photovoltaic Solar Energy Conference and Exhibition, Paris, France, 2013.

[75] K. Looney, B. Brennan, Modelling the correlation between DHT and true field lifetimes for PET based backsheets, in: 29th European Photovoltaic Solar Energy Conference and Exhibition, Amsterdam, Netherlands, 2014.

[76] C. Warren, Foiled again: Market survey on encapsulation materials, Photon International, September 2009, 292–309.

[77] E.R. Parnham, K. Forsyth, W.A. MacDonald, W.J. Brennan, PET Backsheets: The robust balance between performance and cost, in: Polymers in Photovoltaics, Cologne, Germany, 2014.

[78] J. Scheirs, Modern fluoropolymers: High performance polymers for diverse applications, Wiley, Chichester, New York, 1997.

[79] B. Hirschmann, G. Oreski, G. Pinter, Thermo-mechanical characterisation of fluoropolymer films for concentrated solar thermal applications, Solar Energy Materials and Solar Cells 130 (2014) 615–622.

[80] S. Rhee, J.L. White, Crystal Structure and Morphology of biaxially oriented polamide 12 films, Journal of Polymer Science: Part B: Polymer Physics 40 (2002) 1189–1200.

[81] G. Mikats (ISOVOLTAIC GMBH) WO 2011/066595 A1, 2010.

[82] F. Rummens (RENOLIT BELGIUM N.V.) WO 2011/009568 A1, 2010.

[83] Bayer MaterialScience AG, Makrofol DE 318 2-4 160001; Datasheet download: 15.01.2015.

[84] G. Stollwerck, E.-U. Reisner, K. Petzel-Maryniak, A. Seidel (Bayer MaterialScience AG) EP 2308679 A1, 2009.

[85] Eva Bittmann, Oliver Mayer, Marcus Zettl, Omar Stern (Eds.), Low Concentration PV With Polycarbonate, 2008.

[86] G. Oreski, W. Schoeppel, Degradation behavior and reliability of a novel multi-layer polyolefin backsheet film 3M ScotchShield 800 for PV encapsulation, in: 28th European Photovoltaic Solar Energy Conference and Exhibition, Paris, France, 2013.

[87] G. Stollwerck, W. Schoeppel, A. Graichen, C. Jaeger, M. Kollesch, Life Time Estimate of Solar Modules Polymeric Backsheets, in: 27th European Photovoltaic Solar Energy Conference and Exhibition, Frankfurt, Germany, 2012.

[88] G. Stollwerck, W. Schoeppel, A. Graichen, C. Jaeger, Polyolefin Backsheet and New Encapsulant Suppress Cell Degradation in the Module, in: 28th European Photovoltaic Solar Energy Conference and Exhibition, Paris, France, 2013.

[89] D.C. Jordan, S.R. Kurtz, Photovoltaic Degradation Rates- an Analytical Review, Progress in Photovoltaics: Research and Applications 21 (2013) 12–29.

[90] K.-A. Weiß, Alterung von Materialien für PV Module, in: Workshop Qualität und Zuverlässigkeit in der PV, Leoben, Austria, 2014.

[91] G. Winkler, Transport von PV-Modulen: Konzepte und Schäden, in: 8. Workshop "Photovoltaik-Modultechnik" TÜV Rheinland, Köln, Germany, 2011.

[92] D. DeGraaff, R. Lacerda, Z. Campeau, Degradation Mechanisms in Si Module Technologies Observed in the Field; Their Analysis and Statistics, in: Photovoltaic Module Reliability Workshop, NREL, Golden, USA, 2011.

[93] W.J. Gambogi, H. Yushi, J.G. Kopchick, T. Felder, S.W. MacMaster, A.Z. Bradley, B. Hamzavytehrany, B.-L. Yu, K.M. Stika, J.T. Trout, L. Garreau-Iles, O. Fu, H. Hu, Assessment of PV Module Durability Using Accelerated and Outdoor Performance Analysis and Comparisons, in: 40th IEEE Photovoltaic Specialists Conference, Denver, USA, 2014.

[94] W.J. Gambogi, J.G. Kopchick, T.C. Felder, S.W. MacMaster, A.Z. Bradley, B. Hamzavy, E.E. Kathmann, T.J. Stika, T.J. Trout, L.G. Garreau-Iles, T. Sample, Backsheet and Module Durability and Performance and Comparison of Accelerated Testing to Long Term Fielded Modules, in: 28th European Photovoltaic Solar Energy Conference and Exhibition, Paris, France, 2013.

[95] M. Köhl, Grundlegende Untersuchungen zur Gebrauchsdaueranalyse von Photovoltaik-Modulen. Doctor thesis, Hagen, 2011.

[96] A. Richter, Schadensbilder nach Wareneingang und im Reklamationsfall, in: 8. Workshop Photovoltaik-Modultechnik TÜV Rheinland, Cologne, Germany, 2011.

[97] T. Friesen, PV modules failure modes observed in real use and long term exposure, in: PV Module Reliability Workshop, Berlin, Germany, 2011.

[98] G.W. Ehrenstein, Alterung und Stabilisierung, in: G.W. Ehrenstein (Ed.), Polymer Werkstoffe, Carl Hanser Verlag GmbH & Co. KG, 2011, pp. 275-291.

[99] L.-E. Perret-Aebi, H.-Y. Li, R. Théron, G. Roeder, Y. Luo, T. Turlings, R. F. M. Lange, C. Ballif, Insight on EVA lamination process: Where do the bubbles come from?, in: 25th European Photovoltaic Solar Energy Conference and Exhibition, Valencia, Spain, 2010.

[100] G. Oreski, M. Knausz, G. Pinter, C. Hirschl, G.C. Eder, Advanced methods for discovering PV module process optimization potentials and quality control of encapsulation materials, in: 28th European Photovoltaic Solar Energy Conference and Exhibition, Paris, France, 2013.

[101] J. Coello, C. Lopez, F. Cornacchia, Impact of the EVA Yellowing of 20 Commercial Modules on Performance and Durability, in: 25th European Photovoltaic Solar Energy Conference and Exhbition, Valencia, Spain, 2010.

[102] W.J. Gambogi, Y. Heta, K. Hashimoto, J.G. Kopchick, T. Felder, S.W. MacMaster, A. Bradley, B. Hamzavytehrany, L. Garreau-Iles, T. Aoki, K.M. Stika, T.J. Trout, T. Sample, A Comparison of Key PV Backsheet and Module Performance from Fielded Module Exposures and Accelerated Tests, IEEE Journal of Photovoltaics 4 (2014) 935–941.

[103] T. Sample, Failure modes observed in real use and long-term exposure, in: PV Module Reliability Workshop, Berlin, Germany, 2011.

[104] C. Peike, L. Purschke, K.-A. Weiß, M. Köhl, M.D. Kempe, Towards the origin of photochemical EVA discoloration, in: 39th Photovoltaic Specialists Conference IEEE, Tampa Bay, USA, 2013.

[105] F.J. Pern, A.W. Czanderna, Characterization of ethylene vinyl acetate (EVA) encapsulant: Effects of thermal processing and weathering degradation on its discoloration, Solar Energy Materials and Solar Cells (1992) 3–23.

[106] F. J. Pern, Factors that affect the EVA encapsulant discoloration rate upon accelerated exposure, Solar Energy Materials & Solar Cells (1996) 587–615.

[107] F.J. Pern, Factors that affect the EVA encapsulant discoloration rate upon accelerated exposure, Solar Energy Materials and Solar Cells (1996) 587–615.

[108] S.I.N. Ayutthaya, J. Wootthikanokkhan, Investigation of the photodegradation behaviors of an ethylene/vinyl acetate copolymer solar cell encapsulant and effects of antioxidants on the photostability of the material, Journal of Applied Polymer Science 107 (2008) 3853–3863.

[109] A. Beinert, C. Peike, I. Dürr, M. Kempe, K.-A. Weiß, The Influence of the Additive Composition on the Photochemical Degradation of EVA, in: 29th European Photovoltaic Solar Energy Conference and Exhibition, Amsterdam, Netherlands, 2014.

[110] J.H. Wohlgemuth, M.D. Kempe, Equating Damp Heat Testing with Field Failures of PV Modules, in: 39th Photovoltaic Specialists Conference IEEE, Tampa Bay, USA, 2013.

[111] N. Park, J. Jeong, B. Kang, D. Kim, The effect of encapsulant discoloration and delamination on the electrical characteristics of photovoltaic module, Microelectronics Reliability 53 (2013) 1818–1822.

[112] P. Hülsmann, K.-A. Weiß, M. Köhl, Temperature-dependent water vapour and oxygen permeation through different polymeric materials used in photovoltaic-modules, Progress in Photovoltaics: Research and Applications 22 (2012) 415–421.

[113] A. Ioannidis, Haftvermittler auf Basis organofunktioneller Silane. Company presentation EVONIK, Leoben, Austria, 2014.

[114] Y. Voronko, B.S. Chernev, G.C. Eder, Spectroscopic investigations on thin adhesive layers in multi-material laminates, Applied Spectroscopy 68 (2014) 584–592.

[115] Y. Voronko, G. Eder, B. Chernev, M. Knausz, G. Oreski, T. Koch, K. Berger, Analytical Evaluation of the Ageing Induced Changes of the Adhesive within Photovoltaic Backsheets, in: 28th European Photovoltaic Solar Energy Conference and Exhibition, Paris, France, 2013.

[116] C. Peike, T. Kaltenbach, K.-A. Weiß, M. Koehl, Non-destructive degradation analysis of encapsulants in PV modules by Raman Spectroscopy, Solar Energy Materials and Solar Cells 95 (2011) 1686–1693.

[117] M. Schütze, M. Junghänel, O. Friedrichs, B. Jäckel, R. Wichtendahl, J. Müller, P. Wawer, Untersuchung von PID bei Silizium PV Modulen, in: 8. Workshop Photovoltaik-Modultechnik TÜV Rheinland, Cologne, Germany, 2011.

[118] S. Pingel, Potential Induced Degradation (PID), in: Fraunhofer ISE: PV Module Reliability, Berlin, Germany, 2011.

[119] S. Koch, Potential Induced Degradation (PID) effects on crystalline solar modules, in: ATLAS® Technical Conference on Accelerated Ageing and Evaluation (ATCAE), Berlin, Germany, 2011.

[120] C. Reid, S.A. Ferrigan, J.I. Martinez, J.T. Woods, Contribution of PV Encapsulant Composition to Reduction of Potential Induced Degradation (PID) of Crystalline Silicon PV Cells, in: 28th European Photovoltaic Solar Energy Conference and Exhibition, Paris, France, 2013.

[121] C. Liciotti, M. Cardinali, J.D. Lavandera Antolin, Temperature dependence of encapsulant volumetris resistivity and influence on potential induced degradation of c-Si modules, in: 29th European Photovoltaic Solar Energy Conference and Exhibition, Amsterdam, Netherlands, 2014.

[122] S.A. Ferrigan, J.G. Bokria, K.B. Smith, Functionality of Vinyl Acetate in the Reduction of Potential Induced (PID) of Crystalline Silicon PV Cells, in: 29th European Photovoltaic Solar Energy Conference and Exhibition, Amsterdam, Netherlands, 2014.

[123] J. Kapur, A. Bennett, J. Norwood, B. Hamzavytehrany, I. Kueppenbender, Tailoring Ionomer Encapsulants as a low cost solution to potential induced degradation, in: 28th European Photovoltaic Solar Energy Conference and Exhibition, Paris, France, 2013.

[124] S.C. Pop, R. Schulze, X. Wang, B. Yuan, J. Kapur, K. Stika, C. Westphal, H. Antoniadis, A. Meisel, Ionomer-based PID-resistant encapsulant for PV modules,

in: 29th European Photovoltaic Solar Energy Conference and Exhibition, Amsterdam, Netherlands, 2014.

[125] M. Köntges, I. Kunze, V. Naumann, S. Richter, C. Hagendorf, Schneckenspuren, Snail Tracks, Worm Marks und Mikrorisse, in: 8. Workshop "Photovoltaik-Modultechnik" TÜV Rheinland, Cologne, Germany, 2011.

[126] S. Meyer, S. Timmel, U. Braun, C. Hagendorf, Polymer Foil Additives Trigger the Formation of Snail Trails in Photovoltaic Modules, Energy Procedia 55 (2014) 494–497.

CHAPTER II:

INVESTIGATIONS IN SHORT-TERM AGING PROCESSES

2 Introduction to investigations in short-term aging processes

In a PV module, the silicon cell and its connections are responsible for the production and transport of electricity. All other components are needed to support and enable this main function by a) giving structural support for the solar cell with its electrical connections from fabrication to the whole operation time of the module, b) providing optical coupling between solar cell and the incident light in a prescribed spectral region, c) protecting the solar cell and its electrical connections from environmental influences (hail, wind loads etc.) and d) providing electrical isolation [1].

The most common c-Si PV module consists of glass on the front side, a polymeric encapsulant surrounding the cell with its electrical connections and a polymeric backsheet on the back side. In some cases, the glass on the front side can be replaced by a transparent polymeric film (mainly fluoropolymers) to get higher flexibility and reduce weight. On the back side, instead of a backsheet, also glass can be used. The so-called glass/glass modules give the high mechanical stability required for the use in building integrated PV elements.

During its service time a PV module undergoes diurnal and seasonal thermal cycles; the different thermal expansion behavior of the components of a PV module results in internal stresses [1] [2]. For example, the CTE of a commonly used encapsulant e.g. ethylene vinyl acetate (EVA) is about 10 times higher than that for metals and about 35 times higher than for silicon (see also Table 1) [3]. Overstressing may result in fractured cells, broken interconnectors or cracks and delamination in the encapsulation material. These failure modes could be reduced by the right choice of an encapsulant and backsheet with the required thermo-mechanical properties [1].

Moreover, the thermal expansion behavior of solar cell encapsulants is a key parameter for a stable PV module lamination process and high product quality. During heating up/production of a PV module, stresses caused by shrinkage or excessive thermal expansion of the encapsulant can lead to sliding of cells or other components

[1] [4]. For example, a previous study reported that there was a single wrinkle in the backsheet of about 5 cm height across the whole PV module after lamination. A rotation of the EVA film by 90° before lamination yielded a corresponding rotation of the wrinkle by 90° [4]. The formation of the wrinkle was attributed to excessive shrinkage of the EVA film in machine direction during the lamination, before crosslinking started.

As encapsulant, ethylene vinyl acetate (EVA) has been the main material used since the early 80`s more for cost reasons than for better applicability. Over the years several other materials have been introduced into the market, but up to now EVA is still by far the dominating encapsulation material. In general, EVA for PV applications is a random copolymer of ethylene with vinyl acetate between 27 and 33 % (weight). During lamination, the copolymer chains get crosslinked, transforming the thermoplastic EVA into an elastomeric and dimensionally stable polymer. However, the chemical aging behavior of EVA and other materials for solar cell encapsulation is well described in the literature e.g. [1] [5] [6] [7]. But these investigations concentrate mainly on chemical aging, i.e. changes in chemical structure and composition of the polymer itself and its impact on PV module performance. By contrast, physical aging, i.e. changes in polymer morphology without changing the chemical structure, is mentioned only in a few publications [8] [9]. The thermal and thermo-mechanical properties of unaged and also artificially aged EVA types are described in several papers [8] [10]. Regarding thermoplastic solar cell encapsulants, except for ionomers, nearly no data has been published so far [8].

Table 1 lists the thermal expansion coefficients of different materials used in PV modules which were found in the literature. A principal problem is the comparability of the given data due to different temperature ranges, which were used for the measurements. So far, nearly no data of the thermal expansion behavior and material anisotropy of solar cell encapsulants have been published in scientific literature. For EVA only two values were found in the literature, valid only for the crosslinked material with no information on the temperature range or anisotropy [11] [2].

Moreover there is a complete lack of data for different PV encapsulation materials apart from EVA.

Table 1: List of CTE values for materials used in a PV module

	CTE [10^{-6}/K]		
	[2] [11]	[12]	[13]
EVA	270, 300*[1]		
Glass	3.25-9.24*[1]		4.6-70*[2]
Silicon	2.61*[2]		7.63*[2]
Aluminum		23.5*[3]	23.6*[2]
Copper	16.8-17.7*[1]	16.4*[3]	16.5*[2]

*[1]Temperature range for determined CTE not given!
*[2]CTE at room temperature
*[3]CTE in the temperature range 20-100°C

Therefore the main objective in chapter 2.2.1 is a systematic investigation of the thermal expansion behavior and material anisotropy of different solar cell encapsulation materials. High dimensional stability of the encapsulant is of great importance in PV module production to avoid problems during lamination and/or in application. Hence, the results should also identify possible deficiencies in production processes and allow for the optimization of the process parameters for encapsulants. Furthermore, the influence on the lamination process and production yield will be discussed. For this purpose the samples were heated two times in a thermo-mechanical analyzer (TMA) in tensile mode and the coefficient of thermal expansion (CTE) over temperature was evaluated. To get additional information about transition temperatures of the encapsulants differential scanning calorimetry (DSC) measurements were done.

The role of the backsheet in a PV module is to give structural support via mechanical strength, to be a barrier against humidity and oxygen, to provide electrical isolation and weathering protection. To fulfill these requirements, in most cases multi-layer laminates are used mainly with polyethylene terephthalate (PET) as middle layer. The core layer is protected by weathering resistant outer and inner layers e.g.

fluoropolymers. A relatively new approach for the setup of backsheets is the use of co-extruded multi-layer backsheets consisting of polyamide (PA) or polyethylene (PE) [14].

Mechanical stability of backsheets during PV module production and after weathering play an important role in PV module reliability. It compensates the stresses generated from different thermal expansion coefficients of the PV module materials during elevated temperatures at production and due to the seasonal and diurnal thermal cycles. Mechanical stability can be influenced by chemical and physical aging processes in backsheets. Chemical aging processes like photo-oxidation or hydrolysis may lead to a reduction of the molar mass caused by polymer chain scission. Polymer chain scission and the resulting embrittlement is usually followed by the formation of (micro-)cracks. Consequently, these cracks allow for an enhanced moisture ingress and subsequent delamination as well as faster degradation of other components within the PV module. Among others an often used technique for reliability testing of backsheets is the tensile test [15], and especially elongation at break values proved to be a very sensitive indicator for chemical aging (degradation) effects like the reduction of molar mass, but also for physical aging effects like post- and re-crystallization [15]. For all backsheets containing a PET middle layer, in the course of damp heat (DH – 85 % RH/ 85°C) aging a significant decrease in the elongation at break can be seen. This is induced by hydrolysis of PET leading to polymer chain scission [16]. Polymers with ester (e.g. PET) and amide groups (e.g. PA) are known to be susceptible to hydrolysis [17]. Hydrolysis occurs under humid atmospheres and gets enhanced at elevated temperature [18]. It induces chain scission which decreases the mechanical strength. Previous studies revealed once the decrease is detectable for PET it does not take a long time until the material loses its mechanical strength completely [15]. Also physical aging effects like re-orientation or changes in the crystalline regions can affect the mechanical properties like modulus or elongation at break [19]. Investigations on PV backsheets containing polyvinylidene fluoride (PVDF) showed significant post-crystallization of α-PVDF, which resulted in a strong embrittlement of

the material [20]. Crack formation of backsheets containing PVDF has been observed in PV modules under accelerated aging conditions [21] [22].

In 2009 co-extruded polyamide based backsheets were introduced in the PV market. The main benefit of co-extruded films is that they do not exhibit delamination during service life time. Another advantages of this material is its single step processing via extrusion, where each layer can be tailored according its requirements. So far, for polyamide based backsheets nearly no data about physical and chemical aging processes under PV module relevant conditions is published with respect to its influence on the mechanical stability.

But polyamides as poly-condensation polymers in general are sensitive to hydrolysis. Also, polyamides are known to be polymorphous, i.e. having various crystalline structures for the same material and therefore also leaving the possibility of post- and recrystallization processes after exposure to elevated temperatures [23]. Both aging mechanisms have a strong impact on the mechanical behavior of this material which is usually followed by a decrease in elongation at break. However, as post- and recrystallization effects are usually driven by elevated temperatures it may already happen during PV module lamination. Consequently, these effects can possibly result in an unavailability to prevent overstressing of components in PV modules and/or (micro-)cracks.

The main aim of chapter 2.2.2 was to investigate the aging related effects on the mechanical properties of coextruded polyamide based backsheets for photovoltaic (PV) modules. Furthermore also aging related changes on the long term reliability of PV modules are discussed. Therefore samples were exposed to damp heat (DH; 85% RH and 85°C) and dry heat (85°C) conditions. Using differential scanning calorimetry (DSC) information about chemical and physical aging mechanisms was gained. To give information about changes in mechanical properties during artificial aging, tensile tests were realized.

2.1 Experimental procedure

The encapsulation films investigated in chapter 2.2.1 are listed in Table 2. To detect the expansion behavior during the lamination cycle before the crosslinking reaction starts, samples in the original, not crosslinked, state were chosen for the investigations. As the expansion behavior of polymeric films can have a directional dependence due to the drawing off during film extrusion, all samples were measured in the machine (md- direction of extrusion) and the transversal direction (td) [12] [24].

Table 2: Investigated solar cell encapsulant films in chapter 2.2.1

name	composition	thickness [µm]
EVA 1	standard cure ethylene vinyl acetate	460
EVA 2	ultra fast cure ethylene vinyl acetate	465
EVA 3	standard cure ethylene vinyl acetate	460
PO 1	linear low density polyethylene	210
PO 2	linear low density polyethylene	600
PO 3	ethylene methyl acrylate	400
PO 4	ethylene methyl acrylate	450
PVB	polyvinylbutyral	780
TPSE	thermoplastic silicone elastomer	460

The thermal expansion behavior was characterized by thermo-mechanical analysis (TMA). TMA was done in tensile mode using a Mettler Toledo TMA/SDTA 840 (Schwerzenbach, CH). The measurements were all performed under air atmosphere, the first and the second heating run of each sample were carried out according to the parameters given in Table 3. The CTE was evaluated from both, the first and the second heating curve. In the first heating curve, reversible and irreversible effects are overlapping. Due to higher temperatures all irreversible effects (e.g. relaxation of orientations and introduced internal stresses, post- and re-crystallization etc.) are eliminated by the end of the first heating run. To get information about the thermal history from the production process of the films the first heating curves were taken

for evaluation. To demonstrate influences of production parameters, such as cooling rate on the films, the CTE of the second heating curve were taken into account. The second heating curve reflects only the reversible material behavior and therefore the material specific CTE value. This means the CTE will not change even by heating up several times.

During heating, transition temperatures like the ones at glass transition or softening of polymers increase the CTE [17]. So determination of the thermal expansion is often used for evaluating the glass transition temperature or, if the specific CTE is required in temperature ranges without transitions. But the change of the CTE in the beginning of melting can be attributed to the enhanced molecular chain mobility which enables the relaxing of stresses and orientations, which are the effects we are looking for [17]. The resulting increase depends also on the chosen static load. At temperatures above glass transition its influence is low but with beginning of melting its influence increases [24]. However, a static load is necessary to avoid sample buckling and to keep the sample in tension. For films, a static load in a range of 0.01-1 N is recommended. For our measurements, a static load of 0.02 N (resulting in stresses from 4.3 to $15.9*10^{-3}$ N/mm^2) was used. All measurements were repeated at least once, depending on the reproducibility; the measurement parameters are summarized in Table 3.

Table 3: Experiment parameters for TMA measurements in chapter 2.2.1

measuring program no.	**start temperature** [°C]	**end temperature** [°C]	**heating/cooling rate** [°C/min]	**static load** [N]	**initial length** [mm]	**width** [mm]
1	25	55	2	0.02	10	6
2	25	80	2	0.02	10	6

The evaluation of the data was done according to ISO 11359-2 or DIN 53 752 (see Equation 1) [25] [26]

$$\boldsymbol{CTE(T_1, T_2) = 1/l_0 * (l_2 - l_1)/(T_2 - T_1)} \qquad \textbf{Equation 1}$$

where CTE is the mean coefficient of thermal expansion in $10^{-6}K^{-1}$. l_0 is the initial length of the sample at room temperature, l_1 is the length of the sample at temperature T_1 (25°C) and l_2 is the sample length at temperature T_2 (end temperature). The evaluated CTE is dependent on the chosen temperature range. Therefore it is not suitable to use it as a general material property but for specific applications [17].

The thermal behaviors of the polymeric encapsulants were characterized by differential scanning calorimetry (DSC). The tests were performed using a Mettler Toledo DSC 1 (Schwerzenbach, CH). The measuring program and parameters are listed in Table 4. The first heating run gives information on the current state of a polymer (reversible + irreversible effects), including the thermal and mechanical history of the polymer while in the second heating run information about material specific constants (reversible effect) are obtained [17].

Table 4: Experiment parameters for DSC measurements in chapter 2.2.1 (air atmosphere)

air atmosphere	start	end	heating rate
1. heating	-60°C	150°C	10°C/min
2. cooling	150°C	-60°C	
3. heating	-60°C	350°C	

In chapter 2.2.2 the aging behavior of a polyamide based PV backsheet was investigated. The backsheet is a coextruded multilayer with all layers consisting mainly of polyamide 12 (PA 12). The thickness of the inner (encpasulant side) and outer (air side) layers are 25 µm, the core layer is 300 µm.

Two artificial aging methods were used to get a full understanding about the aging-related changes in the material and its temperature and time dependence (see Table 5). The main focus will be on the results of the DH aging. The DH aging was done twice with different measurement intervals of 250 and 24 h. Second, the effect of temperature on the aging processes was investigated in separate dry heat tests at different temperatures and intervals. One dry heat test was performed at 85°C with

250 h intervals. Additional dry heat tests with temperatures of 145 and 150°C with 0.33 h intervals were taken according to a PV module lamination process.

Tensile tests were carried out on a Zwick Z001 according to EN ISO 527-3 [27], the test specimens were cut before accelerated aging according to specimen type 2 (150 mm x 15 mm) for the machine (MD) and the transversal direction (TD) of the films [15]. A load cell for 1 kN was used due to expected loads of about 250 N. The test speed used was 50 mm/min. From a total of at least five specimens for each test series, the average values for yield stress (σ_Y), yield strain (ε_Y), stress at break (σ_B) and strain at break (ε_B) were deduced.

Table 5: Parameters for the artificial aging methods in chapter 2.2.2

type of artificial aging	temperature [°C]	humidity [% RH]	storage time [h]	intervals [h]
damp heat (DH)	85	85	2000	250
	85	85	144	24
dry heat	85	-	1000	250
	145; 150	-	0.33	0.33

The thermal behavior was characterized by differential scanning calorimetry (DSC) using a Perkin Elmer DSC 4000. Measuring program and parameters are listed in Table 6. Samples of the backsheets (~10 mg) were cut and put into 50 µl pans with perforated lids. Melting points, melting enthalpies and crystallization temperatures were evaluated according to ISO 11357-3 [28]. For each evaluation, the average value of at least two independent results was taken.

Additional DSC measurements were performed to evaluate the thermal behavior after lamination by reproducing commonly used lamination temperatures (140 and 145°C) at the DSC runs. After holding the sample for 15 min at the chosen temperature it was cooled down to 20°C with a rate of 10°C/min. After this thermal treatment the DSC followed the same measuring program and parameters as in the earlier measurements (see again Table 6).

Table 6: Experimental parameters for DSC measurements in chapter 2.2.2 (nitrogen atmosphere)

	start	**end**	**time/ramp**
isotherm segment		20°C	5 min
1. heating	20°C	230°C	10°C/min
isotherm segment		230°C	5 min
2. cooling	230°C	20°C	10°C/min
isotherm segment		20°C	5 min
3. heating	20°C	230°C	10°C/min

2.2 Results and discussion

2.2.1 Thermal expansion behavior of solar cell encapsulation materials

In the following the thermal expansion behavior of the investigated materials will be shown. At first the results for all EVA films will be discussed. The thermal expansion coefficient over temperature with the standard deviation as the envelope for the first and the second heating curves for the investigated EVA materials are shown in Figure 36 (EVA1), Figure 37 (EVA2) and Figure 38 (EVA3).

In the first heating curve the results show a significant anisotropy for the materials EVA1 and EVA2 in contrast to EVA3. Anisotropic expansion due to drawing off is a well-known behavior of extruded polymer films [3] [17] [29] [30]. The extent of increased expansion in td, in contrast to the shrinkage in md, results from a too high drawing speed of the film. As a result the polymer molecules get aligned in md (remember =drawing direction) and remain oriented due to the fast cooling process. Another heating up of the film gives the frozen chains mobility and allow the oriented chain molecules to move into their thermo-dynamic preferred isotropic position. Therefore the first change of the slope of CTE values in the first heating run at 40°C for EVA1 and EVA2 (more distinct for EVA1) can be related to the relaxation of orientations, which were introduced during the film extrusion process. The change of the slope at 40°C also correlates with the onset temperature of melting in the first heating run of the DSC for the investigated EVAs (see exemplarily Figure 39). The start of melting gives the chain mobility and supports, therefore, our assumption of the relaxation of orientations which were introduced previously. Supportive of the assumption is an absence of the slope change for EVA3, although its onset of melting is at the same temperature (see Figure 40).

The second change of the slope at ~50°C is more distinct for the results in md and also appears for EVA3. This change in thermal expansion behavior can be explained by the thermal behavior of the investigated EVA films (see Figure 39 and Figure 40). All investigated EVA films showed in the first heating run a broad area of melting, starting immediately above the glass transition around -40°C to about 80°C with a melting

temperature around 50°C and a shoulder at 65°C [31]. The first heating run gives information on the current state of a polymer, including the thermal and mechanical history and the second heating run about material-specific behavior for known cooling conditions [17]. Hence the occurrence of a single melting peak at 65°C in the second heating run corresponds to the thermo-dynamical melting point of the EVA. The peak at 50°C in the first heating run can be attributed to a less organized crystal phase, which is formed in the area among the primary crystals during slow cooling or storage at ambient temperatures [32] [33]. Due to the absence of this less organized crystal phase after heating up, also the slope for CTE at ~50°C disappeared in the second heating run (see Figure 36 to 38). Furthermore it has to be taken into account that the absolute values of the thermal expansion after melting begins are influenced to some extent from the static load [24]. As the static load is necessary to keep the sample in tension, it is chosen at a low level (0.02 N) to keep the influence at a minimum.

The values for the CTE evaluated from 25 to 55°C of the first heating curves in md ranged from -231 to 697 [$*10^{-6}K^{-1}$] (standard deviation-SD ≤81) and for td from 855 to 2710 [$*10^{-6}K^{-1}$] (SD ≤123). At the second heating curves significantly lower values for the CTE were detected. The negative CTE values at the start of the second heating run can be attributed to a small decrease in the initial length (<10 mm). For md the CTE values ranged from 222 to 366 $*10^{-6}K^{-1}$ (SD ≤29) and for td from 337 to 444 $*10^{-6}K^{-1}$ (SD ≤28). There is obviously, as described above, a wide spread of the results for the CTE.

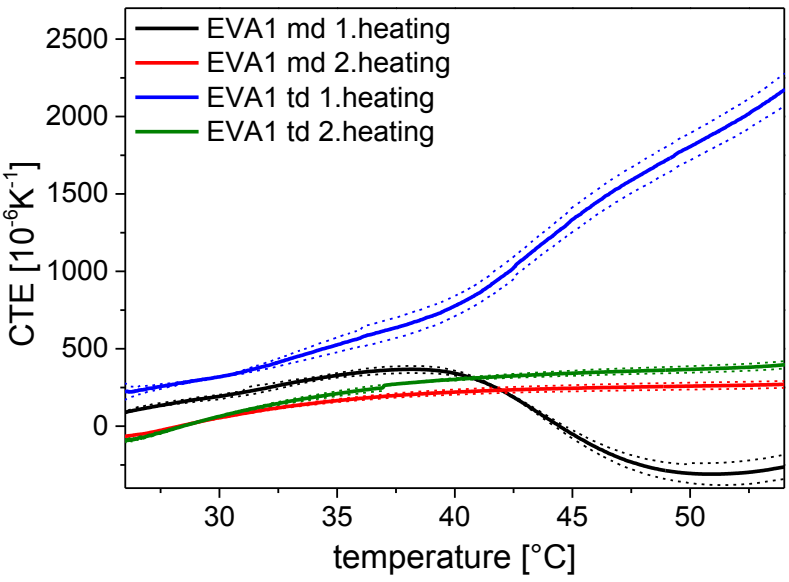

Figure 36: Coefficient of thermal expansion (CTE) with its standard deviation as the envelope in machine (md) and transversal (td) direction of the first and second heating curve for EVA1

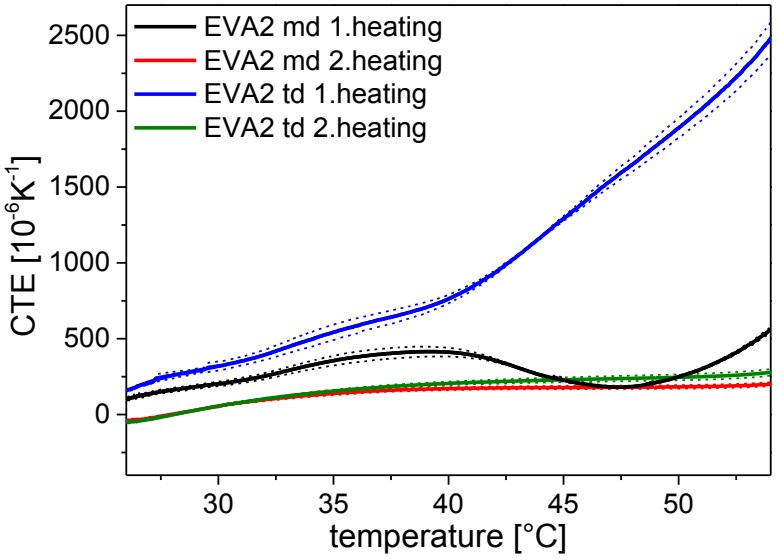

Figure 37: Coefficient of thermal expansion (CTE) with its standard deviation as the envelope in machine (md) and transversal direction (td) of the first and second heating curve for EVA2

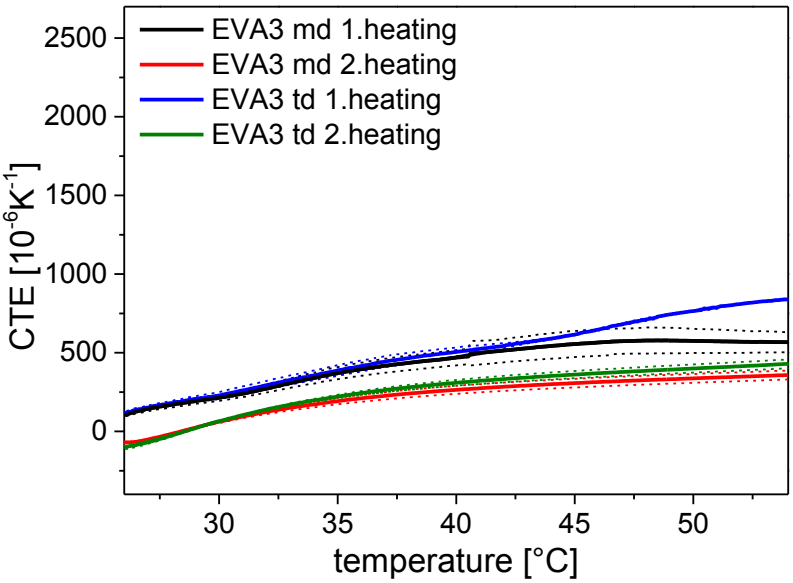

Figure 38: Coefficient of thermal expansion (CTE) with its standard deviation as the envelope in machine (md) and transversal (td) direction of the first and second heating curve for EVA3

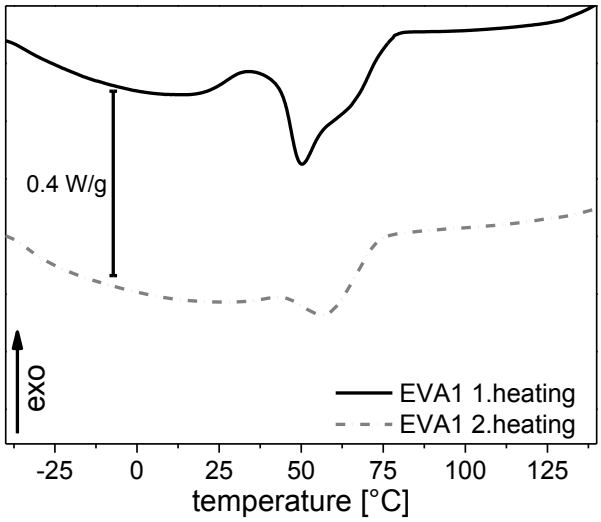

Figure 39: DSC curves of the first and second heating of EVA1

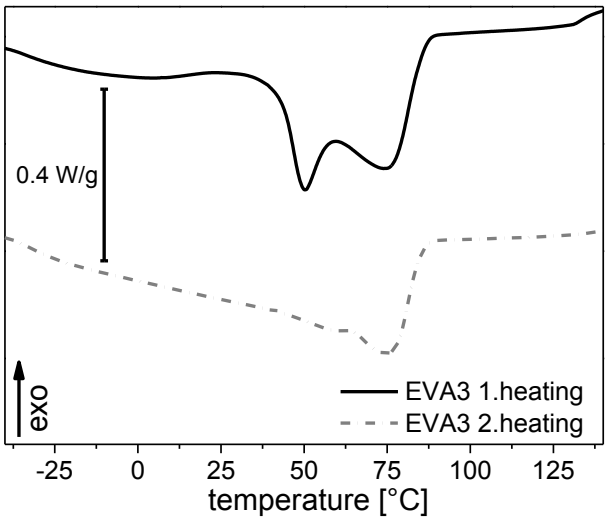

Figure 40: DSC curves of the first and second heating of EVA3

In the next step several thermoplastic solar cell encapsulants were investigated. In general the CTE curves showed the same trend and approximately same values as those for EVA3. Deviating behavior (e.g. enhanced CTE, anisotropy, etc.) were detected for the materials PO1, PO4 and PVB, which are depicted in the Figures 41 to 45. The results for all measured encapsulants are then summarized in Figure 46. For all semi-crystalline thermoplastic encapsulants (PO1- PO4) the same temperature range as those for the EVAs was chosen. Hence the end temperatures were below the main maximum melting temperature but slightly above the secondary crystallization region to enable a detection of relaxation effects.

In general the calculated CTE values for PO1 are moderate in comparison to EVA1 and EVA2 and comparable to those of EVA3 (see Figure 41 and also Figure 46). But in contrast to all other materials, the detected expansion in td (504 ±37 $*10^{-6}K^{-1}$) in the first heating curve for PO1 is lower than in md (990 ±372 $*10^{-6}K^{-1}$). The difference in the expansion of md to td could indicate a biaxial stretching of the film. The high standard deviation (±372) in md gives a hint to inhomogeneity in between the polymer film. The change in the slope of the first heating curve in md of PO1 at ~37°C can be related to relaxation of orientations (see Figure 41). The onset of melting of the material is at the same temperature, which enables the reorientation (see Figure 42). For low density polyethylene (LDPE), a semi-crystalline polymer, the melting

temperature given in literature is about 105- 118°C [30] [3]. By introducing side chains density and morphology (i.e. crystallinity) of PE can be tailored. This results also in a change of the melting temperature. The lower melting point can be attributed to a less organized crystal phase, which is formed in the area among the primary crystals during slow cooling or storage at ambient temperatures [32] [33]. Therefore the lower melting temperature of PO1 is an indication of many branched side-chains which results in a very low crystallinity as well as a broad distribution of lamellae thicknesses in the material. As expected the anisotropy disappeared at the second heating curve, due to reorientation of the chain molecules and remained with values in between those for the second heating of all EVA types (see Figure 46).

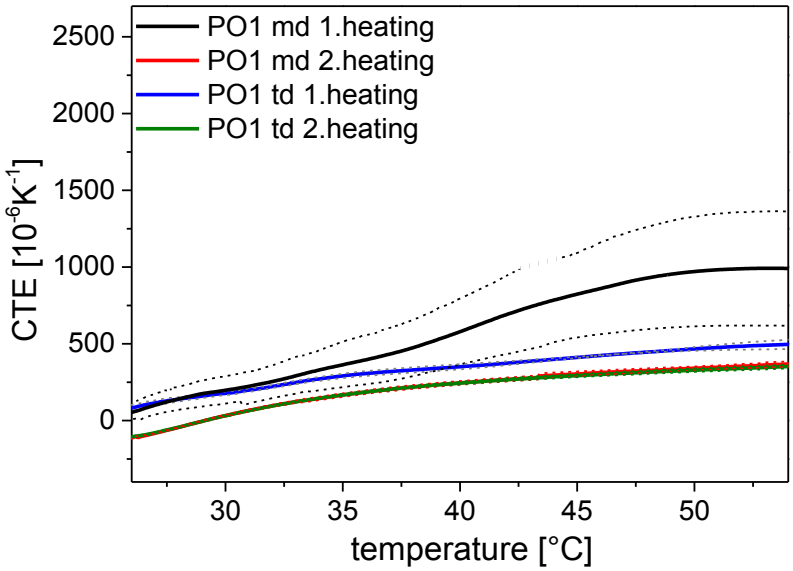

Figure 41: Coefficient of thermal expansion (CTE) with its standard deviation as the envelope in machine (md) and transversal (td) direction of the first and second heating curve for PO1

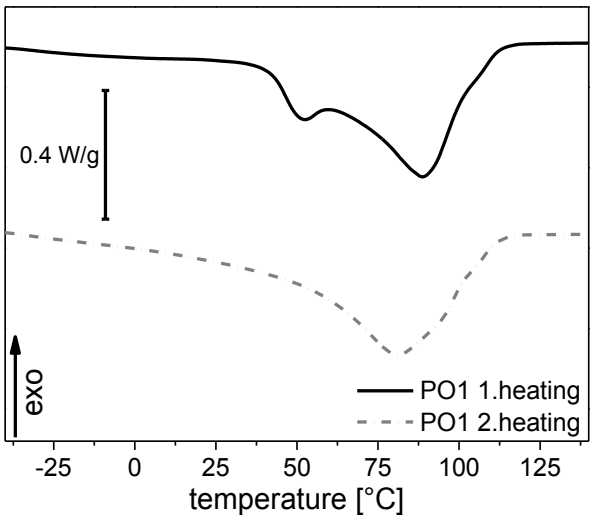

Figure 42: DSC curves of the first and second heating of PO1

The thermal expansion behavior of PO4 is shown in Figure 43. In the first heating curves the results for PO4 showed an anisotropic behavior of the film with values of -394 ±13 *10-6K-1 in md and 1044 ±5 *10-6K-1 in td (see Figure 43). PO4 has, like EVA1, a negative expansion, and therefore shrinkage, in md. The resulting difference between the expansions in md to td is lower than this for EVA1 (2499) and EVA2 (2013). The change of the slope of CTE values for both directions at 40°C can be related to the relaxation of molecular orientations.

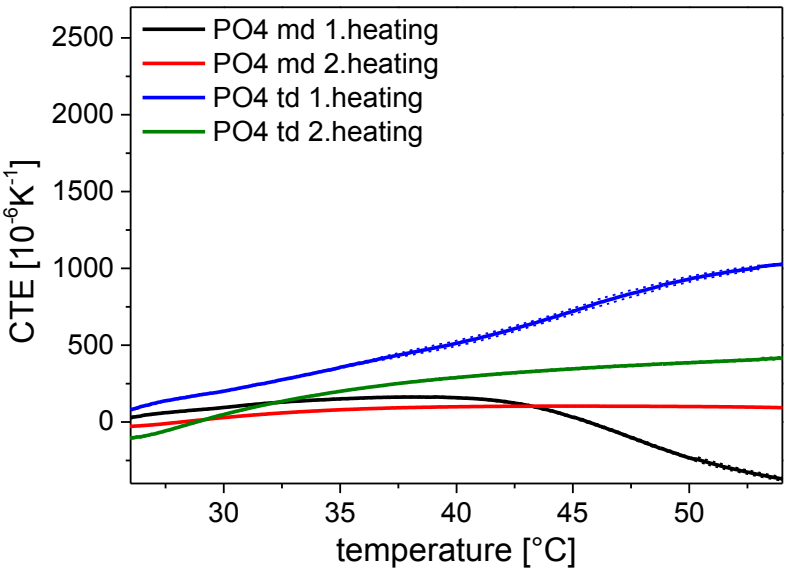

Figure 43: Coefficient of thermal expansion (CTE) with its standard deviation as the envelope in machine (md) and transversal direction (td) of the first and second heating curve for PO4

As it was the case for the materials EVA1, EVA2 and PO1 there is a reorientation of chain molecules at raised temperatures into their preferred position. For the film PO4 the expansion in md and td decreased with a remaining difference of 344 (see also Figure 46) at the second heating curve.

In the first heating curve the results for PVB showed also enhanced anisotropy for the material (see Figure 44). The CTE in the temperature range from 25 to 80°C showed a negative value for md (-916 ±169 $10^{-6}K^{-1}$) and an elevated one for td (1890 ±65 $10^{-6}K^{-1}$). This is the highest detected shrinkage in md of all materials. PVB is an amorphous polymer which passes the glass transition at ~20°C (see Figure 45). Therefore it can be excluded that the inhibition of enhanced expansion with simultaneous shrinkage in md starting at ~50°C is inhibited from passing the glass transition of this polymer. The change of the slope of CTE values at ~50°C can may also related to the relaxation of orientations.

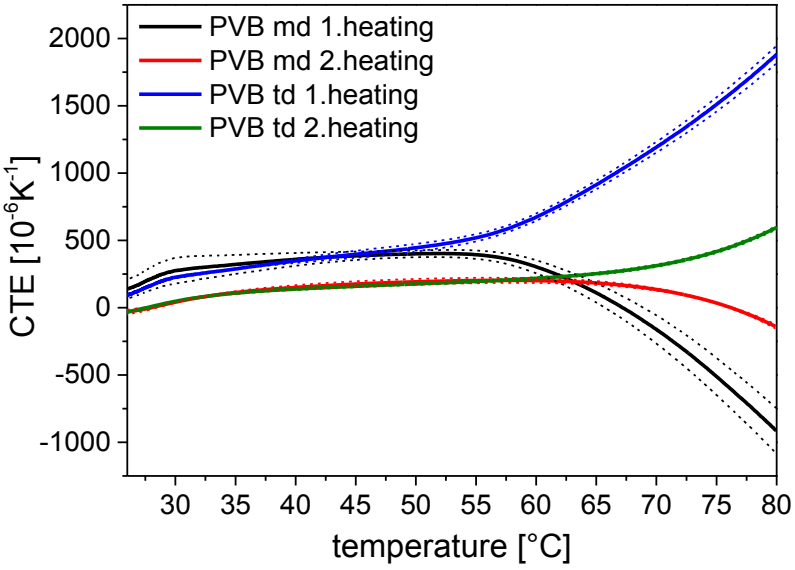

Figure 44: Coefficient of thermal expansion (CTE) with its standard deviation as the envelope in machine (md) and transversal direction (td) of the first and second heating curve for PVB

DSC curves of PVB from the first heating run revealed an expanded glass transition to around 60°C (marked in Figure 45 with a grey circle). As shown in [17] this effect may be accorded to a relaxation of oriented molecules. Nevertheless the detected temperatures of ~50°C for the change of the slope for CTE with 60°C for relaxation deflection in DSC do not fit perfectly. It is assumed that a preliminary reinforcement of

this effect occurs due to the high amount of plasticizer in the material (up to 40 %) which enables an easier sliding of the molecule chains [34]. The difference in the thermal expansion behavior between the first and the second heating curve can possibly be attributed to the not fully extended relaxation of orientations and/or an enhanced sliding of molecule chains due to the plasticizer in the material.

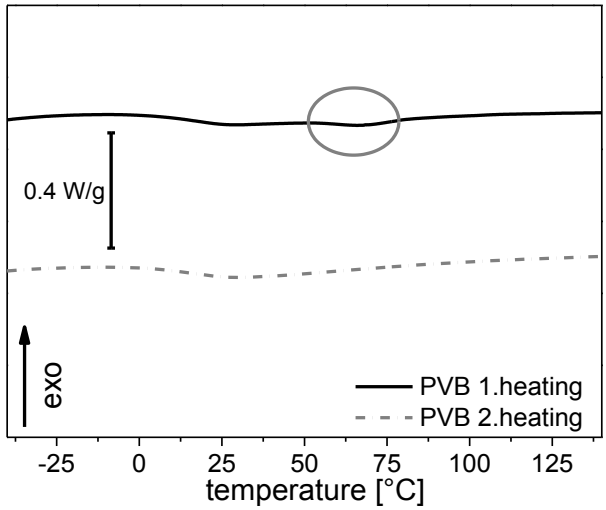

Figure 45: DSC curves of the first and second heating of PVB

We depicted as the comparative factor among all encapsulants studied the CTE values of 25-55°C. These results are shown in Figure 46 as well as those for the two amorphous polymer films PVB and TPSE also the CTE from 25-80°C of the first and second heating curves. The CTE results for the first heating curves revealed a high spread of thermal expansions in md and td among the encapsulants. For EVA it shows also a spread in among the same polymer, which indicates the importance of well-chosen process parameters (see explanation above and Figure 46). In general all encapsulants with anisotropic behavior showed higher CTE values in td, which ranged from 2710 ±123 $10^{-6}K^{-1}$ for EVA2 to 394 ±21 $10^{-6}K^{-1}$ for TPSE. The only exception was PO1 with 990 ±372 $10^{-6}K^{-1}$ in md to 504 ±37 $10^{-6}K^{-1}$ in td. The CTE values in md ranged between -916 ±169 $10^{-6}K^{-1}$ for PVB and 990 ±372 $10^{-6}K^{-1}$ for PO1. PO2 and TPSE showed approximately no anisotropy. For EVA3, PO3 and PVB the anisotropy was vanishingly small between 25-55°C. EVA1, EVA2 andPO4 showed an enhanced anisotropy, also PVB for values from 25-80°C. Results for the second heating curves

indicated the processing influence on the anisotropy as it decreased for all materials, except PVB, to negligible values.

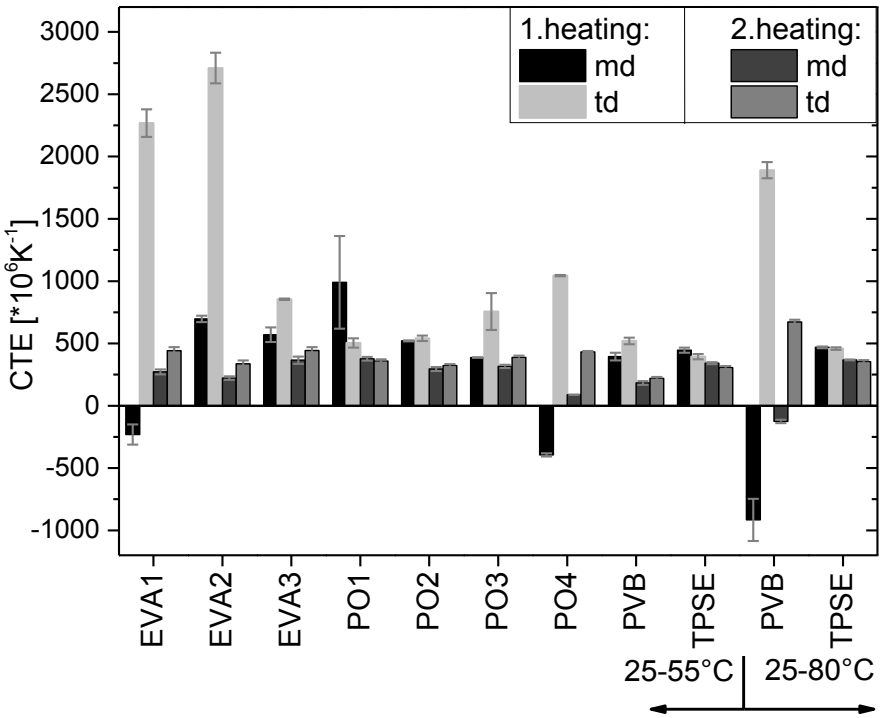

Figure 46: CTE (25-55°C) of the first and second heating curve for all tested encapsulants and CTE (25-80°C) for PVB and TPSE

To show a direct relationship to the influence of CTE during the lamination of a PV module we calculated the expected increase in length from CTE results. The size of the PV module was chosen with a standard dimension of 1.6 m x 1 m. The calculated values are shown in Table 7. Please be aware that these values are calculated for the individual films, not taking into account hindered mobility due to the multi-layer structure of a PV module. The calculated deformations do not appear in the module, but such hindered mobility leads to mechanical stress within the module. As explained in the introduction EVA1 and 2 induced wrinkles in a PV module [4]. For example the calculated expansion for EVA1 revealed -11 in md to 68 mm in td. The difference between the calculated expansions in both directions is 79 mm. As the materials PO1, PO4 and PVB revealed the similar differences one would expect the same problems. But as PVB is generally used in glass/glass modules, no problems during production are expected, assumedly due to the symmetrical construction and higher stiffness of

glass. For this reason the values for PVB were not calculated. The two other films, as well as EVA1 and 2 are highlighted in bold in the Table. However, we assume that not only anisotropy is the problem. Only EVA1 and 2 showed a significant shrinkage with subsequent expansion. This effect induces stresses to the backsheet which may not relax resulting in a contraction of the backsheet.

Table 7: Calculated thermal expansions of the investigated encapsulants related to a standard module size (1.6 m x 1 m)

encapsulant	**ΔL in md [mm]** per 1.6 m	**ΔL in td [mm]** per m	difference in **ΔL** md to td
		25-55°C	
>EVA1	***-11.0***	***68.0***	***79.0***
>EVA2	***33.4***	***81.3***	***47.9***
EVA3	27.3	25.7	1.6
>PO1	***47.5***	***15.1***	***32.4***
PO2	25.0	16.2	8.8
PO3	18.6	22.7	4.1
>PO4	***-18.9***	***31.3***	***50.2***
TPSE	21.4	11.8	9.6

The main conclusion is that if a polymer film/ encapsulant is produced with well-chosen production parameters, the anisotropy/ thermal expansion should be in a good/ low range. If the parameters are not chosen well, the resulting expansion can induce problems during lamination. TMA measurements can be a good tool for quality control of these production parameters and/or for testing incoming materials to avoid problems during lamination.

2.2.2 Reliability of polyamide based PV backsheets

Tensile test curves give information about general mechanical properties of a material. In the case of backsheets used for PV modules all materials show a yield point indicating that they are thermoplastic polymers with a ductile behavior. The yield point is a local maximum where the plastic deformation of the polymer begins. Its increase is an indicator for physical changes like post-crystallization [16].

Exemplarily the stress-strain curves from tensile tests on the polyamide based backsheet in its initial stage for the MD and the TD tested backsheet samples are shown in Figure 47. A clear anisotropic behavior can be seen. This is generally the case for most extruded films as drawing off after extrusion introduces orientations [17] [35].

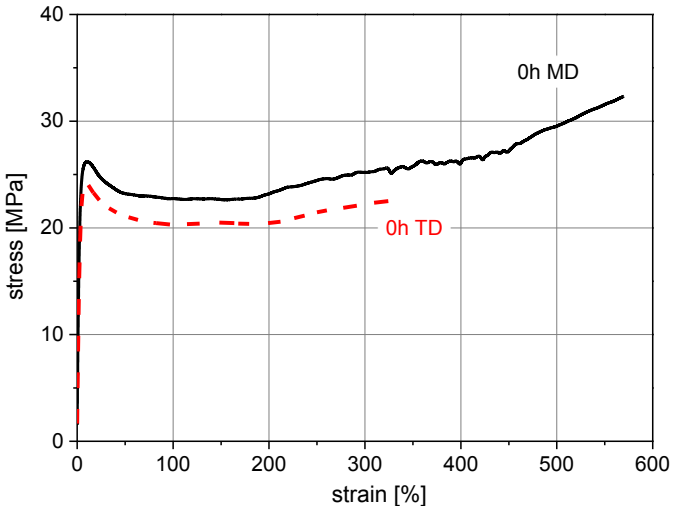

Figure 47: Stress- strain curves for the initial polyamide backsheet tested in the machine direction (MD) and the transverse direction (TD)

After passing the yield point the stresses in the MD and the TD started to increase again. If the stresses reach values above the yield point (like for the polyamide backsheet in MD) a full orientation of the polymer chains in load direction occurs. Then the load gets absorbed via the main valence bonds and no longer by intermolecular forces [35]. Hence the elongation at break is dependent on the polymer chain length as well as the resulting entanglements: The higher the molecular weight the longer the chains and consequently there are more entanglements. As hydrolysis results in chain scission it goes along with a significant decrease in

molecular weight and therefore elongation at break. Is there no further increase in stresses above the yield stress (like for the TD of the polyamide backsheet) the alignment is not completed and the load gets absorbed via intermolecular forces. For this behavior the orientation plays a major role as it directly influences the amount of intermolecular forces. An increase in yield stress after artificial aging with elevated temperatures of semi-crystalline polymers is a common behavior [16] [35]. During artificial aging elevated temperatures enable chain mobility and allow post-crystallization to occur. The increase in the yield stresses observed with the polyamide backsheet upon DH aging in the MD (26 to 28 MPa) and the TD (22 to 26 MPa) was not very pronounced which indicates a moderate increase in crystallization. The results for the change in the elongation at break during DH storage are more significant (see Figure 49). For the initial samples in both directions a necking at several locations was observed. While this behavior was observed for all tested samples in the MD, in the TD it was only observed for the initial state samples. Exemplarily the 250 h DH aged samples after the MD and the TD testing are shown in Figure 48. This behavior is also reflected via a high standard deviation in the elongation at break values for all results in the MD and the initial in the TD tested samples in Figure 49.

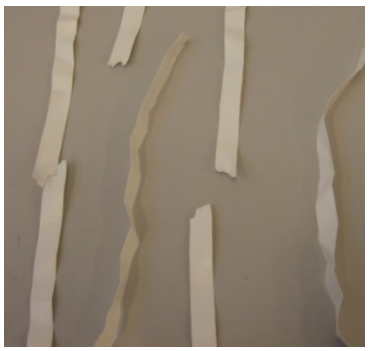
a)

b)

Figure 48: Tensile test samples of 250 h DH aging of AAA after measurements samples tested in the **a)** MD and the **b)** TD

For both directions (MD and TD) a decrease in the elongation at break can be seen in Figure 49. While the elongation at break decreased continuously in MD, the values for TD showed a significant decrease right after 250 h of DH storage. As explained above,

all the aged samples tested in the TD showed a different behavior. However, after this sharp initial decrease, surprisingly, the elongation at break of the DH stored samples was almost constant over storage time up to 2000 h. For the 2000 h DH aged samples there was still an elongation at break from ≥20 % for both directions. From the general trend of the results in MD and TD, one would assume the material would lose its mechanical strength by further storage. For PET based backsheets such a trend in elongation at break values is a sign for beginning reduction of molecular weight, which is observable via embrittlement [15]. But compared to PET based backsheets no embrittlement could be detected for the polyamide backsheets under investigation. Simulations from PV modules revealed a maximum tensile strain of 18 % occurring between the area of the cells and the backsheet [2]. In these simulations extreme conditions - cooling down from the initial stress-free state after lamination at 150°C to -40°C - were considered [2]. Hence we assume that the residual elongation at break, with no observation of embrittlement, is sufficient for the use in PV modules. But there remains still the question: Does the big drop in the elongation at break after 250 h DH storage for the samples in TD result from physical and not chemical aging?

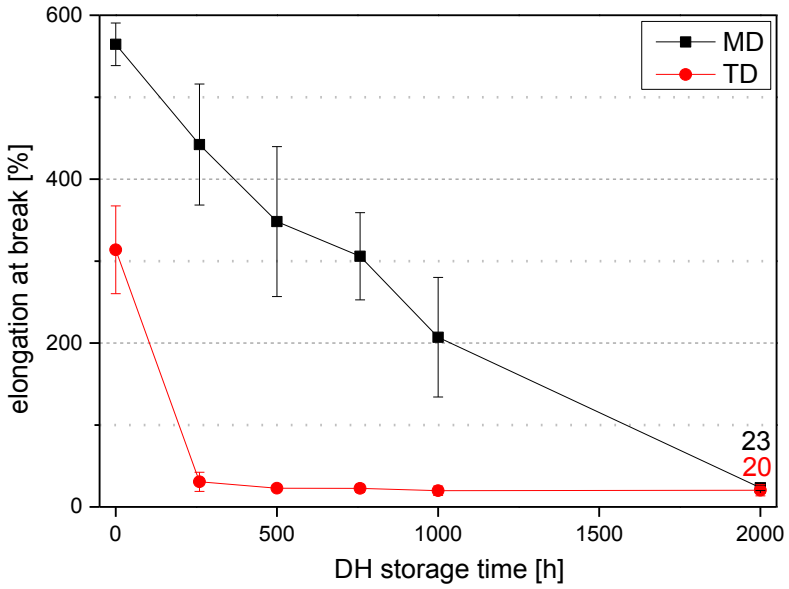

Figure 49: Change of the elongation at break during DH storage of the polyamide backsheet for MD and TD

Thermal analysis via DSC measurements was chosen for further investigations to find an answer. In Figure 50 the DSC curves of the initial polyamide backsheet samples are

shown. In the first heating curve two melting peaks were detected. The first melting peak at 167°C can be related to polypropylene (PP) [29], which was found in the polyamide core layer [36]. The amount of PP was not determinable via thermogravimetric analysis, as the decomposition temperatures of PA 12 and PP lie in the same regions. The second peak in the first heating curve at 178°C can be attributed to polyamide 12 (PA 12) [29]. In the cooling curve a shoulder of the crystallization peak of PA 12 (153°C) was detected at 149°C. The shoulder may be associated with PA 12 in the outer layers as these polyamides have a different additive formulation compared to the PP modified core layer and might thus show a slightly varied crystallization behavior. A similar effect was reported by Ogunniran, where different crystallization temperatures were determined for pure PA 12 and a PA 12 blended with PP [37]. Additional DSC measurements of a single PA 12 layer confirmed a crystallization temperature at 149°C for this material. For PP a double crystallization peak was detected (113°C and 96°C). The occurrence of the double peak may be associated with a further additive in PP which disturbs the perfect crystallization [37]. In the second heating run the PP melting peak was again at 167°C, an additional third peak at 172°C was found and the PA 12 melting peak was at 178.5°C.

PA 12 exhibits the γ-form as its most stable crystal structure [38] [39]. Therefore we assume that the peak at 178.5°C refers to the melting of γ-PA 12 crystals [37] [39]. However the co-existence of α- and γ-crystal forms for PA 12 are reported when PA 12 is treated and/or produced under specific conditions [40] [23] [41] [37] [38] [39]. The unit cell of PA 12 is monoclinic; its dimensions are summarized in [41]. PA 12 establishes perfect hydrogen bonding between two adjacent chain molecules in a layer whether they are parallel or antiparallel to each other [41]. From the parallel alignment, the γ-crystal is formed having shortened chain axis repeat distances as a result of a kink that is caused by gauche conformations around the amide groups. The antiparallel alignment produces the α-unit cell having fully extended trans chain conformation [41].

Thus, the occurrence of the additional melting peak at 172°C in the second heating run in our DSC measurement might be caused by the existence of α-crystals of PA 12,

as a re-crystallization of parts of the γ-crystals has occurred in the 1.heating run. Ogunniran et al. assigned the two peaks (172 and 178.5°C) in the second heating run to less dominant α-crystals (172°C) and predominant γ-crystals (178°C) [37]. Ishikawa claimed that the occurrence of a double peak at the second heating run does not imply the presence of α-crystals, but is due to the melting of γ-crystals: the lower-temperature peak arises from rather smaller and/or more imperfect crystallites formed during cooling [42]. However, as the measurement conditions and materials under investigation were not exactly the same we can not give a proof for one of either assumption.

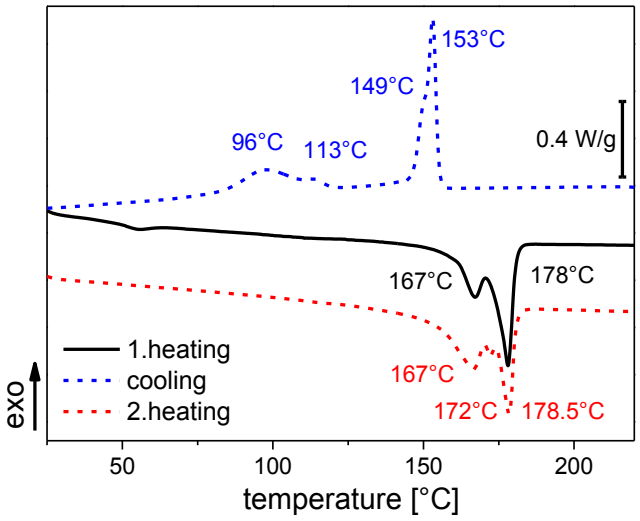

Figure 50: DSC curves for the initial polyamide backsheet samples

DSC measurements were performed for samples taken at all removal intervals during DH aging. Exemplarily the 1.heating curves of the initial, 250 h and 1000 h DH aged samples are shown in Figure 51. For the initial samples, the two peaks at 167 und 178°C, as described above, were detected. For all aged samples an additional peak at 112°C was observed.

This peak can be attributed to a post-crystallization of PA 12 which occurred at the storage temperature of 85°C and did not change over storage time. The same effect for the polyamide backsheet was seen for other artificial aging methods with shifted peak maximum temperature corresponding to the storage temperature used. E.g. for storage at 60°C the peak maximum was at 90°C. This effect is a common behavior of

polymers and is assumed to occur from post-crystallization [17]. The assignment of the peak to PA 12 and not PP is supported by results with stored APA (PA 12/ polyethylene terephthalate/ PA 12) samples. The 250 h DH aged samples showed in the first heating curve additionally a shoulder at 176°C attached to the 178.5°C PA 12 melting peak. The change of the shoulder into a peak was detected for all ≥500 h DH aged samples. It was revealed that the occurrence of a double melting peak of PA 12 in the first DSC heating run can be related to a presence of γ and α-crystal modifications [37] [38] [39] [43]. During artificial aging and/or storage at elevated temperatures, crystallization occurs from solid state in the amorphous regions of the polymers. We assume that the melting temperature at 176°C in the first heating run can be associated with α-PA 12 and is enhanced (e.g. 174°C in [39]; 173°C in [38] [43] and 170.6°C [37]) as no clear separation from the γ-crystals is possible in the solid state.

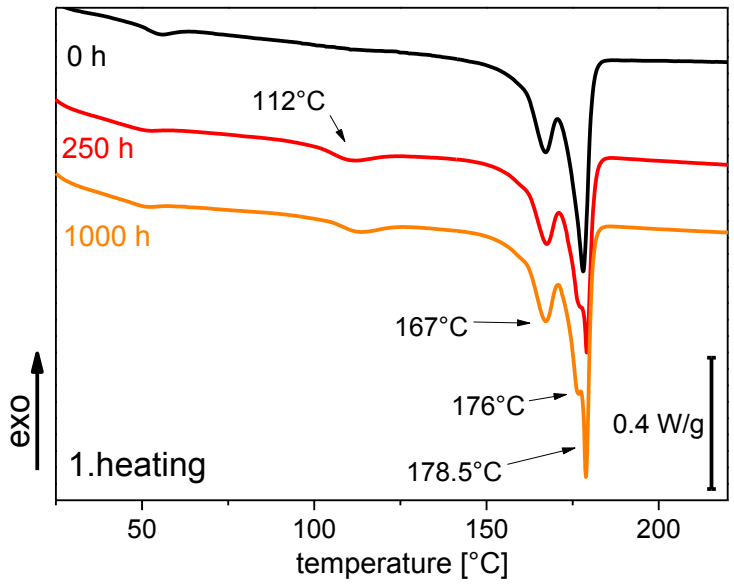

Figure 51: DSC curves of the first heating for the initial- 250 h- 1000 h DH aged polyamide backsheet samples

Hiramatsu et al. claimed the γ-form not to be transferable in α-form, but introduced a γ`-crystal form which is formed due to drawing of γ-PA 12 above 50°C under atmospheric pressure [40]. Both crystal forms (γ and γ`) were not distinguishable in WAXD patterns and/or melting peak temperatures in DSC curves [39]. However he

denoted the γ`-form as transformable into α-PA 12 when treated under high pressure (500 MPa) and temperatures lower than the melting point [40]. As the polyamide backsheet is coextruded and, due to this production process, drawn with temperatures over 50°C and then, in our DH storage, treated at temperatures lower than the melting region (but without pressure) this could be one reason for the double peak.

Another possibility could be that the lower-temperature peak arises from rather smaller and/or more imperfectly γ-crystallites. Both possibilities were not verifiable as the corresponding PP, γ- and α-PA 12 peaks in WAXD patterns are overlaid. Therefore in the following the re-crystallized γ-PA 12 will be called r-PA 12.

The melting peaks observed in the second heating run (167°C-PP, 172°C and 178.5°C-PA 12) remained at the same values for all initial and artificially aged samples.

The evaluated melting enthalpy for PA 12 in the second heating curves stayed constant at about 22 J/g ±0.8 for initial and all aged samples. Chemical aging of PA 12 via chain cleavage would result in differing enthalpies and a possible lower melting peak temperature in the second heating curve as well as changes in the crystallization temperature at the cooling run [17]. As all these indicators were not detected, the chemical aging processes of this material can be neglected.

To find out if there is a correlation between the sharp decrease in mechanical values for the polyamide backsheet (elongation at break in TD-tensile tests) to the physical changes (enthalpy -1.heating run DSC) in the PA 12 layers during the DH storage, we compared both measurement results. In Figure 52 the schematic evaluation of the enthalpy results for the PA 12 are shown. The chosen method uses a simplified evaluation for the detected double peaks since a clear separation of the peaks is not possible. Deviating absolute values can be a result, but the general trend will not be influenced by that. The resulting relation of the tensile tests to the DSC results can be seen in Figure 53. The melting enthalpies of the whole PA 12 in the polyamide backsheet showed a slight increase until 500 h of storage (see Figure 53). The enthalpies of γ-PA 12 (according to peak 178.5°C) showed a decrease from start to 250 h storage, then the values stayed constant. For the recrystallized γ-PA 12 (r-PA

12), as it first appeared in the DSC measurements for the 250 h stored samples, an increase was detected. Also a further small increase from 250 to 500 h was observed, which also seems to cause the small increase of the enthalpy for the whole PA 12 in polyamide backsheet. The progression of the enthalpies of the r-PA 12 over time directly correlates with the decrease in the elongation at break in TD for the polyamide backsheet, while in MD a continuous decrease was detected. The elongation at break in TD is more sensitive to changes which are influencing the intermolecular forces. The re-crystallization of PA 12 from γ in α leads to antiparallel alignment and extended chain lengths. It seems reasonable that this change in conformation leads to fewer intermolecular forces and furthermore lower elongation at break values. Also a re-crystallization from γ to smaller and/or more imperfect crystallites can have an influence on the elongation at break. However once the re-crystallization is finished no further decrease in the elongation at break happens for TD and also MD. Therefore the re-crystallization has a direct correlation to the mechanical behavior of the polyamide backsheet.

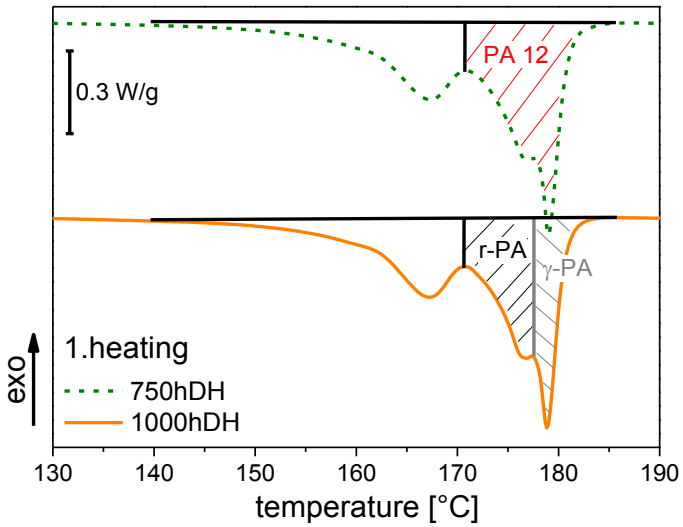

Figure 52: Schematic picture of the evaluation of the polyamide enthalpy results

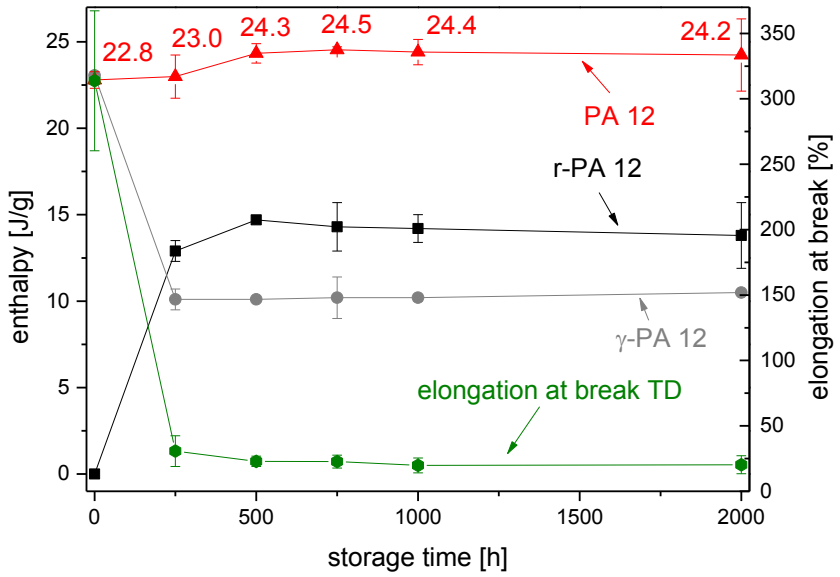

Figure 53: Comparison of the DSC- enthalpy (PA 12 in whole, r-PA 12 for the recrystallized and γ-PA 12 for the main crystal form) to tensile test- elongation at break (polyamide backsheet) results for DH storage

In a second phase further investigations were done for a more detailed description of the physical aging process regarding the following aspects: (1) influence of time during DH aging - start of the re-crystallization process; (2) influence of humidity. The second DH storage, with smaller measurement intervals (24 h), revealed that the re-crystallization starts after about 144 h of storage where the first occurrence of a shoulder was detected. No reverse effect could be found for samples with a detected PA 12 double peak by further room storage (3 weeks) or drying (24 up to 72 h). To see if there is a requirement for the presence of water vapor for the re-crystallization process, dry heat storage was also performed. Already after 250 h re-crystallization via an occurrence of a double melting peak was detected (see Figure 54). Therefore it can be stated that the re-crystallization process is only induced by temperature.

As the re-crystallization process of γ-PA 12 into r-PA 12 occurs at raised temperatures, it is likely that it occurs already during the PV module lamination process. To get a reliable answer we annealed polyamide backsheet samples at different temperatures (140 and 145°C) for 15 min. Then the thermal properties were measured by DSC. These results were compared to measurements of samples taken from a PV module after lamination.

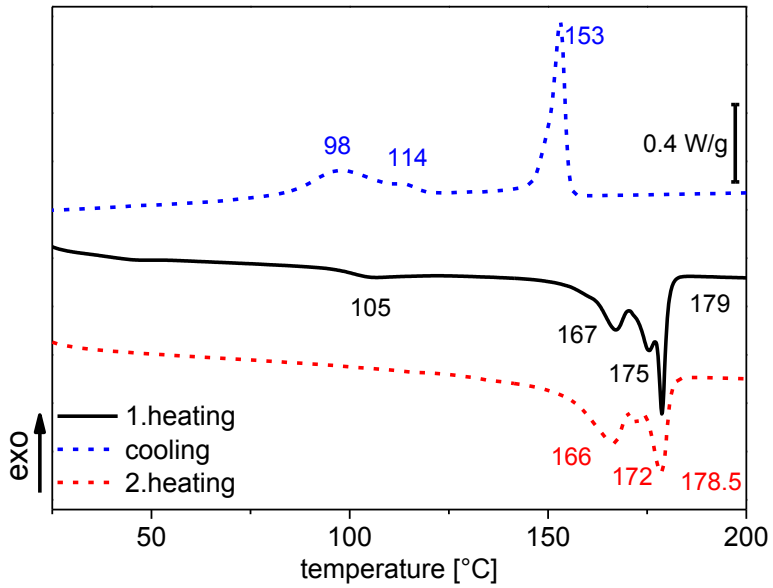

Figure 54: DSC curves for the polyamide backsheet samples after 250 h of dry heat storage

Annealing of the polyamide backsheet in the DSC for 15 min (0.25 h) at 145°C showed the best fit with samples taken from a polyamide backsheet after PV module lamination (see Figure 55). The lamination temperature of the module was held at 146°C for 20 min. For both samples an occurrence of a PA 12 double peak can be seen. Therefore this temperature loading already induced the re-crystallization of PA 12. For the samples annealed at 140°C for 15 min in the DSC device the re-crystallization process was not detectable. Consequently, the lower the annealing temperature the longer the time necessary for re-crystallization.

One interesting fact we found was an occurrence of a peak, which changes its maximum in relation to the chosen annealing temperature. For example for the module backsheet and the DSC samples, annealed at 146 (module) and 140°C (DSC), the peak was at 146°C. It seems to be the same peak detected for the DH samples (at 112°C) and dry heat aging (105°C) but more pronounced. As explained before it belongs to PA 12.

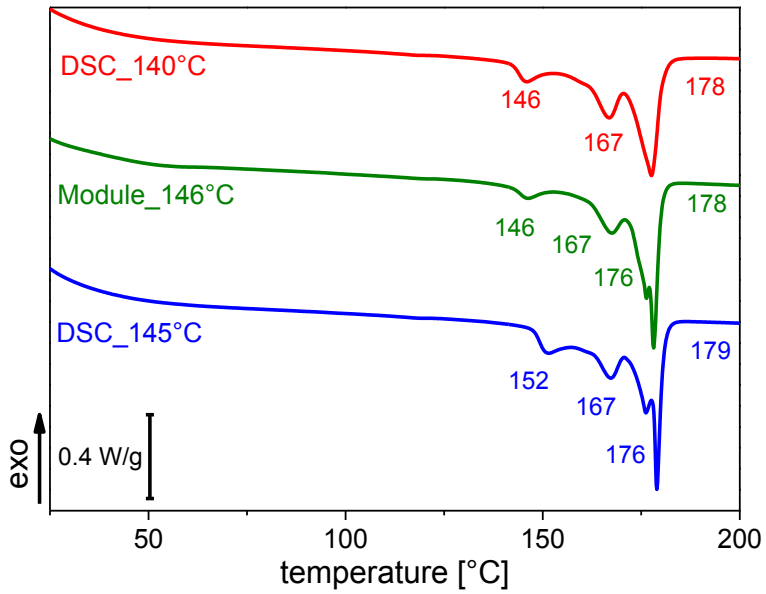

Figure 55: Comparison of the DSC first heating run curves for the DSC lamination measurements and module laminated polyamide backsheet samples

For all measurement results it can be said if there was a double peak detected in the first heating run the low temperature peak for PA 12 was at 176°C (for dry heat aging it was 175°C) and the one for the γ-crystals was always between 178 and 179°C. The peak maximum for PP was always at 167°C. For all second heating run curves the melting temperatures did not change (166, 172, 178.5°C). This also holds true, as said before, for the samples from DH and dry heat storage and indicates no significant chemical changes in the material [17] [42].

In Figure 56 the results of the tensile tests for the initial polyamide backsheet samples in comparison to the dry heat stored and the 2000 h DH aged ones are shown. The results for the initial in TD tested samples and the 145°C stored samples in MD show a high standard deviation, although for every measurement five samples were evaluated. This may can be attributed to inhomogeneity's in the film. The temperature loading for the samples of the dry heat stored samples was 20 min at the shown temperatures. For both testing directions a decrease in the mechanical values can be seen. Therefore the re-crystallization in the DSC curves for the lamination experiments (at 145°C) can be related to a decrease in mechanical values as also seen for the DH aged samples. The difference between the evaluated values from the 2000

h DH aging may be explained via different resulting morphologies between the storages with different conditions. However it proves that the re-crystallization process induces a decrease in mechanical values which can already happen during the lamination of a PV module.

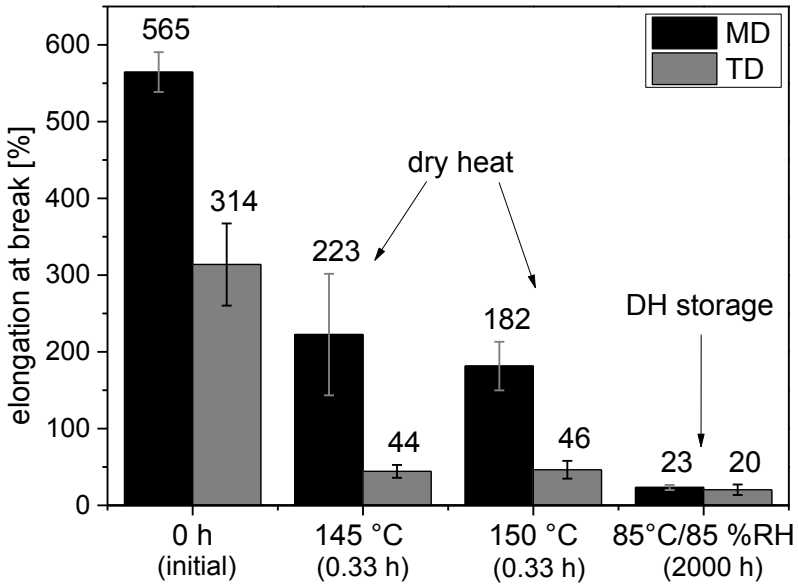

Figure 56: Change of the elongation at break during dry heat and DH storage of polyamide backsheet for MD and TD

Simulations from PV modules revealed a maximum tensile strain of 18 % occurring between the area of the cells and the backsheet [2]. In these simulations extreme conditions - cooling down from the initial stress-free state after lamination at 150°C to -40°C - were considered. The polyamide backsheet samples annealed at 150°C were taken from the oven and cooled down to room temperature. However the measured value for the elongation at break was still at 46 % in TD which is significantly above the required tensile strain. Although this re-crystallization, followed by a decrease in strain at break value happens during PV module lamination, its effect on PV module reliability and crack formation is assumed to be less critical. Only after permanent storage at 85°C were strain at break values between 20 and 23% measured, which is only slightly above the simulated maximum strain of 18 % [2]. But it was shown by Koehl et al. [44], that permanent temperatures above 65°C are very rare even for hot climate zones under standard operating conditions without clouding. Therefore also in

case of hot climates only limited influence of weathering-induced polyamide re-crystallization on the mechanical stability of the backsheet, and consequently PV module reliability, can be expected.

2.3 Summary and conclusions

So far, nearly no data on the thermal expansion behavior and material anisotropy of solar cell encapsulants have been published in scientific literature. Therefore in chapter 2.2.1 an overview on the thermal expansion behavior for nine different encapsulants is discussed. In the first heating run for all materials anisotropic expansion behavior was found, which was significantly reduced in the second heating run. Anisotropic expansion due to drawing off is a well-known behavior of extruded polymer films that usually results from a too high drawing speed of the film. As a result, the polymer molecules get aligned in extrusion direction and remain oriented due to the fast cooling process. Another heating up of the film enables enhanced mobility and allows the oriented chain molecules to move into their thermo-dynamic preferred isotropic position, causing shrinkage. For three encapsulant films a significant shrinkage with subsequent expansion was detected during heating up. This material behavior can result in a dislocation of components and/or distortion or even deformation of the backsheet during PV module lamination.

To summarize, knowing the thermal expansion behavior of the solar cell encapsulants is highly relevant for the PV module lamination process, and Thermo-Mechanical Analysis proved to be a suitable method for ability but also for quality control of solar cell encapsulation films.

The aging behavior of a co-extruded polyamide based backsheet under DH (damp heat 85 % RH/ 85°C), dry heat (85°C) and PV module lamination conditions was investigated in chapter 2.2.2. The investigation was done by detection of the changes in thermal behavior via DSC (differential scanning calorimetry) and mechanical behavior via tensile tests.

Although polyamides are known to be susceptible to hydrolysis no significant chemical aging mechanisms could be found with thermal analysis. For all samples aged under elevated temperatures a physical change was detected. The polyamide showed a re-crystallization peak which indicates the formation of a different crystal formation into the general existing γ-crystals. It was shown that this re-crystallization process is

dependent on time and temperature. It can already be induced during lamination of a PV module, depending on the lamination temperature. The influence of the physical changes on the mechanical behavior was examined via tensile tests. A drop in elongation at break for the transversal direction of the backsheet was the result. For the machine direction a continuous decrease was detected as there is a lower influence of morphological changes on it. Once the re-crystallization is completed no further loss in mechanical values were found. As this process results from physical and not chemical changes no embrittlement could be observed.

In simulations with considering extreme conditions a maximum tensile strain of 18 % between the area of the cell and the backsheet was calculated. The values for the elongation at break for samples loaded with temperatures according to common lamination temperatures (145 and 150°C) and time (0.33 h) were still above 44 % in TD which is significantly above the required tensile strain of 18 %. Only after permanent storage at 85°C (2000 h) were strain at break values between 20 (TD) and 23 % (MD) measured. But as permanent temperatures above 65°C are rare even for hot climate zones under standard operating conditions without clouding, not only after lamination but also in case of hot climates only limited influence of weathering-induced polyamide re-crystallization on the mechanical stability of the backsheet, and consequently PV module reliability, can be expected.

2.4 References

[1] A.W. Czanderna, F.J. Pern, Encapsulation of PV modules using ethylene vinyl acetate copolymer as a pottant: A critical review, Solar Energy Materials and Solar Cells (1996) 101–181.

[2] U. Eitner, Thermomechanics of photovoltaic modules. Doctor thesis, Martin-Luther-Universitaet Halle-Wittenberg, 2011.

[3] H. Domininghaus, P. Eyerer, P. Elsner, T. Hirth, Kunststoffe: Eigenschaften und Anwendungen, Springer, Berlin Heidelberg, 2007.

[4] G. Oreski, M. Knausz, G. Pinter, C. Hirschl, G.C. Eder, Advanced methods for discovering PV module process optimization potentials and quality control of encapsulation materials, in: 28th European Photovoltaic Solar Energy Conference and Exhibition, Paris, France, 2013.

[5] P. Klemchuk, E. Ezrin, G. Lavigne, W. Holley, J. Galica, S. Agro, Investigation of the degradation and stabilization of EVA-based encapsulant in field-aged solar energy modules, Polymer Degradation and Stability (1997) 347–365.

[6] M.D. Kempe, G.J. Jorgensen, K.M. Terwilliger, T.J. McMahon, C.E. Kennedy, T.T. Borek, Acetic acid production and glass transition concerns with ethylene-vinyl acetate used in photovoltaic devices, Solar Energy Materials and Solar Cells 91 (2007) 315–329.

[7] C. Peike, T. Kaltenbach, K.-A. Weiß, M. Koehl, Non-destructive degradation analysis of encapsulants in PV modules by Raman Spectroscopy, Solar Energy Materials and Solar Cells 95 (2011) 1686–1693.

[8] G. Oreski, G.M. Wallner, Damp Heat induced physical ageing of PV encapsulation materials, in: 12th Intersociety Conference on Thermal and Thermomechanical Phenomena in Electronic Systems, Las Vegas, USA, 2010.

[9] Klemens Grabmayer, Physikalische Charakterisierung des Vernetzungsgrades von EVA Einbettmaterialien für Solarzellen. Diploma thesis, Leoben, 2009.

[10] K. Agroui, G. Collins, Determination of thermal properties of crosslinked EVA encapsulant material in outdoor exposure by TSC and DSC methods, Renewable Energy 63 (2014) 741–746.

[11] U. Eitner, S. Kajari-Schröder, M. Köntges, R. Brendel (Eds.), Non linear mechanical properties of ethylene-vinyl acetate (EVA) and its relevance to thermomechanic of photovoltaic modules.

[12] VDI-Gesellschaft Verfahrenstechnik und Chemieingenieurwesen Hrsg., VDI-Wärmeatlas. 11., bearbeitete und erweiterte Auflage, VDI-Verlag, Düsseldorf.

[13] S. Kalpakjian, S.R. Schmid, E. Werner, Werkstofftechnik: Herstellung, Verarbeitung, Fertigung, 5th ed., Pearson Studium, Munich, 2011.

[14] G. Stollwerck, W. Schoeppel, A. Graichen, C. Jaeger, M. Kollesch, Polyolefin Backsheet Protects Solar Modules for a Life Time, in: 28th European Photovoltaic Solar Energy Conference and Exhibition, Paris, France, 2013.

[15] G. Oreski, G. Pinter, Aging Characterization of Multi-Layer Films Used As Photovoltaic Module Backsheets, in: 28th European Photovoltaic Solar Energy Conference and Exhibition, Paris, France, 2013.

[16] G. Oreski, Untersuchung des Delaminationsverhaltens von Folienverbunden für die Einkapselung von PV-Modulen. Master thesis, Montanuniversitaet Leoben, 2004.

[17] G.W. Ehrenstein, G. Riedel, P. Trawiel, Thermal analysis of plastics: Theory and practice, Carl Hanser Verlag, Munich, 2004.

[18] K. Looney, B. Brennan, Modelling the correlation between DHT and true field lifetimes for PET based backsheets, in: 29th European Photovoltaic Solar Energy Conference and Exhibition, Amsterdam, Netherlands, 2014.

[19] G. Oreski, G.M. Wallner, Aging mechanisms of polymeric films for PV encapsulation, Solar Energy 79 (2005) 612–617.

[20] G.W. Ehrenstein, S. Pongratz, Beständigkeit von Kunststoffen, 1st ed., Carl Hanser Verlag, Munich, 2007.

[21] W.J. Gambogi, J.G. Kopchick, T.C. Felder, S.W. MacMaster, A.Z. Bradley, B. Hamzavy, E.E. Kathmann, T.J. Stika, T.J. Trout, L.G. Garreau-Iles, T. Sample,

Backsheet and Module Durability and Performance and Comparison of Accelerated Testing to Long Term Fielded Modules, in: 28th European Photovoltaic Solar Energy Conference and Exhibition, Paris, France, 2013.

[22] W.J. Gambogi, H. Yushi, J.G. Kopchick, T. Felder, S.W. MacMaster, A.Z. Bradley, B. Hamzavytehrany, B.-L. Yu, K.M. Stika, J.T. Trout, L. Garreau-Iles, O. Fu, H. Hu, Assessment of PV Module Durability Using Accelerated and Outdoor Performance Analysis and Comparisons, in: 40th IEEE Photovoltaic Specialists Conference, Denver, USA, 2014.

[23] C. Ramesh, Crystalline Transitions in Nylon 12, Macromolecules 32 (1999) 5704–5706.

[24] Mettler-Toledo AG, UserCom: Interpretation von TMA-Kurven, 2001.

[25] International Organisation for Standardisation, ISO 11359-2, Plastics-Thermomechnical Analysis (TMA). Determination of CTE and Tg, 1999.

[26] DIN, Normausschuss Kunststoffe (FNK), Bestimmg der Thermischen Längenausdehnungskoeffizienten, 1980.

[27] International Organisation for Standardisation, ISO 527-3, Determination of Tensile Properties - Test conditions for films and sheets, 1995.

[28] International Organisation for Standardisation, ISO 11357-3, Plastics-Differential scanning calorimetry (DSC) - Part 3: Determination of temperature and enthalpy of melting and crystallization, 1999.

[29] E. Baur, J.G. Brinkman, T.A. Osswald, E. Schmachtenberg, Saechtling Kunststoff Taschenbuch, 30th ed., Carl Hanser, Munich, 2007.

[30] C. Choy, F. Chen, E. Ong, Anisotropic thermal expansion of oriented crystalline polymers, Polymer 20 (1979) 1191–1198.

[31] R. Androsch, Melting and crystallization of poly(ethylene-co-octene) measured by modulated d.s.c. and temperature-resolved X-ray diffraction, Polymer 40 (1999) 2805–2812.

[32] M. Brogly, M. Nardin, J. Schultz, Effect of Vinylacetate Content on Crystallinity and Second-Order Transitions in Ethylene–Vinylacetate Copolymers, Journal of Applied Polymer Science 64 (1997) 1903–1912.

[33] Y.-L. Loo, K. Wakabayashi, Y.E. Huang, R.A. Register, B.S. Hsiao, Thin crystal melting produces the low-temperature endotherm in ethylene/methacrylic acid ionomers, Polymer 46 (2005) 5118–5124.

[34] F. Ensslen, Zum Tragverhalten von Verbund-Sicherheitsglas unter Berücksichtigung der Alterung der Polyvinylbutyral-Folie. Doctor Thesis, Bochum, 2005.

[35] W. Grellmann, S. Seidler, Kunststoffprüfung, 2nd ed., Carl Hanser Verlag, Munich, 2011.

[36] G.M. Wallner, K.J. Geretschläger, M. Dankl, I. Hinersteiner, Aging Behavior of Polyamide Based Backsheet Films, in: 28th European Photovoltaic Solar Energy Conference and Exhibition, Paris, France, 2013.

[37] E.S. Ogunniran, R. Sadiku, S. Sinha Ray, N. Luruli, Morphology and Thermal Properties of Compatibilized PA12/PP Blends with Boehmite Alumina Nanofiller Inclusions, Macromolecular Materials and Engineering 297 (2012) 627–638.

[38] T. Ishikawa, S. Nagai, The gamma -> alpha Partial Transformation in Nylon 12 by Drawing, Makromolekulare Chemie 182 (1981) 977–988.

[39] S. Gogolewski, K. Czerniawska, M. Gasiorek, Effect of annealing on thermal properties and crystalline structure of polyamides. Nylon 12 (polylaurolactam), Colloid Polymer Science 258 (1980) 1130–1136.

[40] N. Hiramatsu, K. Haraguchi, S. Hirakawa, Study on Transformations among alpha, gamma, gamma' Forms in Nylon 12 by X-Ray and DSC, Japanese Journal of Applied Physics 22 (1983) 335–339.

[41] S. Rhee, J.L. White, Crystal Structure and Morphology of biaxially oriented polamide 12 films, Journal of Polymer Science: Part B: Polymer Physics 40 (2002) 1189–1200.

[42] A. Frick, C. Stern, DSC-Prüfung in der Anwendung, Carl Hanser Verlag, Munich, 2006.

[43] T. Ishikawa, S. Nagai, Thermal Behavior of alpha Nylon 12, Journal of Polymer Science Part A-2: Polymer Physics 18 (1980) 1413–1419.

[44] M. Koehl, M. Heck, S. Wiesmeier, J. Wirth, Modeling of the nominal operating cell temperature based on outdoor weathering, Solar Energy Materials and Solar Cells 95 (2011) 1638–1646.

CHAPTER III:

INVESTIGATIONS IN LONG-TERM AGING PROCESSES

3 Introduction to investigations in long-term aging processes

To simulate failures in polymeric materials, which would be observed in the field, accelerated aging via enhanced stress loads (e.g. temperature, humidity, UV irradiation) in research, is used. In PV industry, discussions about reliability testing of materials/modules are still holding on as it is beyond controversy that accelerated aging on components of PV modules via enhanced stress loads can induce degradation mechanisms which are not occurring during outdoor operation. For example the discussion on the relevance of the enhanced stress loads and/or duration in the standard damp heat (DH- 85°C/ 85 % RH for 1000 h; IEC 61215) test is still going on [1] [2]. For research it is established to extent the exposure up to 2000 h in case of polymer testing as it gives a better correlation to failure mechanisms in outdoor use. But it is still a test procedure to determine the infant failures of the used polymers. Therefore a further discussion is about combining the DH test with UV irradiation in the standard as it includes the main stress factors (especially for polymers) during service life of a module.

Also of special interest is the question, whether the individual components/materials should be tested as single materials or laminated within a PV module. On the one hand component testing would simplify sample preparation, lower the costs and offer more testing options for the materials as they are often destructive. On the other hand there remains always the important question of material (in)compatibilities and synergistic effects and thus, how results of tested single aged materials correlate with materials aged within PV modules. Interestingly no literature could be found which deals with this question.

In case of solar cell encapsulants, testing of whole modules is preferred as some interactions (e.g. PID, snail tracks, corrosion, yellowing…) can`t be reproduced by aging of the single materials. Merely a principal applicability, pre-selection or process improvements can be achieved by testing of encapsulants as single materials.

Accelerated aging and testing of backsheet films, instead, seem to be less critical with respect to the installation situation as fewer failure/degradation cases occur in combination with other PV module components. For repetition -reported failures of backsheets are delamination within the multi-layer laminate, embrittlement leading to cracks or yellowing etc. [3] [4] [5]. Yellowing of backsheets, however, is reported to have no influence on the electrical performance of the modules [3]. The worst failures within backsheets are cracks and delaminations as they allow enhanced water vapor and oxygen ingress into the PV module and can cause safety problems due to the loss in isolation properties. Water vapor is known to have a critical impact on various degradation phenomena like corrosion of metal-, cell parts, potential induced degradation (PID), snail tracks of PV modules and encapsulant decomposition [6] [7]. Therefore, these failure modes can reduce the performance of a PV module and shorten its lifetime.

Previous studies have shown that hydrolysis is the dominant aging mechanism of PET under DH conditions, whereas the other materials used in the backsheets like e.g. fluoropolymers but also polyamides are not affected significantly by exposure to high humidity at elevated temperatures [8] [9] [10] [11]. Hydrolysis of PET results in chain scission (=polymer degradation) leading to embrittlement, but also to physical aging processes like post-crystallization. Both may lead to a loss in the mechanical stability like e.g. crack formation in the inner PET layer of the backsheets [11] [12] [13]. Therefore under DH aging conditions the PET core layer defines the reliability of the whole backsheet.

Published results, where enhanced temperatures and humidity combined with UV was used, focused on the aging mechanisms of the encapsulants in whole modules [14]. Peike showed that this combination showed the best correlation with the mechanisms detected for outdoor exposure of PV modules, but in relation to the encapsulant. Eder et al. also showed that this combination leads to significant yellowing in modules which can be referred to the EVA encapsulant [15]. This clearly indicates the combined UV and DH aging is very critical to the encapsulant. However there are some works published where some failure modes of the investigated PV modules

from field were related also to the backsheet as thoroughly discussed in part I of this work. All three failure modes can be observed during DH aging after more or less time, but the absorption of UV light of the outer/inner polymer layers in the backsheets can also induce yellowing and/or loss in mechanical strength due to photo-oxidation, which leads to cracking [16] [17]. Liu et al. reported cracks and yellowing of backsheets after UV aging [18]. Summarized it can be said, that UV aging has some impact on the reliability of backsheets. However, the resulting question is how much and its relevance as the backsheet is incorporated in the PV module and therefore to some part “protected” as the glass and the encapsulant in front of the backsheet are absorbing parts of the incoming UV light [19].

In the third part of this work all artificial aged backsheets were exposed as single films and laminated within PV modules. All initial samples (module and single sheets) will be investigated as well as the artificial aged ones. The aging method chosen in chapter 3.2.1 is the DH storage up to 2000 h which was applied on samples from four different PET based backsheets. The stage of hydrolytic degradation/chain scission was determined by differential scanning calorimetry (module and single aged films) and tensile tests (single aged films). In order to support the results, additional rheological measurements were carried out to verify the assumption of polymer chain degradation (decrease of average molecular mass) upon aging. The influence of material interactions on the reliability of the PET core layer within the PV module will be discussed.

In chapter 3.2.2 the focus was on the simultaneously impact load of enhanced temperature (50°C), humidity (80 %) and irradiation (300-2800 nm metal halide lamp, 1000 W/m²) for 1000 h on samples from six different backsheets. Due to the usage of a halide lamp with also longer wavelengths (300- 2800 nm) a warm up of the PV modules to 70-80°C should be taken into account [20]. Differences between results for the single to module aged sheets will give a conclusion about the temperature influence on the aging mechanisms.

3.1 Experimental procedure

In chapter 3.2.1 and 3.2.2 the aging behavior of four and six different types of backsheets from three different producers was investigated, all of them containing PET core layers with one exception. The outer/inner layers of the backsheets were (i) fluoropolymers (symmetric composition) or (ii) stabilized PET on the outer side and ethylene vinylacetate (EVA)/ polyethylene (PE) as primer on the inner side or (iii) polyamide 12 (PA 12). (iiii) The sixth material was a coextruded 3-layered backsheet consisting mainly of PA 12. Test modules comprising of a glass front sheet (float glass, 2 mm), fast cure EVA as encapsulant (Vistasolar 486.00, SolutiaSolar GmbH, 455 µm), 4 polycrystalline Si-cells and polymeric backsheets were fabricated in a standard lamination process. The composition of all test modules was identical except for the type of backsheet used, a description of the backsheet films investigated within chapter 3.2.1 (B1- B4) and chapter 3.2.2 (B1- AAA) is given in Table 1.

Table 8: List of backsheets used

abbr.	inner layer	core layer		outer layer	thickness [µm]
B1	PVF *(37)*	PET *(250)*		PVF *(37)*	340
B2	PVDF *(19)*	PET *(250)*		PVDF *(19)*	325
B3	EVA/PE *(125)*	PET *(190)*	aluminum *(12)*	PET *(50)*	390
B4	EVA/PE *(125)*	PET *(190)*		PET *(50)*	370
APA	PA 12 *(25)*	PET *(250)*		PA 12 *(25)*	305
AAA	PA 12 *(25)*	PA 12 *(300)*		PA 12 *(25)*	350

The single backsheet films and one set of test modules were exposed to damp heat (DH) conditions at 85°C and 85 % relative humidity (RH) for 1000 and 2000 h in chapter 3.2.1 and to 50°C (leads to about 70-80°C temperature in module), 80 % RH and 1000 W/m² (300-2800 nm) for 1000 h in chapter 3.2.2. The impact of UV irradiation in chapter 3.2.2 was equivalent to about 1 year outdoor operation with a global irradiation dose of 1000 kWh/m² as an enhanced incoming of UV light of about

10 % is reached with metal halide radiation sources. Test conditions of the climate and irradiation (Climate) as well as the DH storage are summarized in Table 9. A second set of test modules and backsheets were kept as original reference samples in both chapters.

Table 9: Test conditions of applied accelerated aging tests

name	temperature [°C]	irradiation [W/m²]	irradiation source	humidity [%]
DH	85	-	-	85
Climate	50	1000	300-2800 nm metal halide lamp	80

The thermal behavior was characterized with differential scanning calorimetry (DSC) using a Perkin Elmer DSC 4000. Measuring program and parameters are listed in Table 10. Samples of the backsheets (~10 mg) were cut and put in 50 µl pans with perforated lids. Samples of module sheets were taken from the edge areas of the modules. For every evaluation, an average of at least two sample runs was taken. Melting points, melting enthalpies and crystallization temperatures were evaluated according to ISO 11357-3 [21].

Table 10: Experimental parameters for DSC measurements (nitrogen atmosphere)

	start	end	time/ramp
isotherm segment	20°C		5 min
1. heating	20°C	270°C*	10°C/min
isotherm segment	270°C*		5 min
2. cooling	270°C*	20°C	10°C/min
isotherm segment	20°C		5 min
3. heating	20°C	270°C*	10°C/min

* for AAA samples 230°C

Tensile tests were carried out on a Zwick Z001 according to EN ISO 527-3 [22], the test specimen were cut before accelerated aging according to specimen type 2 (150 mm x 15 mm). A load cell of 1 kN was used due to expected loads of ≤900 N. The test speed

used was 50 mm/min. From a total of at least five specimens for each test series, the average values for yield stress (σ_Y), yield strain (ε_Y), stress at break (σ_B) and strain at break (ε_B) were deduced. The DH aged backsheets were measured only in machine direction due to the high amount of samples necessary for all measurements. As the peeling-off of the backsheets from the modules was not possible, only single backsheets were measured with this technique.

As a good verification of changes in molecular mass, melt rheological measurements were carried out on an Anton Paar MCR 301 device in oscillatory mode in chapter 3.2.1. A parallel plate geometry (diameter 25 mm) was used. As the PET core layer is the dominating material in the backsheet and to eliminate overlaying effects the outer and inner layers and the adhesives were removed. As this sample preparation is a very demanding and time-consuming task only single backsheets were measured. To achieve a gap width, i.e. sample height, of 0.6 mm the dried films were carefully stacked to ensure a bubble free melt. Oszillation amplitude γ was 6 % and the angular frequency ω was 1 rad/s. The measurements were done at 270 °C under nitrogen atmosphere.

UV/Vis/NIR measurements in chapter 3.2.2 were done using a Lambda 950 UV/Vis/NIR spectrometer with integrating sphere. Hemispherical and diffuse reflectance spectra were recorded from 250 to 2500 nm in 5 nm steps. From these results also CIE L*a*b color scale evaluation was done. For the assessment the b values were used, as this is the parameter for indicating yellowing. The b value can range from -80 for yellow to +80 for blue. Hence the more positive the value for b the yellower is the sample.

3.2 Results and discussion

3.2.1 Aging induced changes on module and component level under DH storage

In the following the results will be described and discussed considering at first the differences in the DSC curves between single backsheets and sheets incorporated into modules in the original state. Then the aging (DH storage) induced changes on module and component level will be compared. These results obtained from the thermal analysis of the polymeric sheets will then be compared to results from tensile tests (only from the single backsheets) and the rheological measurements on the PET core layers. The description of the results is focused on the aging behavior of the PET core layer, which is mainly responsible for the mechanical stability [9] [10].

3.2.1.1 DSC results

Initial state

Processes like melting of crystallites formed during post-crystallization or tempering are irreversible as their impact on the DSC curve can be seen only in the first but not in the second heating run. Glass transitions or the thermodynamic melting of a polymer are reversible effects and will, thus, be seen in each heating run irrespective of the history of the polymer. Therefore in the first heating curve of a DSC measurement all reversible and irreversible effects are determined including the information on the thermal and mechanical history of a polymer like physical changes (post-crystallization, changes in the crystal structure…) having taken place in the material upon processing or aging [23]. It reflects the so called “current state of a polymer” and is the commonly used curve for the evaluation of the application relevant behavior of a material. The second heating run gives information on material specific constants and includes only reversible effects. It plays a subordinate role for the analysis of aging induced changes.

The information obtainable from the crystallization behavior (= cooling run) is rarely discussed in standard literature. However, it bears evidence about changes in the chemical structure of a material like e.g. the decrease of molecular mass due to

polymer chain scission etc. [23] [24]. As this work focuses on the aging behavior of PET which means post-crystallization (physical aging) and hydrolysis (chemical aging) both, 1.heating and cooling curves were evaluated and are presented in this point of investigation.

Post-crystallization of polymers results in an increase in the melting enthalpy as well as a shift to higher melting temperatures. Hydrolysis induces polymer chain scission which goes along with a decrease in the molecular mass and leads to a shift of the crystallization temperature to higher values as well as to an increase in the crystallization enthalpy [23].

Exemplarily the DSC runs (1.heating, cooling, 2.heating) of the backsheet B1 (single and module laminated sheet of the initial state) are shown in Figure 57. In the 1.heating curve, the first melting peak can be attributed to the PVF outer layer (T_m = 194°C). The highest melting peak with respect to temperature and area is attributed to the melting of the main fraction of the PET crystallites (T_m = 256°C).

A secondary melting peak of the PET core layer was found at 219°C. This secondary melting peak can be attributed to small crystallites, which are formed during exposure at elevated temperatures. This peak was not detected in the second heating run which confirms its irreversible, aging induced character. The first crystallization peak in the cooling curve is attributed to PET (T_c = 205°C) and the second to PVF (T_c = 169°C). At the second heating run the PVF melting peak was detected at 192°C and the PET melting peak at 248°C.

In general, all backsheets showed comparable DSC curves for samples taken from single sheets to those taken from modules (exemplarily see Figure 57). This confirms that the lamination process of the PV module, although enhanced temperatures (up to 150 °C) are involved, have no influence on the thermal properties of the backsheets. Assumedly the lamination times of maximum 30 min do not lead to physical changes in the PET core layer. As expected there were also no glass transitions and/or cold-crystallization peaks observable for PET. This is an indication for a high crystalline material [14]. PET used for PV module backsheets has to be

hydrolysis resistant, which can be achieved by enhancing the crystallinity of the material by heat treatment as well by the addition of stabilizers.

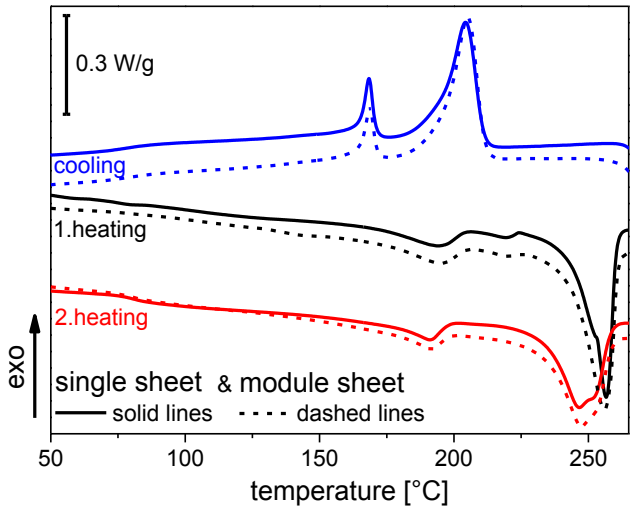

Figure 57: DSC curves of the initial state of single (line) and module laminated backsheet (dotted line) of B1

The detected temperature maxima of the peaks in the heating/cooling curves of the fluoropolymer outer layers (B1 and B2, see Figure 58), EVA/PE inner layers of B3 and B4 (see Figure 59) are compiled in Table 11. The melting peaks observed at 110 and 127°C of samples B3 and B4 are attributed to the melting of the inner layers (see Figure 59). Crosslinked EVA commonly used as encapsulant for PV modules has a vinylacetate (VA) content of ~30 % (w/w) and melts in the temperature region between 30 and 70°C [25]. Therefore the first melting peak at 110°C indicates that the ethylene-vinylacetate has a very low VA content and mainly consists of longer chain segments of ethylene (melting region PE~ 130-145°C). The second melting peak at 127°C can be attributed to an additional PE layer in the backsheet. Both assumptions were confirmed by additional ATR imaging measurements.

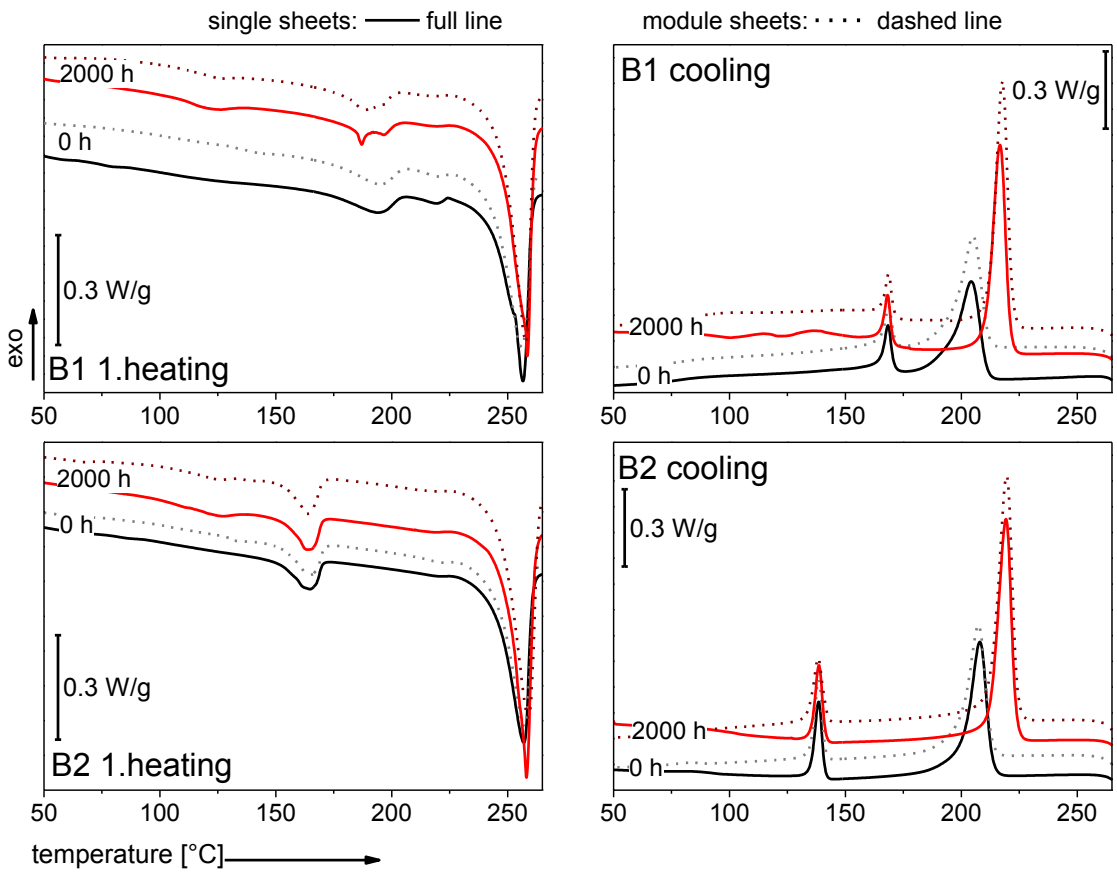

Figure 58: DSC heating and cooling curve of B1 (top) and B2 (bottom) for the initial state and aged (2000 h DH) samples

Table 11: Detected peaks from the DSC heating/cooling curve of the outer and/or inner layers of the single backsheets in the initial state

Backsheet		1.Heating melting peak [°C]				Cooling cooling peak [°C]			
Abbr.	**Layer**	**single sheet**		**module sheet**		**single sheet**		**module sheet**	
B1	PVF	194		195		168		169	
B2	PVDF	165		165		139		139	
B3	EVA/ PE	109	128	109	127	96	114	95	113
B4	EVA/ PE	111	127	111	126	99	113	98	112

The melting region of PET for all backsheets was found to be rather broad (230-270°C) but the maximum of the peak was constant in a very narrow temperature range between 256 and 258°C (standard deviation of each materials melting point

smaller than 0.4°C). Semi-crystalline polymers have more or less perfect crystallites with different lamellae thicknesses [23]. A broad melting range, as observed for our samples, reflects this non-uniform structure. The maxima in the crystallization curves of PET varied between 204 and 214°C (standard deviation smaller than 1.2°C). For the backsheets B3 and B4 a double peak of PET in the crystallization curves can be seen (see Figure 59), which can be attributed to the two PET layers (core and outer layer) which vary in composition. The outer PET layer is claimed to be hydrolysis- and UV resistant, thus, a different additive formulation, molecular mass distribution and/or crystallinity of the material is expected.

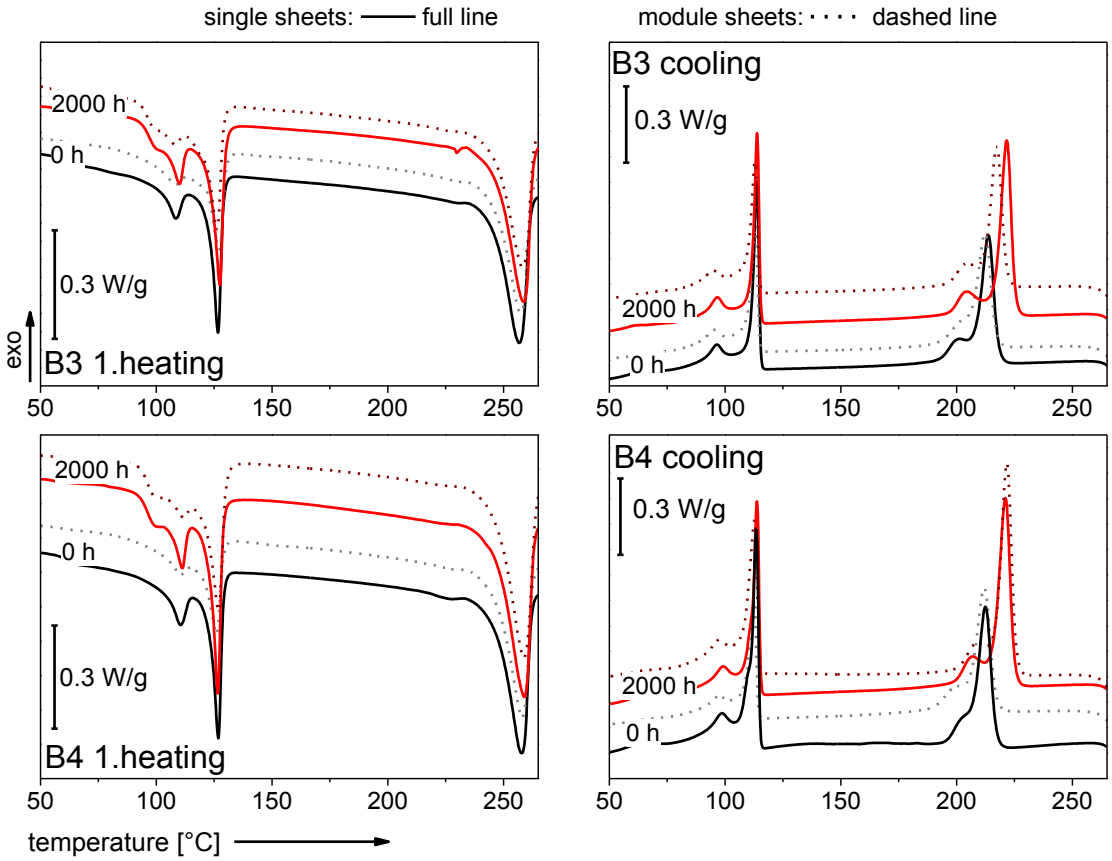

Figure 59: DSC heating and cooling curves of B3 (top) and B4 (bottom) for the initial state and aged (2000 h DH) samples

Heat/crystallization enthalpies are not as precise as melting/cooling temperatures. Usually backsheets are multilayer films consisting of different polymers. As the whole weight of the sample (with all layers) is used for the calculation of the enthalpies this results in a larger uncertainty. Furthermore, small differences in the thicknesses of the

individual layers within the multilayer composite of a backsheet are observed. Also the difficult sample preparation of the backsheets that have been laminated within the modules introduces additional uncertainty as a clear separation of the backsheet from the encapsulant is a very demanding task.

Artificially aged backsheets (DH storage)

The maxima of the melting peaks of the PET materials lie between 258 and 259°C with a standard deviation smaller than 0.3°C. In comparison to the initial state samples, this means a small increase in the melting temperature of about 1-2°C. The melting enthalpies, on the other hand show a significant increase (see Table 12). Both facts indicate a post-crystallization, which generally appears due to aging of PET at elevated temperatures [23]. The mechanism is enhanced due to the storage over the glass transition temperature (~80°C) of PET.

Table 12: PET melting enthalpies of initial and aged single and module laminated backsheets

	Melting enthalpy (0 h)				**Melting enthalpy (2000 h)**			
	Sheet		Module		Sheet		Module	
Abbr.	**[J/g]**							
B1	30,9	±0,2	33	±0,7	34,8	±0,7	41,4	±2,6
B2	32,4	±0,4	33	±0,3	36,4	±0,9	41	±1
B3	25,6	±0,8	26,6	±1,4	28,2	±0	24,7	±0,2
B4	29,6	±0,2	28,3	±0,2	33,7	±0,2	31	±1,4

The most significant changes of the initial to the aged sheets can be seen in the cooling curve of the DSC runs. Changes in the DSC cooling curve are related to chemical changes in the polymers [23]. For example polyolefins build a double crystallization peak when molecule chain scission happens due to aging [23] [17]. Polycondensation polymers are susceptible to hydrolysis, which in case of PET is the cleavage of the ester groups in the polymer chain by addition of water. Also polyamides are susceptible to hydrolysis, but as shown in chapter 2.2.2 this aging effect was not detected for the DH stored samples. The hydrolysis reaction leads to

chain scission and therefore reduction of the average molecular weight. Crystalline parts of the polymer can be seen as impermeable to water vapor, therefore hydrolysis occurs solely in amorphous parts of the polymer or imperfections in the crystalline zones [26] [27]. All produced terminal groups during artificial aging act as nucleating agents for new crystals which results in the formation of smaller crystallites and significantly higher crystallization temperatures [23] [24] [26]. Besides the higher crystallization temperature for the degraded polymer also a narrowing of the crystallization peak can be observed. The polymer itself is more mobile and therefore the crystallization process is faster [28].

The maxima of the PET crystallization peaks of the various backsheet materials were found between 217 and 222°C with a standard deviation smaller than 0.4°C. In comparison to the initial samples, this means an increase in the crystallization temperature of about 5-13°C. The increase in the maximum of crystallization temperature for B1, B2 and B4 are identical for samples taken from the single backsheets and taken from the modules (see Table 13). The slight temperature increase of +1°C for the samples of the modules with B2 and B4 seems negligible.

Table 13: Increase in the maximum of PET crystallization temperatures for the initial to the 2000 h DH aged samples

	increase in the crystallization temperature [Δ°C]	
	sheet sample	**module sample**
B1	13	13
B2	11	12
B3	8	5
B4	9	10

In contrast to the other samples, for B3 a significant increase of the crystallization temperatures of the PET core layer was observed for the samples taken from the single sheets to those taken from the module (see Table 13). The reason for this effect

is maybe the additional aluminum barrier layer which is the only difference between B3 and B4. In the module, with the impermeable glass front sheet on the one side and the impermeable aluminum layer between the outer and core layer on the other side the ingress of water vapor to the PET core layer is reduced and therefore hydrolysis/degradation is reduced [20]. As the same shift in the crystallization temperature of the outer PET layer is measured for both sheets, single and module laminated, this assumption is supported as the pathway for water vapor from the outer side is feasible in both cases (sheet and module aging).

The DSC results showed that for reliability testing of backsheets for PV modules no significant differences between single and module aged sheets can be found. The only exception is backsheet B3 containing a gas tight Al barrier layer.

As described above evidence for the reliability and long-time stability of backsheets with PET layers can be deduced from the aging related changes as derived from the thermal analysis. DSC results of the aged backsheets taken from single and module sheets indicated post-crystallization and hydrolysis/degradation of PET. Both aging mechanisms cause embrittlement. As hydrolysis induces chains scission it gives additional possible pathways for water vapor and oxygen. Especially permeation of water vapor is often discussed in literature as a problem which can cause corrosion of metallic components as well as polymer degradation of the encapsulant [29] [30] [31].

To correlate the detected results with the mechanical behavior of the backsheets tensile tests were performed and the results are shown and discussed in the next section.

3.2.1.2 Tensile test results

Exemplarily the stress-strain curves of backsheet B2 in the initial state and after 1000 h-2000 h aging under DH conditions are shown in Figure 60. In the initial state, the investigated materials exhibit a ductile behavior with distinct yield points. After 1000 h DH aging, an increase of the yield stress and a decrease of the strain at break value were detected for all materials. The increase of the yield stress is an indicator for physical aging like e.g. post-crystallization. A decrease in the strain at break values

can be related to chemical aging with chain scission and, therefore, with polymer degradation via hydrolysis in respect to PET [10]. The strain at break values for all materials decreased with increasing aging time (see Figure 61).

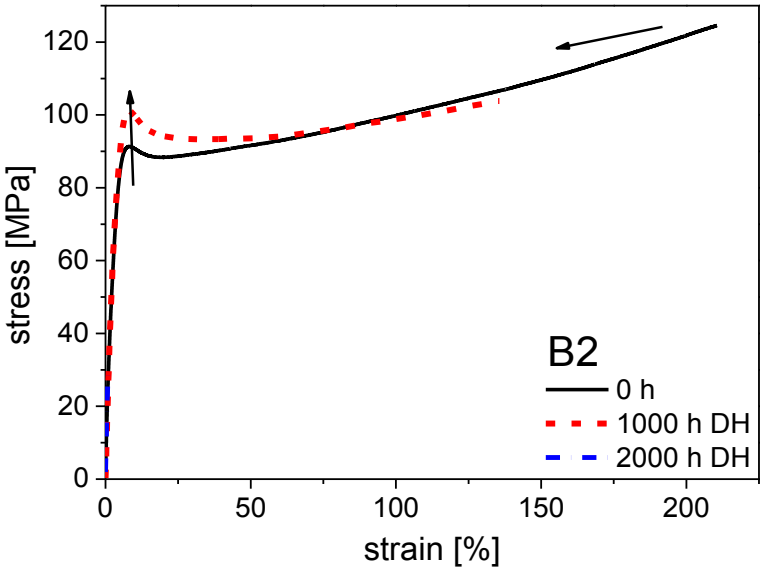

Figure 60: Stress-strain curves of backsheet B2 in the initial state, after 1000 h, and after 2000 h DH storage

The 2000 h aged tensile test samples did not show a yield point due to the high embrittlement of the PET layers. Strain at break decreased to values below 1 % (Figure 61). Breakage of samples during tensile tests starts on a defect. This defect has a notching effect with a stress concentration where crack formation begins and results in a full break of the according polymer layer. Defects can be generated mechanically from sample preparation, different thickness distributions, enclosures, bubbles, density differences occurring due to hydrolytic degradation etc. The initiation of crack formation differs especially for aged samples as the spreading of defects is statistical. Therefore the high standard deviation of strain at break for the 2000 h DH aged samples can be attributed to differences in the crack initiation from local defect spots. For B3 and B4 the inner EVA layer showed a ductile behavior with a very high elongation at break after the breakage of the other (relevant) layers (see Figure 62).

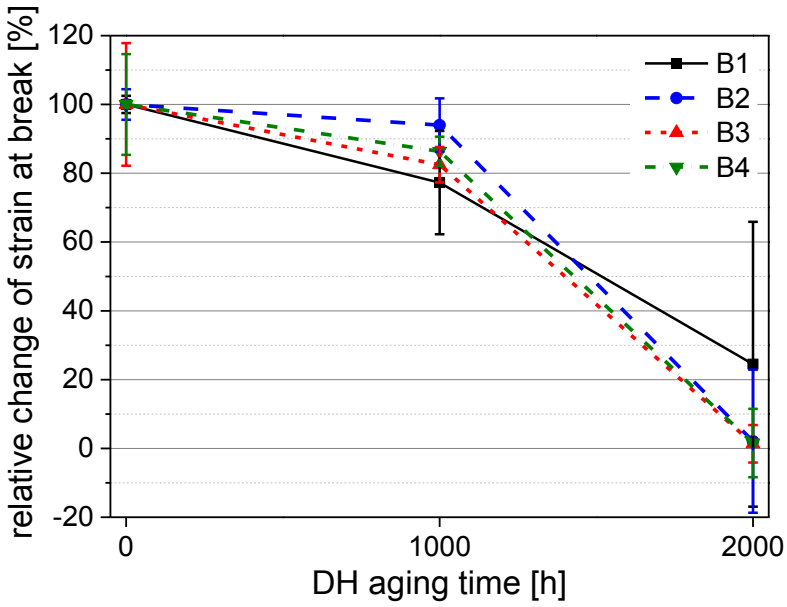

Figure 61: Relative change of the strain at break values of the backsheets B1-B4 in the initial state, after 1000 h and after 2000 h DH storage

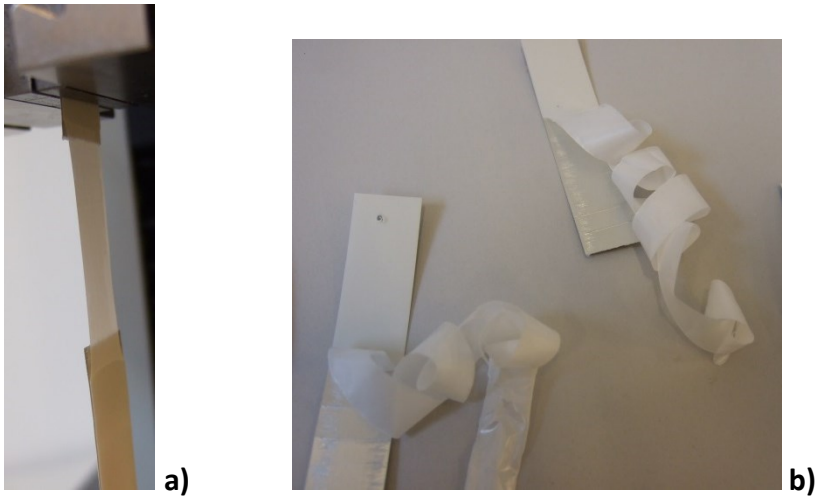

Figure 62: Tensile test sample of 2000 h DH aged B3 **a)** during and **b)** after testing

The increase in the yield stress followed by the disappearance of the yield point indicated post-crystallization and the decrease in strain at break values indicated chain scission (hydrolysis). Therefore tensile tests proved to be a good tool for detecting aging in PET based backsheets. Post-crystallization and hydrolysis have also been detected via the DSC measurements and are in good correlation with the tensile test results.

3.2.1.3 Oscillatory time sweep test results

Oscillatory time sweep tests, often called thermal stability tests, were performed to examine if the PET materials show time-dependent rheological properties due to thermal degradation and/or chemical reactions. Looking exemplarily on the results of backsheet B1 two characteristic phenomena are clearly visible, the strong drop of melt viscosity after DH testing and the increasing viscosity with increasing measuring time (Figure 63). The lower values of viscosity after DH storage (dashed line) result from hydrolytic degradation and by that from a decrease in molar mass. At temperatures higher than T_m, an increasing viscosity with time is a well-known effect observed in thermal stability tests of PET and can be related to (poly)condensation which is the dominating process under nitrogen atmosphere [32]. By that, molar mass M increases which is shown by an increasing zero shear viscosity η_0. This well-known relation is given by $\eta_0 = KM^{\alpha}$, K and α are polymer specific constants. Time-sweep tests were performed at ω = 1 rad s^{-1} and, as shown in Figure 63 (inserted graph) at this angular frequency the η_0 is reached.

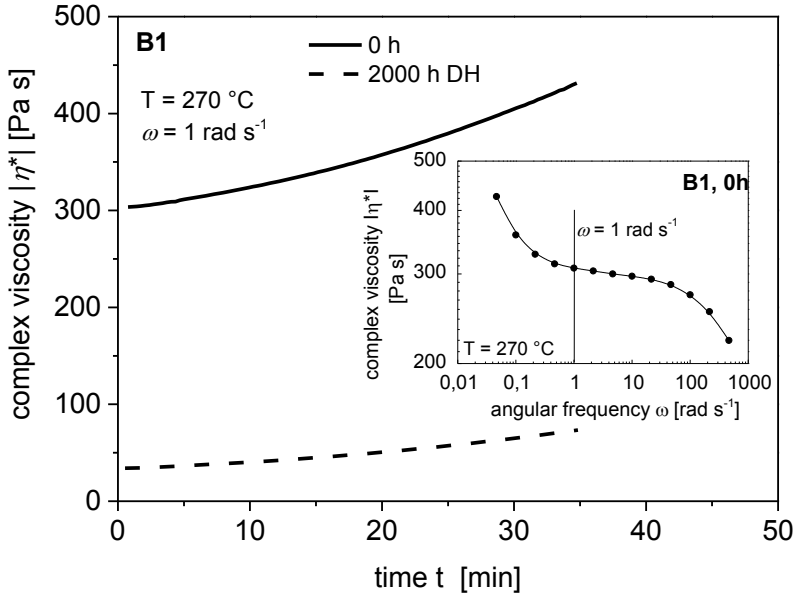

Figure 63: Complex viscosity |η*| at ω= 1 rad s^{-1} and 270°C as a function of time of the core PET layer taken from an initial and aged single backsheet B1

However, due to changes in the molar mass long-term rheological methods like frequency sweeps and their interpretation are an awkward procedure. Only a short

time window of about 10 minutes (including sample load) is available [33] [34]. Therefore, and to give a qualitative proof of chain scission (decreasing molar mass) during DH storage the η_0 after a measuring period of 1 min was read out and compared (Figure 64). All backsheets show this strong decrease in viscosity reflecting the hydrolytic degradation.

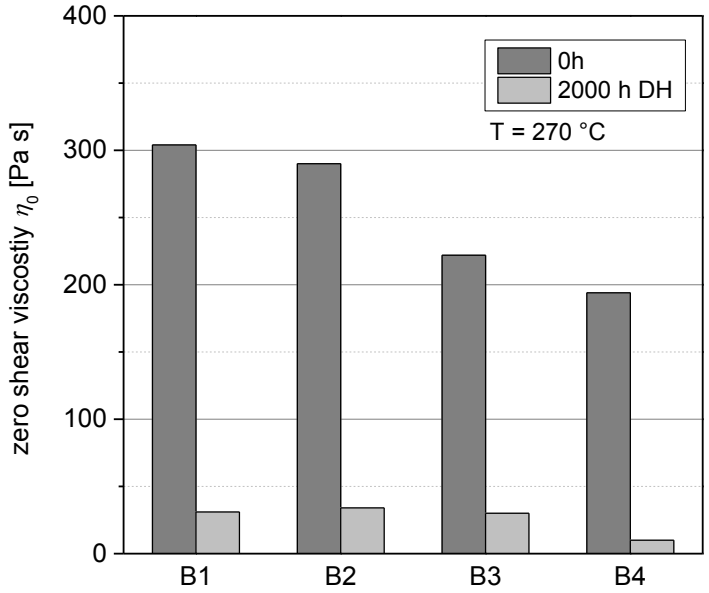

Figure 64: Complex viscosity |η*| at ω= 1 rad s^{-1} and 270°C of the PET core layer taken from the initial and aged single backsheets

3.2.2 Aging induced changes on module and component level under climate and irradiation

In the following the results will be described and discussed considering at first the differences in the DSC curves between single and module backsheets for the initial and artificial aged (Climate) state of PET and then in consideration of all other layers. From the thermal behavior of the backsheets a conclusion about the physical and chemical aging will be given. Then tensile test curves will be discussed to see the aging influence on the mechanical behavior. Both (physical and chemical aging) can have an influence on yellowing of the sheets. Therefore also UV/Vis/NIR measurement results will be shown.

3.2.2.1 DSC results

In Figure 65 to Figure 67 the DSC 1.heating and cooling curves for all investigated backsheets are shown. The main melting/crystallization regions were assigned in the figures to the according polymeric layers EVA, PE, PET, PA 12, PVF and PVDF. Changes in the DSC curves which will be discussed in detail are marked in the shown DSC curves.

Middle layers (PET)

PET absorbs light in the wavelength regions between 290-330 nm [17]. This absorption leads to chemical changes causing both yellowing and loss in mechanical performance [16]. As the PET layer is protected from the inner and outer layers in the backsheet, minor changes due to incoming of UV light are expected. Only B3 and B4 had also a PET outer layer. Elevated temperatures and humidity in the Climate aging can cause hydrolysis of PET as shown in chapter 3.2.1. Both chemical aging mechanisms going along with a decrease in molar mass and would be seen in changes of the PET crystallization temperature of the DSC cooling run [28] [23]. This was also confirmed from the results in chapter 3.2.1. Due to the elevated temperatures also post-crystallization can occur. This physical aging effect can be seen in the first heating run via an enhanced melting enthalpy and temperature. All these possible aging mechanisms can lead to embrittlement and cracks within a backsheet.

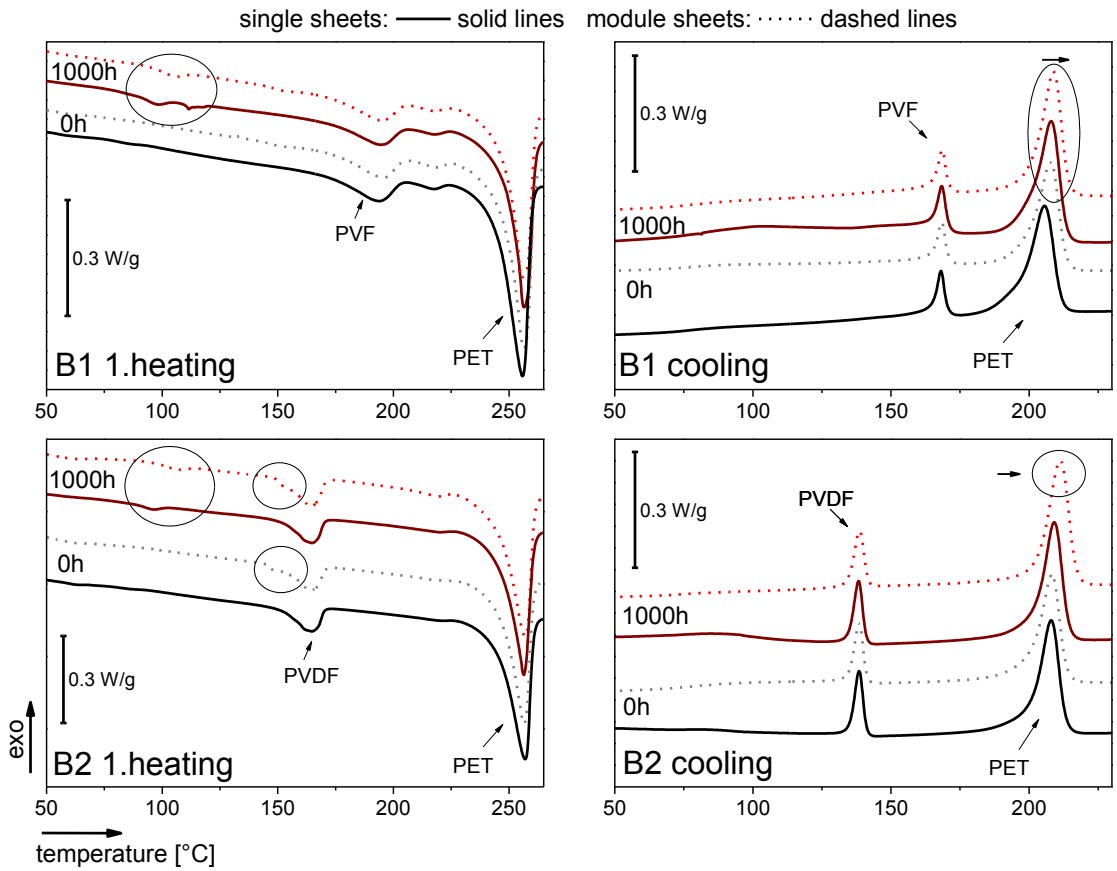

Figure 65: DSC heating and cooling curve of B1 (top) and B2 (bottom) for the initial state and aged (1000 h Climate) samples.

The PET melting enthalpies for all initial samples in the first heating run ranged between 26 and 33 J/g. Due to the temperature load during the production of the modules post-crystallization and therefore a higher enthalpy for the module samples is expected. Surprisingly B1 and B2 showed a lowered enthalpy (-1.2 and -1.6 J/g), while B3, B4 and APA showed the expected slight increase (+1.1– 2.2 J/g). However the amount of the changes in the enthalpy is not significant. Additionally in Table 14 differences in the PET melting enthalpies in the course of Climate aging are depicted and imply an uncertainty in the enthalpies. Due to the elevated temperatures at Climate storage also an increase due to post-crystallization was expected. Surprisingly just the B2 and B4 module samples showed an increase and the other samples even a slight decrease. Two main reasons can be mentioned: As the whole weight of the samples (with all layers) is used for the calculation of the enthalpies this results in a larger uncertainty. Also the difficult sample preparation of the backsheets that having

been laminated within the modules introduces additional uncertainty as a clear separation of the backsheet from the encapsulant is a very demanding task. Hence for the further discussion we focus on the melting/crystallization temperatures of the polymeric layers in the backsheets.

Table 14: Increase in PET melting enthalpies for the initial to aged single and module laminated backsheets of the first heating run

	Δ H_{PET} 0 – 1000 h [J/g]	
	Sheet	**Module**
B1	-1.9	-1.2
B2	-1.5	2.9
B3	-0.9	-1.7
B4	-1.3	3.6
APA	-3.3	-0.5

The melting region of PET in the first heating run for all backsheet samples was found to be rather broad (230- 265°C), but the maximum of the peak was constant in a very narrow temperature range between 255.9 and 258.7°C (standard deviation smaller than 0.9°C). A broad melting range, as observed with our samples, reflects a non-uniform structure due to more or less perfect crystallites with different lamellae thicknesses [23]. All backsheets showed no significant differences (≤1°C) between single to module initial as well as aged sheets (see Figure 65 to Figure 67). A small, but not significant, deviation can be seen for B3 where the melting temperature of the initial to aged module sheet increased about 1.2 to 258.7 ±0.9°C. This was also the highest detected PET melting temperature (see Figure 66). This is possibly induced by the aluminum barrier layer in between the polymer layers of this backsheet. It may induce higher temperatures in the module sheet and therefore slightly enhanced post-crystallization. As explained above elevated melting temperatures are an indication for post-crystallization. Hence from the results of the first heating curves no significant changes in crystallinities were detected. This can be attributed to the storage under the glass transition temperatures (T_g) of PET (~80°C). The storage

temperatures for the single aged sheets were around 50°C and those of the module aged sheets due to irradiation warming between 70- 80°C. Permanent temperatures above 65°C are rare even for hot climates zones under standard operating conditions without clouding [20]. Hence from our results only limited influence of weathering induced post-crystallization on the mechanical stability of the investigated backsheets is expected, as even for the module aged samples no significant differences could be seen. This can also be stated for the temperature loads and its duration during PV module production, as also here in respect to the initial samples no significant changes in the first heating runs were detected.

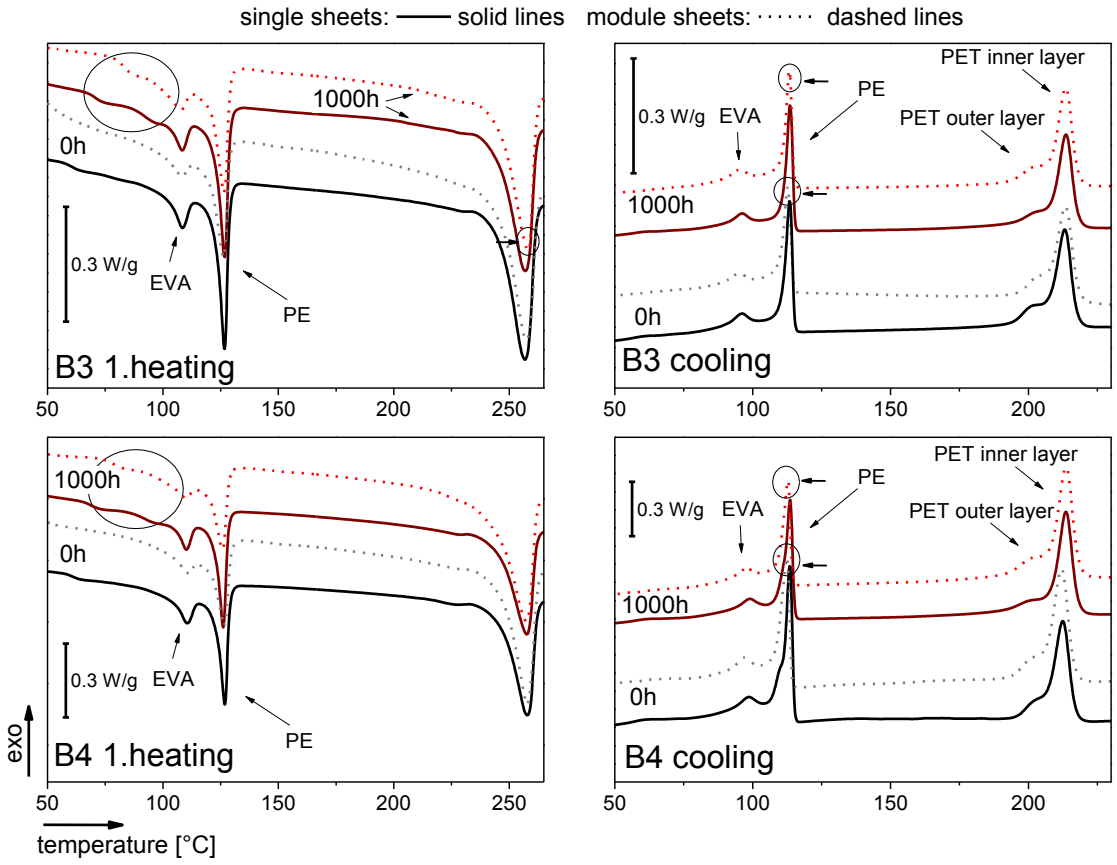

Figure 66: DSC heating and cooling curve of B3 (top) and B4 (bottom) for the initial state and aged (1000 h Climate) samples

The evaluated changes in the PET crystallization temperatures of all backsheets (except AAA- no PET layer) in course of Climate aging are shown in Table 15. The maxima of the PET crystallization temperatures for all backsheets varied between 205.4 and 213.7°C (standard deviation smaller than 0.5°C). The smallest changes were

found for B3 and APA. For the B1 initial single sheet the PET crystallization temperature was about 2°C lower (205.8°C) as all other tested samples of B1 (see Figure 65 and Table 15). As an influence on the cooling run can only be induced via chemical changes we have no explanation for this difference. The temperature loads and its duration for the backsheets during the production of the module samples with 146°C is too low for thermal chain scission [17].

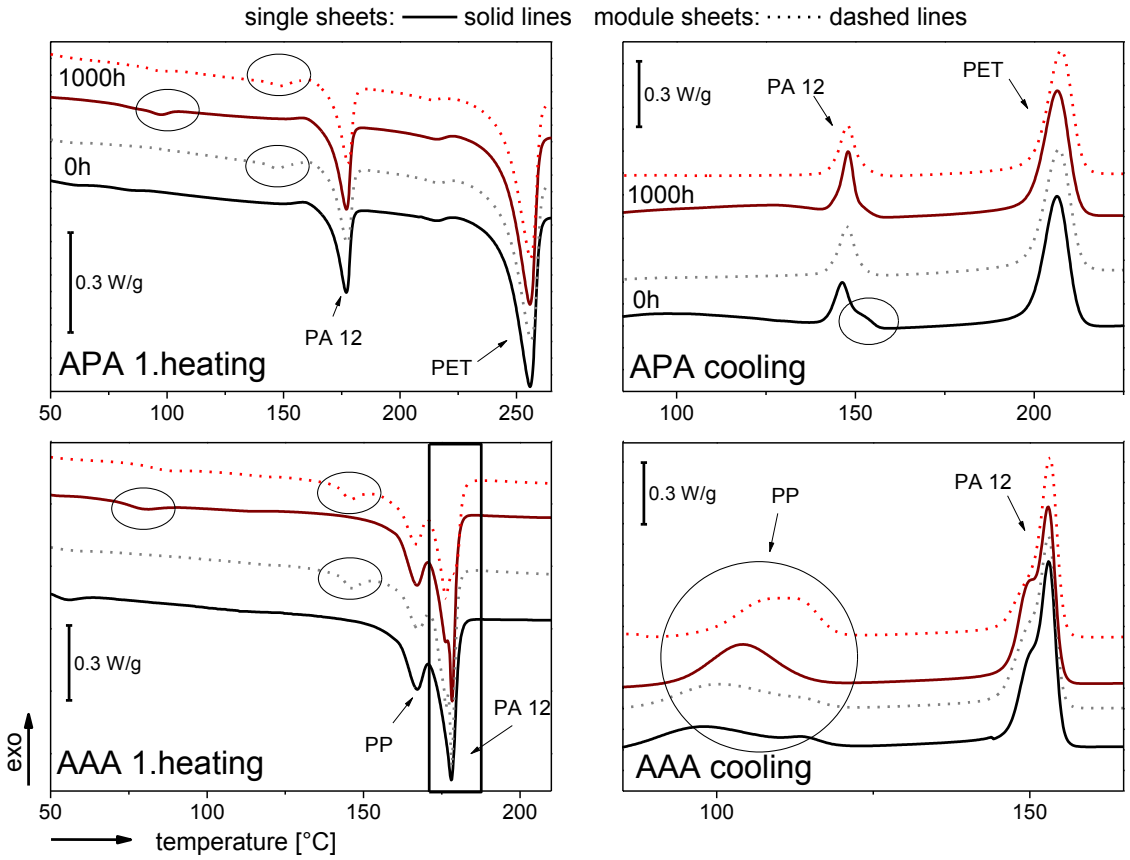

Figure 67: DSC heating and cooling curve of APA (top) and APA (bottom) for the initial state and aged (1000 h Climate) samples

For B2 an enhanced crystallization temperature (+3.1°C) only for the 1000 h aged module sheets was found (see Figure 65). This is an indication for a lowered molecular weight in comparison to the other B2 sheets [28] [chapter 3.2.1]. As it was not detected for the single aged sheet we assume the temperature difference between the single to module sheets during aging is the main driving factor for enhancing the chemical aging process. B4 showed little changes with an increase of 1.3°C for the module sheets and slightly beneath with 1.1°C for the single sheets. The evaluated

differences for the DH aged samples were significant higher. Hydrolysis is a chemical aging process and is enhanced by temperature. The storage beneath the T_g of PET (50°C; 70-80°C) and/or the lower humidity level (80 % RH) in respect to the DH (85°C/ 80 % RH) storage resulted in significant lowered chain scission due to hydrolysis. Hence from the results of the PET layers it can be concluded that no significant changes in the tensile test curves will be seen for all PET based backsheets as PET is the responsible layer for mechanical strength.

Table 15: Increase in PET crystallization temperatures for the initial to the 1000 h Climate aged sheets

	increase in the crystallization temperature of PET [Δ°C]	
	sheet sample	**module sample**
B1	2.2	1
B2	1	3.1
B3	0.2	0.1
B4	1.1	1.3
APA	0.2	0.9

Inner/outer layers

The maximum melting and crystallization temperatures of all other layers than PET in the initial state of the backsheets are listed in Table 16. All evaluated values therein have a standard deviation smaller than 0.3. In the course of Climate aging more significant changes within the outer/inner layers for B1- B4 in respect to the DH aging were detected. Differences between single to module aged sheets may give a hint to processes which are enhanced from UV light, as the single aged backsheets are directly exposed to the incoming UV irradiation. Differences for the single to module sheets (initial and aged) in the main melting peaks were only detected for PA 12 in AAA and in respect to the crystallization temperatures for PE in B3 and B4, for PA 12 in APA and AAA. For all layers additional melting peaks were observed.

Table 16: Melting peak temperatures of the outer and/or inner layers for B1- APA and of all layers for AAA (standard deviations ≤0.3) in the initial state

		1.Heating melting peak [°C]				Cooling cooling peak [°C]			
Abbr	Layer	single sheet		module sheet		single sheet		module sheet	
B1	**PVF**	194.1		195.9		168.3		168.4	
B2	**PVDF**	164.9		163.5		138.5		138.5	
B3	**EVA / PE**	108.6	127.0	108.4	126.3	96.3	113.5	95.2	112.8
B4	**EVA / PE**	110.6	126.8	110.9	126.4	98.6	113.4	97.4	112.4
APA	**PA 12**	177.1		177.3		146.5		147.6	
AAA	**PA 12**	177.9		178.2		152.8		153.0	

The fluoropolymers PVF (outer layers of B1) and PVDF (outer layers of B2) are known to have an excellent weatherability. Their strong carbon-fluorine-bonds to carbon-hydrogen-bonds from common polymers are the reason for a very low absorption in the UV wavelength region [17]. For B1 the only differences can be seen for the initial sheets compared to the aged sheets (see Figure 65). An additional small melting peak appearing after aging at about 105.4°C for the module aged sheet and slightly below for the single aged sheet at ~99.6°C was observed. This was also the case for B2 (106.2°C and 95.8°C; see again Figure 65). This small post-crystallization peak belongs to the PVF and PVDF inner/outer layers [35] [36]. The melting enthalpy is ~0.8 J/g and independent on the melting temperature and or single/module sheet. The melting peak for the module aged sheets is at higher temperatures but with no increase in enthalpy. Hence, the enhanced temperatures due to the irradiation warming of the modules induced more perfect crystallites, but not a higher degree of crystallization. This post-crystallization peak was also observed for the DH aged single and module samples of PVF and PVDF at ~125°C. This confirms the assumption of the temperature dependence for this melting peak.

One additional effect which was observed for the B2 module samples was a peak which merges with the main PVDF melting peak at 165°C. For the initial module sample the peak temperature/shoulder was at 148°C and for the aged ones at 156°C.

This peak occurs due to the “annealing” effect on the module samples during lamination. The lamination temperature for the modules was about 146°C. Therefore the occurrence of this peak at 148°C fits with the described behavior of PVDF after annealing [37] [38]. The post-crystallization starts from the amorphous phase of PVDF and so the initial nucleus or crystal lamellae grow with further storage at elevated temperatures. This is the reason for the enhanced melting temperature of this additional peak (156°C) for the aged module sample. This effect was not seen for the samples investigated in the former chapter. It indicates that the temperature loads during PV module sample production therein were lower than 146°C. It gives a hint to post-crystallization with formation of another crystal form as such processes require temperatures above a specific temperature. In [36] the additional peak was related to the arising of α-crystals into the general existing β-crystals, but the investigated samples therein were aged under DH (85°C/ 85 % RH) conditions. FTIR-ATR spectra were made to give an answer on that as there are specific absorption bands for both crystal forms [36]. It revealed no occurrence of α-crystals in this material.

EVA (inner layers of B3 and B4) degradation and yellowing during UV aging is reported to be strongly dependent on the additive system and presence of oxygen [39] [40]. Within the EVA UV induced degradation mechanisms volatile compounds such as acetic acid and hydroperoxides are formed as degradation products [40]. PET (outer layers of B3 and B4) requires an adequate stabilization against thermo-oxidation, photo-oxidation (PET absorbs UV light between 290 and 330 nm) and hydrolysis [17]. For B3 and B4 it can be said that the used EVA inner layers are with low vinyl acetate contents. This is indicated by the high melting peak at ~109°C (see Figure 66) [41]. For the PE layer the melting peak was ~127°C. For both backsheets all aged samples showed multiple peaks for EVA. For the single aged sheets two additional melting peaks at ~74 and 96°C (B3 and B4) and for the module aged sheets one additional melting peak at 87 (B3) or 82°C (B4) has been detected. During aging the ethylene chain segments of EVA are able to re-arrange and form secondary crystallization regions, which are the cause for the multiple endotherms [42]. This less organized secondary crystal phase is formed in the area between the primary crystals during

elevated temperatures [43] [44]. Another indication for that is the uniform melting peak at the second heating run. The melting enthalpy increased significant from ~6 to 15 (module sheet) and to 18 J/g (single sheet) for B3 and ~9 to 19 (module sheet) and to 23 J/g (single sheet) for B4. In the cooling curves for the PE inner layer of B3 and B4 a small decrease of crystallization temperature for the single (113.5°C ±0.2) to module sheets was observed. For the initial sample it was -0.7°C for B3 and -1°C for B4. For the 1000 h aged sample it was -0.5°C for B3 and -0.9°C for B4. The decrease for the module aged samples were lower, although these samples are to some part protected from the UV-light and therefore it has to have a lower tendency to UV chain scission. In [23] it is written that there is no influence of physical aging processes on the cooling run in the DSC. The small decrease (≤1°C) possibly occurred due to chain scission.

Aliphatic polyamides like PA 12 (outer layers of APA and all layers of AAA) have no absorption in the 200-300 nm UV wavelength range. However during processing some chromophores are built which absorb UV light at 320 nm. The absorption leads to formation of radicals, with subsequent chain scission [17]. In general this is occurring on the surface and leads to embrittlement and yellowing [45] [17]. In presence of special stabilisator systems and weatherable pigments the requirements for outdoor applications can be fulfilled [17]. In Figure 67 the DSC heating and cooling curves for all APA and AAA backsheet samples are shown. The additional small melting peak for APA 147.1°C (initial) and 148.7°C (aged) for the module sheets and 97.5°C for the single aged sheets can be attributed to a post-crystallization melting peak of PA 12. For AAA the same peaks occurred slightly above with 145.9°C (initial and aged) for the module sheets and below with 80.8°C for the single sheets. It is a post-crystallization effect due to elevated temperatures during lamination and/or aging and was already explained in chapter 2.2.2. In chapter 2.2.2 investigated AAA single sheet samples with storage under DH (85°C/ 85 % RH; 2000 h) conditions showed the post-crystallization peak at 112°C. In chapter 2.2.2 also samples taken from one module were investigated and they showed the same melting peak as the module sample at 146°C.

The most changes were found for the AAA samples. Therefore in Figure 68 an excerpt of the first heating curve is depicted. As explained in chapter 2.2.2 the peak at 167°C belongs to PP, which is incorporated in the middle layer of AAA [46].

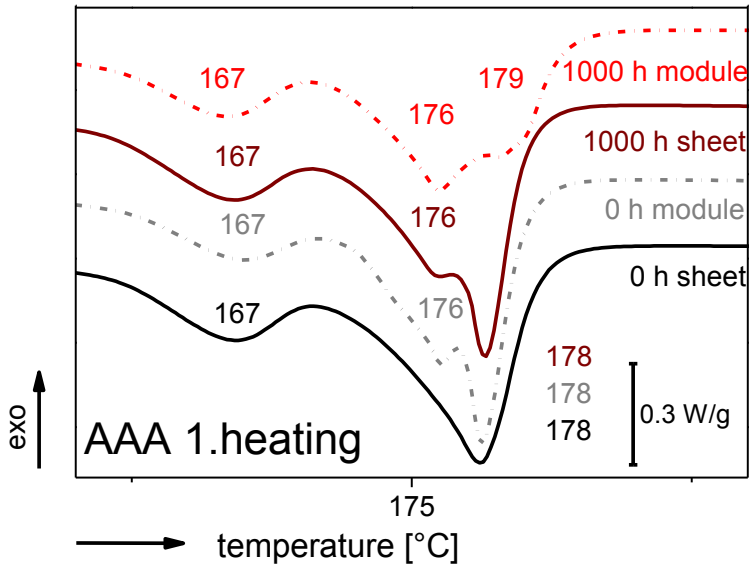

Figure 68: DSC heating and cooling curve of the inner and outer layers from APA for the initial state and aged (1000 h Climate) samples

For all investigated samples this peak was at the same temperature, which was also the case for all artificial aged samples in chapter 2.2.2. The occurrence of the double peak in chapter 2.2.2 was attributed to two possible reasons. On the one hand it can be the re-crystallization of the PA 12 γ-crystals into α-crystals or on the other hand due to smaller and/or more perfect γ-crystals in the amorphous phase. In both cases it is a physical aging process. The PA 12 melting enthalpies for the single sheets changed in the course of Climate aging with -1 J/g, while the change for the module samples was -2 J/g. This is in contrast to the results for the DH aged samples. In chapter 2.2.2 the enthalpy increased with 1.6 J/g for the initial to 1000 h DH aged single sheet. The melting behavior of the 1000 h module Climate aged samples differs from all other results. The height of the main melting peak for γ-PA 12 decreased significantly and the melting temperature increased by 1°C to 179°C.

In the cooling curves a slight shoulder for the APA initial sheet at the PA 12 crystallization peak was detected (see Figure 67). This peak shows the same crystallization temperature (~153°C) as those for all main PA 12 crystallization peaks

of AAA. The detected shoulders for the AAA sheets were at ~148°C like the main PA 12 crystallization peak of APA. As explained in chapter 2.2.2 and also in [23] some additional polymers incorporated in the main polymer matrix can act as nucleating agent which enhances the crystallization temperatures. At the cooling curve the shoulder of the crystallization peak for the PA 12 module aged backsheet was hardly detectable. However, in chapter 2.2.2 it was assumed that the double crystallization peak may be associated to PA 12 in the outer layers as this polyamides have a different additive formulation compared to the PP modified core layer and might thus show a slightly varied crystallization behavior. In [47] it is written that TiO_2 is incorporated in the inner PA 12 layer in AAA to enhance the reflectance. TiO_2 in polyamides is also used as nucleating agent to enable a faster crystallization process [45]. The results for APA and AAA confirm the assumption. The little crystallization shoulder for the initial APA sample which correlates with the main one for PA 12 in AAA also confirms the assumption. For PP a double crystallization peak was detected (113°C and 98°C) for both initial samples. The occurrence of the double peak may be associated to a further additive in PP which disturbs the perfect crystallization [48]. The crystallization area of PP changed for both aged samples to a more uniform area with a melting peak of 103°C for the single aged sheet sample and 110°C for the module aged sample. Also the melting enthalpies showed an increase from about 13 J/g to 16 J/g.

Only APA and AAA showed differences in the cooling run of the other layers than PET in the DSC. Therefore no significant chemical changes were found for the other outer/inner layers of the backsheets.

3.2.2.2 Tensile test results

For tensile tests of backsheets for PV applications an elongation at break of ≥18 % is required [49]. This requirement was fulfilled by every backsheet (see Figure 69 and Figure 70). As the main responsible layer for the mechanical strength is the PET middle layer and no significant changes for PET crystallization curves in the DSC

measurements were detected, this was expected. The general lower stresses detected for the MD to the TD can be attributed to a former biaxial stretching of PET layers.

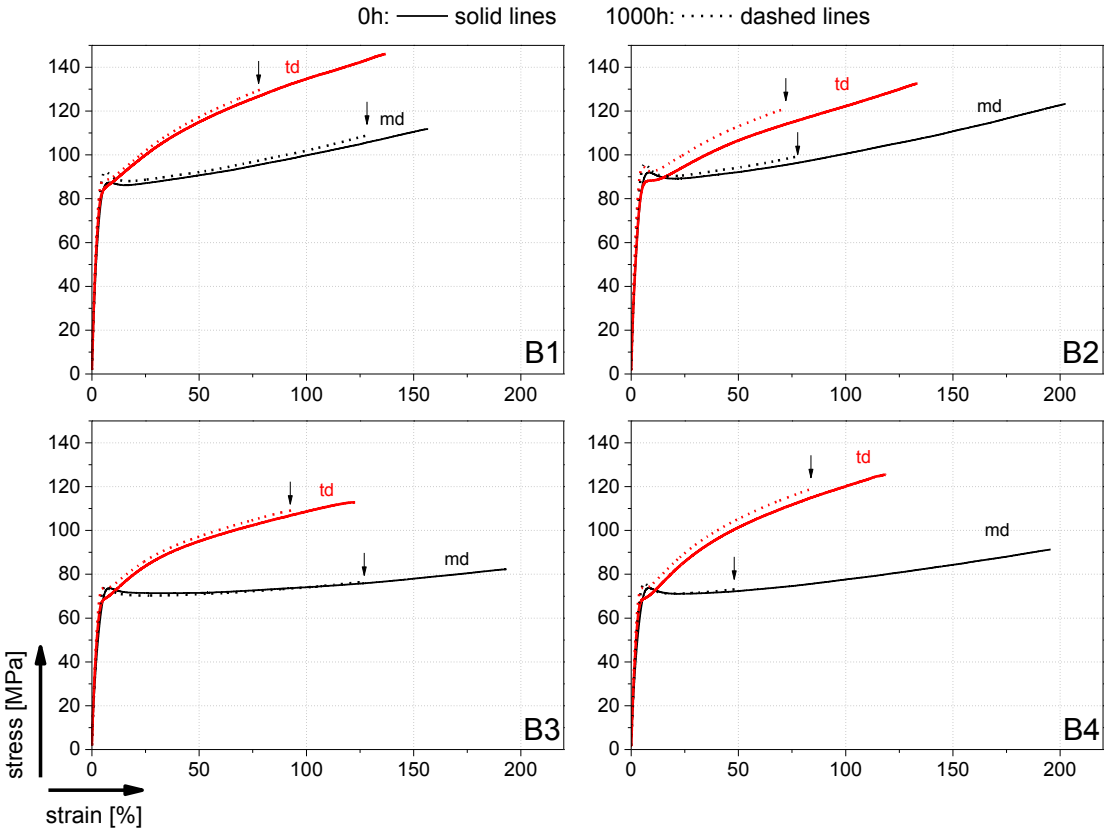

Figure 69: Stress-strain curves of backsheet B1-B4 in the initial state and after 1000 h Climate storage

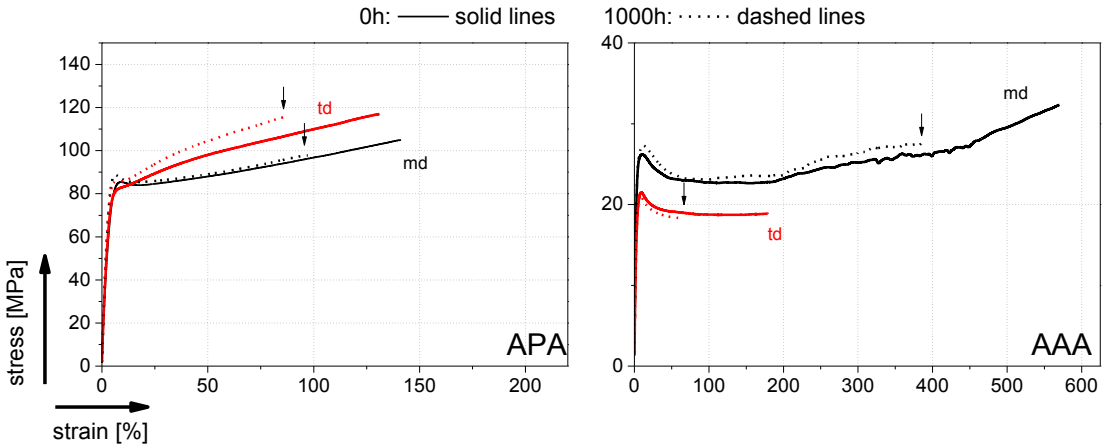

Figure 70: Stress-strain curves of backsheet APA and AAA in the initial state and after 1000 h Climate storage

The most significant decreases in elongation at break were detected for B4 in the MD (204 % to 53 %) and AAA in the TD (314 % to 59 %). This correlates very well with the

detected increase of the crystallization temperatures of the B4 samples and the detected double PA 12 melting peak of AAA, see explanation chapter 2.2.2. One interesting fact was the cracking of the PVDF outer layers for the B2 samples in the TD just when load was applied (see Figure 71). The post-crystallization peak of PVDF, detected in the DSC measurements after aging seems to have a significant impact on embrittlement. Increase in crystallization inhibits increase in stiffness and therefore of the E-modulus. In Table 17 the E-modulus values for all samples are depicted. The evaluation of the E-modulus was done manually.

Table 17: Evaluated E-modulus in the MD and the TD for the initial and aged sheets; M for median value and S for standard deviation

	E-modulus							
	MD				**TD**			
	0 h		**1000 h**		**0 h**		**1000 h**	
	M	S	M	S	M	S	M	S
B1	3105	±25	3194	±17	3539	±24	3601	±24
B2	3072	±25	3182	±17	3276	±34	3614	±29
B3	2563	±38	2756	±53	3029	±49	3057	±31
B4	2313	±9	2428	±42	2775	±15	2987	±27
APA	2688	±185	2911	±20	3025	±49	3097	±153
AAA	891	±27	874	±20	692	±12	595	±10

For all samples an increase in the E-modulus after Climate storage, ranging from +62 MPa to even +339 MPa, was detected. The only exception was AAA, which showed even a decrease of -97 MPa to 595 MPa in the TD and approximately same values for the MD. The highest increase in the TD showed B2 from 3276 to 3614 MPa (+339 MPa). B4 had the second highest increase with +212 MPa to 2987 MPa in the TD (+212 MPa). Both materials showed the strongest decrease in elongation at break, but in the MD. We assume a correlation between those values for PET based backsheets. It should also be mentioned, that Gambogi et al. published a report where detected cracks in backsheets with PVDF outer layers were found [50]. It was assumed it is due to a stiffness change in the PET layer and therefore other thermal expansions in every

layer. We assume, due to the tensile test results, it is possibly the post-crystallization of PVDF but with an influence of the increase in stiffness (see E-modulus values) of the PET middle layer.

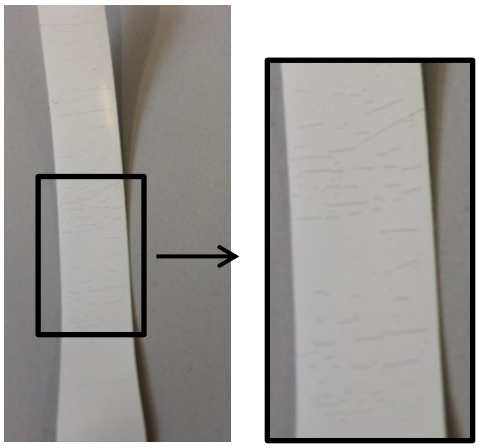

Figure 71: Tensile test sample of B2 in transversal direction after measurement

3.2.2.3 UV/Vis/NIR measurement results

If yellowing occurs in polymeric materials it is always a sign for polymer degradation and furthermore it is unwanted more for optical reasons as power output seems not influenced by yellowing of backsheets [3] [51]. From the general trend of the UV/Vis/NIR measurements changes after accelerated aging for B2 and APA were found (see Figure 72). For APA an increase of reflectance in the UV region for all module sheets in comparison to the single sheets can be seen. It indicates that the elevated temperatures at the PV module lamination process facilitating a partly loss or deactivation of the UV absorber. For the B2 module sheet aged for 1000 h a decrease in reflectance for the blue and green wavelength region was detected. The decrease of the blue wavelength region can also be seen in Figure 73 as the b value decreased. But the resulting decrease in b value with 0.86 for B2 seems not significant. For example Eder et al. detected changes in the b-value after 2000 h of DH storage for a polyamide based backsheet of about 5, which was the only visible color change for the observer [15]. Another issue was that only the PVDF outer layers were very easy to peel off from the module. The underlying region was strongly yellow. This can possibly be attributed to a degradation of the adhesive in this multilayer and therefore loss of adhesion [52]. It may also have a little influence on the b-values of the outer layers for

this backsheet. Additionally FTIR-ATR measurements were taken from the outer layers. The taken spectra showed no significant differences, and therefore chemical changes, in the outer/inner layers of the backsheets.

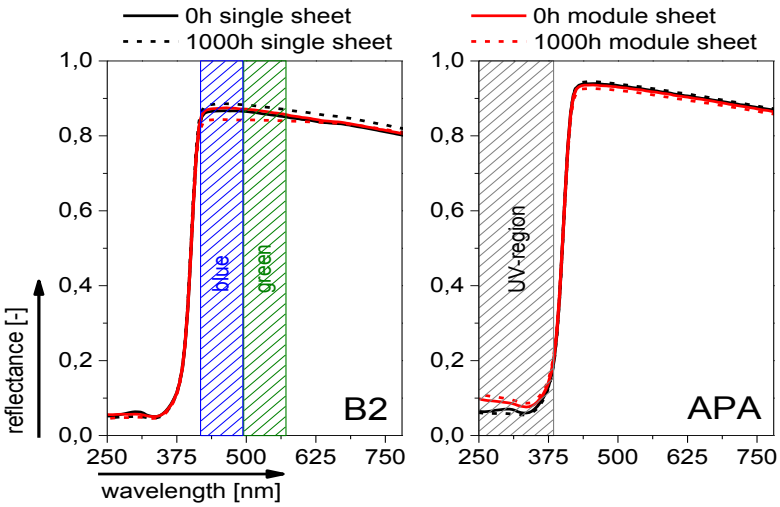

Figure 72: UV/Vis/NIR measurement curves for B2 and APA in the UV to visual wavelength range of 250-780 nm

In Figure 73 all evaluated b values for the backsheets B1 to AAA are shown. In general the inner and outer sides of the single exposed backsheets showed a decrease of the b-value, respectively “bleaching”. In contrast the backsheet B2 and APA showed a slight increase, respectively yellowing, for the inner side. For APA the increase is vanishingly small. The inner sides of the module sheets indicated the strongest increase in b-values for B2 (+0.9) and B3 (+0.4). For APA a slight increase with 0.1 was detected. The storage in the climatic chambers and the handling induced small scratches on the surface of the outer sides of the module backsheets. As this would influence the result, they were not measured. No visible color change was found for them. Therefore from the results of the b-value no significant yellowing was detected for all backsheets.

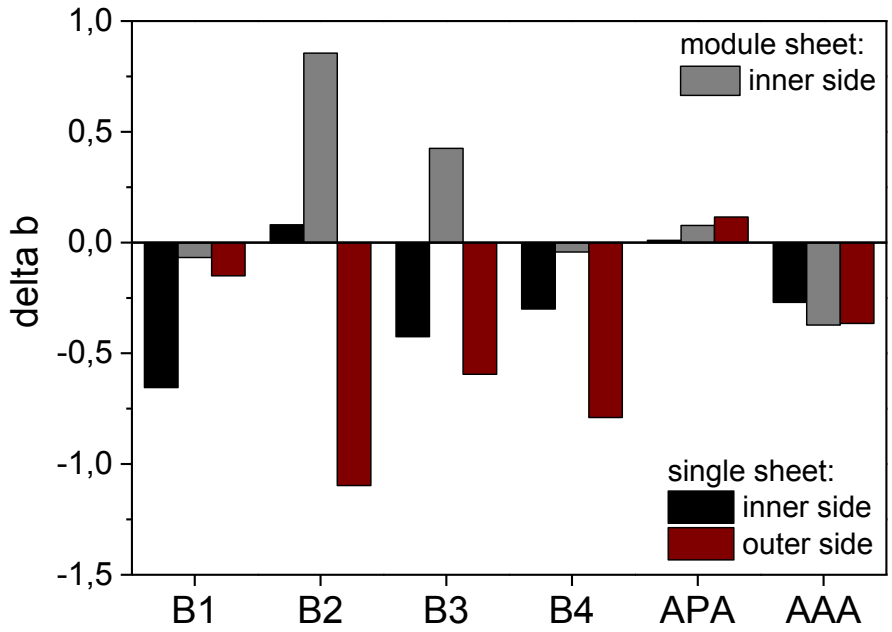

Figure 73: Evaluated b values from UV/Vis/NIR measurements of the module backsheets B1-APA (inner side)

3.3 Summary and conclusions

The focus of the first point of the investigations was the question, whether meaningful DH reliability testing of backsheets should be performed on backsheets laminated within a photovoltaic (PV) module or if testing on single backsheets reveals comparable results. Therefore four different types of backsheets were investigated, all of them containing PET core layers. Test modules using the same components (glass, encapsulant, solar cells etc.), varying only in the backsheet used were produced and artificially aged (damp heat: 85°C/ 85 % RH storage up to 2000 h).

The focus of the second point of investigations was the question, whether in reliability testing a combination of high temperatures and humidity with irradiation can induce service relevant failure mechanisms in backsheets. Six different backsheets were chosen for investigation. Again, as for the DH aging, test modules using the same components (glass, encapsulant, solar cells etc.), varying only in the backsheet used were produced and artificially aged (Climate: 50°C/ 80 % RH and irradiation 300-2800 nm storage up to 1000 h). The artificial aging was done on single backsheets and on backsheets laminated within a PV module to see if there is an influence of microclimate (of the module to single sheets) or if test results are to some extent comparable. The results of the two aging methods were not compared directly, due to different storage times for the modules (DH: 2000 h; Climate: 1000 h) and measurement parameters like temperature and humidity. Another issue was the different lamination temperatures for the DH in respect to Climate modules which can influence the initial samples and therefore further aging processes.

The DSC results showed that for reliability testing of DH aged backsheets of PV modules no significant differences between single and module aged sheets can be found. Reliability of backsheets with PET layers can be deduced from the aging related changes in the core layer, PET. DSC curves of the aged backsheets taken from single and module sheets indicated post-crystallization (physical aging) and hydrolytic degradation (chemical aging) of PET. Both aging effects were confirmed by results from tensile testing and rheological measurements of the single initial and aged

backsheets. The most significant changes of the initial to the aged state can be derived from the cooling curve of the DSC runs. For all materials a significant increase in the crystallization temperatures were found, which can be explained by the presence of a high number of nucleation endpoints formed by chain scission of the PET molecules by hydrolytic degradation.

The DSC results showed that for reliability testing of Climate aged backsheets of PV modules slight differences between single and module sheets can be found. The lamination temperature of the modules for Climate aging (146°C) was slightly above those for the DH aging. It was indicated by a physical aging effect (post-crystallization) obvious for the PVDF, PE and PA 12 inner and/or outer layers of the initial module sheets. For all inner/outer layers of the backsheets little post-crystallization effects in the course of aging were detected. This effect was slightly enhanced for module aged sheets in comparison to the single aged sheets. The enhancement can be attributed to the microclimate of the modules. Due to the irradiation warming of the modules a higher temperature load (70-80°C) for the backsheets occurred during aging [20]. With UV/Vis measurements initiation of chemical aging for the outer/inner layers was detected. While for the single aged sheets even a slight bleaching effect was detected (b-value decreased), the inner sides of the module aged sheets showed slight yellowing (b-values increased). For the PET layers of the backsheets hydrolytic degradation (chemical aging) was indicated, but to a vanishingly small extent. Again, due to the irradiation warming, the effect was slightly enhanced for the module sheets (except B1 and B3). Hence, the storage under Tg (~80°C) of PET induced only slight changes for the PET layers. As PET is the main responsible layer for mechanical strength also little changes in the tensile test curves were obvious. For B2 a cracking of the PVDF layer transversal to the applied load during testing occurred. It was attributed to a stiffness change of the PET middle and PVDF outer layers.

From the presented results it can be stated that for reliability testing of PET based backsheets under DH conditions investigations (aging characterization) on single sheets yield meaningful results which can be directly correlated to the behavior of the backsheets laminated within a module. Exceptions are backsheets with barrier layers.

This allows simplified sample preparation, lower costs and offers more testing options for the characterization of the aging induced changes of the polymeric materials.

For reliability testing of backsheets under Climate conditions the interpretation is more difficult than for DH aging. Irradiation warming induced a different microclimate on modules (higher temperature) compared to the single sheets which went along with enhanced extents in detected aging mechanisms. As irradiation is always a part of external impacts on PV modules in application it is highly relevant for validation of aging induced changes. Additional, the investigations should be extended from the investigated 1000 h to at least 2000 h to see further ongoing chemical aging effects.

One has to keep in mind, however, that this does NOT mean that the type of backsheet used has no influence on the aging behavior of other components within the PV modules. Measurements on the performance of the test modules before and after DH storage e.g. gave a clear indication that the permeation properties of the backsheets for water vapor and oxygen and their aging induced changes strongly influence the performance stability of the test modules [15].

3.4 References

[1] K. Looney, B. Brennan, Modelling the correlation between DHT and true field lifetimes for PET based backsheets, in: 29th European Photovoltaic Solar Energy Conference and Exhibition, Amsterdam, Netherlands, 2014.

[2] H. Eguchi, H. Masuda, E. Soga, Improvement of damping performance by splitting damping material: Microsystem Technologies 17 (2011) 1497-1503.

[3] T. Sample, Failure modes observed in real use and long-term exposure, in: PV Module Reliability Workshop, Berlin, Germany, 2011.

[4] W.J. Gambogi, J.G. Kopchick, T.C. Felder, S.W. MacMaster, A.Z. Bradley, B. Hamzavy, E.E. Kathmann, T.J. Stika, T.J. Trout, L.G. Garreau-Iles, T. Sample, Backsheet and Module Durability and Performance and Comparison of Accelerated Testing to Long Term Fielded Modules, in: 28th European Photovoltaic Solar Energy Conference and Exhibition, Paris, France, 2013.

[5] T. Friesen, PV modules failure modes observed in real use and long term exposure, in: PV Module Reliability Workshop, Berlin, Germany, 2011.

[6] G. Stollwerck, W. Schoeppel, A. Graichen, C. Jaeger, Polyolefin Backsheet and New Encapsulant Supress Cell Degradation in the Module, in: 28th European Photovoltaic Solar Energy Conference and Exhibition, Paris, France, 2013.

[7] C. Reid, S.A. Ferrigan, J.I. Martinez, J.T. Woods, Contribution of PV Encapsulant Composition to Reduction of Potential Induced Degradation (PID) of Crystalline Silicon PV Cells, in: 28th European Photovoltaic Solar Energy Conference and Exhibition, Paris, France, 2013.

[8] G. Oreski, G.M. Wallner, Delamination behaviour of multi-layer films for PV encapsulation, Solar Energy Materials and Solar Cells 89 (2005) 139–151.

[9] G. Oreski, Accelerated indoor durability testing of polymeric photovoltaic encapsulation materials, in: SPIE Solar Energy + Technology, San Diego, USA, 2010.

[10] G. Oreski, G.M. Wallner, Aging mechanisms of polymeric films for PV encapsulation, Solar Energy 79 (2005) 612–617.

[11] G. Oreski, G. Pinter, Aging Characterization of Multi-Layer Films Used As Photovoltaic Module Backsheets, in: 28th European Photovoltaic Solar Energy Conference and Exhibition, Paris, France, 2013.

[12] B. Hirschmann, G. Oreski, Implementation and evaluation of accelerated weathering tests for the aging characterisation of polymer composite films used in photovoltaic modules, in: Austrian-Slovenian Polymer Meeting, Bled, Slovenia, 2013.

[13] G. Oreski, G.M. Wallner, R.W. Lang, Ageing characterization of commercial ethylene copolymer greenhouse films by analytical and mechanical methods, Biosystems Engineering 103 (2009) 489–496.

[14] C. Peike, S. Hoffmann, I. Dürr, K.-A. Weiß, N. Bogdanski, M. Köhl, PV module degradation in the field and in the lab - how does it fit together?, in: 29th European Photovoltaic Solar Energy Conference and Exhibition, Amsterdam, Netherlands, 2014.

[15] G.C. Eder, Y. Voronko, M. Knausz, G. Oreski, T. Koch, K.A. Berger, Correlation of the loss in PV module performance with the characteristics and ageing behavior of the backsheet used.

[16] E.R. Parnham, K. Forsyth, W.A. MacDonald, W.J. Brennan, PET Backsheets: The robust balance between performance and cost, in: Polymers in Photovoltaics, Cologne, Germany, 2014.

[17] G.W. Ehrenstein, S. Pongratz, Beständigkeit von Kunststoffen, 1st ed., Carl Hanser Verlag, Munich, 2007.

[18] F. Liu, L. Jiang, S. Yang, Ultra-violet degradation behavior of polymeric backsheets for photovoltaic modules, Solar Energy 108 (2014) 88–100.

[19] N. Lenck, Polymere Materialien im Modul, in: 12. Österreichische PV-Tagung, Linz, Austria, 2014.

[20] M. Koehl, M. Heck, S. Wiesmeier, Modelling of conditions for accelerated lifetime testing of humidity impact on PV-modules based on monitoring of climatic data, Solar Energy Materials and Solar Cells 99 (2012) 282–291.

[21] International Organisation for Standardisation, ISO 11357-3, Plastics-Differential scanning calorimetry (DSC) - Part 3: Determination of temperature and enthalpy of melting and crystallization, 1999.

[22] International Organisation for Standardisation, ISO 527-3, Plastics - Determination of tensile properties: Part 3: Test conditions for films and sheets, 1995.

[23] G.W. Ehrenstein, G. Riedel, P. Trawiel, Thermal analysis of plastics: Theory and practice, Carl Hanser Verlag, Munich, 2004.

[24] J. Badia, E. Strömberg, S. Karlsson, A. Ribes-Greus, The role of crystalline, mobile amorphous and rigid amorphous fractions in the performance of recycled poly (ethylene terephthalate) (PET), Polymer Degradation and Stability 97 (2012) 98–107.

[25] C. Hirschl, M. Biebl–Rydlo, M. DeBiasio, W. Mühleisen, L. Neumaier, W. Scherf, G. Oreski, G. Eder, B. Chernev, W. Schwab, M. Kraft, Determining the degree of crosslinking of ethylene vinyl acetate photovoltaic module encapsulants—A comparative study, Solar Energy Materials and Solar Cells 116 (2013) 203–218.

[26] G. Menges, E. Haberstroh, W. Michaeli, E. Schmachtenberg, Werkstoffkunde Kunststoffe, 5th ed., Carl Hanser, Munich, 2002.

[27] B. Duncan, J. Urquhart, S. Roberts, Review of Measurement and Modelling of Permeation and Diffusion in Polymers, NPL Report DEPC MPR 012 (2005).

[28] A. Frick, C. Stern, DSC-Prüfung in der Anwendung, Carl Hanser Verlag, Munich, 2006.

[29] G. Jorgensen, K. Terwilliger, G. Barber, C. Kennedy, T.J. McMahon, Measurements of Backsheet Moisture Permeation and Encapsulant-Substrate Adhesion: Preprint, in: NCPV Program Review Meeting, Lakewood, USA, 2001.

[30] G.D. Barber, G.J. Jorgensen, K. Terwilliger, S.H. Glick, J. Pern, T.J. McMahon, New Barrier Coating Materials for PV Module Backsheets: Preprint, in: 29th IEEE Photovoltaic Specialists Conference, New Orleans, USA, 2002.

[31] P. Hülsmann, M. Jäger, K. A. Weiss, M. Köhl, Measuring and simulation of water vapour permeation into PV-modules under different climatic conditions, in:

SPIE 7773; Reliability of Photovoltaic Cells, Modules, Components and Systems III, Bellingham, USA, 2010.

[32] R. Assadi, X. Colin, J. Verdu, Irreversible structural changes during PET recycling by extrusion, Polymer 45 (2004) 4403–4412.

[33] A. Ghanbari, M.-C. Heuzey, P.J. Carreau, M.-T. Ton-That, Morphological and rheological properties of PET/clay nanocomposites, Rheol Acta 52 (2013) 59–74.

[34] R.F. Rosu, R.A. Shanks, S.N. Bhattacharya, Shear rheology and thermal properties of linear and branched poly(ethylene terephthalate) blends, Polymer 40 (1999) 5891–5898.

[35] M. Neidhöfer, F. Beaume, L. Ibos, A. Bernès, C. Lacabanne, Structural evolution of PVDF during storage or annealing, Polymer 45 (2004) 1679–1688.

[36] G. Oreski, Untersuchung des Delaminationsverhaltens von Folienverbunden für die Einkapselung von PV-Modulen. Master thesis, Montanuniversitaet Leoben, 2004.

[37] C. Marega, A. Marigo, Influence of annealing and chain defects on the melting behaviour of poly(vinylidene fluoride), European Polymer Journal 39 (2003) 1713–1720.

[38] I.A. Al-Raheil, A.M. Qudah, Thermal behaviour and annealing of poly(vinylidene fluoride), Polymer International (1996) 323–326.

[39] A. Beinert, C. Peike, I. Dürr, M. Kempe, K.-A. Weiß, The Influence of the Additive Composition on the Photochemical Degradation of EVA, in: 29th European Photovoltaic Solar Energy Conference and Exhibition, Amsterdam, Netherlands, 2014.

[40] C. Peike, L. Purschke, K.-A. Weiß, M. Köhl, M.D. Kempe, Towards the origin of photochemical EVA discoloration, in: 39th Photovoltaic Specialists Conference IEEE, Tampa Bay, USA, 2013.

[41] J. Jin, S. Chen, J. Zhang, UV aging behaviour of ethylene-vinyl acetate copolymers (EVA) with different vinyl acetate contents, Polymer Degradation and Stability 95 (2010) 725–732.

[42] G. Oreski, Polar Ethylene Copolymer Films for Solar Applications - Optical Properties and Aging Behavior. Doctor thesis, Leoben, 2008.

[43] M. Brogly, M. Nardin, J. Schultz, Effect of Vinylacetate Content on Crystallinity and Second-Order Transitions in Ethylene–Vinylacetate Copolymers, Journal of Applied Polymer Science 64 (1997) 1903–1912.

[44] Y.-L. Loo, K. Wakabayashi, Y.E. Huang, R.A. Register, B.S. Hsiao, Thin crystal melting produces the low-temperature endotherm in ethylene/methacrylic acid ionomers, Polymer 46 (2005) 5118–5124.

[45] H. Dominighaus, P. Eyerer, P. Elsner, T. Hirth, Kunststoffe: Eigenschaften und Anwendungen, Springer, Berlin Heidelberg, 2007.

[46] E. Baur, J.G. Brinkman, T.A. Osswald, E. Schmachtenberg, Saechtling Kunststoff Taschenbuch, 30th ed., Carl Hanser, Munich, 2007.

[47] G. Mikats (ISOVOLTAIC GMBH) WO 2011/066595 A1, 2010.

[48] E.S. Ogunniran, R. Sadiku, S. Sinha Ray, N. Luruli, Morphology and Thermal Properties of Compatibilized PA12/PP Blends with Boehmite Alumina Nanofiller Inclusions, Macromolecular Materials and Engineering 297 (2012) 627–638.

[49] U. Eitner, Thermomechanics of photovoltaic modules. Doctor thesis, Martin-Luther-Universitaet Halle-Wittenberg, 2011.

[50] W.J. Gambogi, Y. Heta, K. Hashimoto, J.G. Kopchick, T. Felder, S.W. MacMaster, A. Bradley, B. Hamzavytehrany, L. Garreau-Iles, T. Aoki, K.M. Stika, T.J. Trout, T. Sample, A Comparison of Key PV Backsheet and Module Performance from Fielded Module Exposures and Accelerated Tests, IEEE Journal of Photovoltaics 4 (2014) 935–941.

[51] IEA Task 13, Review on Failures of PV Modules: Report IEA-PVPS T13-01:2013, 2013.

[52] Y. Voronko, B.S. Chernev, G.C. Eder, Spectroscopic investigations on thin adhesive layers in multi-material laminates, Applied Spectroscopy 68 (2014) 584–592.

CHAPTER IV:

PERMEATION PROPERTIES OF BACKSHEETS

4 Introduction to permeation properties of backsheets

Permeation is a mass transport of molecules or gases through permeable materials like polymers. Glasses, ceramics and metals are in contrast to polymers impermeable [1]. Permeation consists of three physically based sequences and occurs only under the basic requirement of partial pressure respectively concentration differences of the molecules between two surfaces. In the first step molecules getting attached to the surface of the separating material (adsorbed) with following absorption. In the second step the molecules will be transferred through the material (diffusion). In the third step the molecules will be released from the inner surface (desorption). Therefore permeation rates are defined as product of the sorption coefficient and the diffusion coefficient (P=D*S) [2]. The transport of the molecules occurs until there is an equal concentration on both sides of the separating material.

The measured variable to quantify the permeation process is given for water vapor by the water vapor transmission rate (WVTR) and for oxygen by the oxygen transmission rate (OTR). It is established to use the unit g m^{-2} day^{-1} for WVTR and cm^3 m^{-2} day^{-1} bar^{-1} in case of OTR. Both rates in this form are dependent on the layer thickness and therefore for each film specific (thickness must be given!). In some cases also differing units are used, dependent on the measurement technique. In [3] [4] all conversion factors are listed. Permeation is a complex issue. But the knowledge of its fundamentals is not necessary to understand the following discussion. Hence, for a further detailed description of the fundamentals of permeation, as well as on sorption and diffusion the reader is referred to [5] [4] [1] [6] [7] [8] [2].

In Figure 74 requirements for WVTR and OTR on polymer films for different application ranges are shown. Therein the range of the WVTR and OTR of common polymers is obviously above the required ranges for the listed applications, but this range is related to 1 µm thick polymer layers. However, the range for commercial polymers will be discussed in detail later on (see also Figure 75). While for food

packaging often a “simple” barrier layer is conducted via a multilayer stack up of for example a polyamide (low OTR) and a polyolefin (low WVTR), for applications like organic light emitting diodes (OLEDs) there is a need for highly sophisticated barrier layers. For OLEDs a local enhanced water vapor can induce black inactive points (“dark-spots”), therefore it is of prime importance to protect the electrical device against incoming water vapor [9].

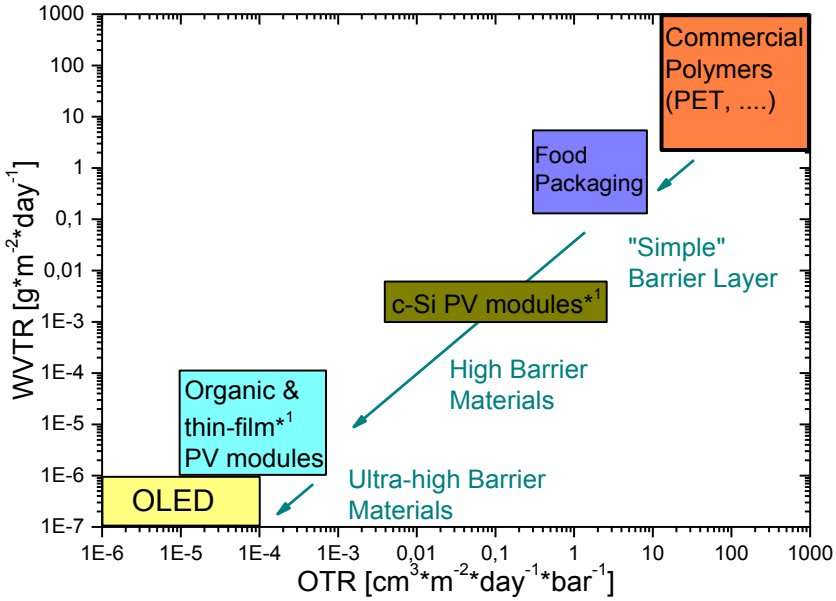

Figure 74: Requirements of permeation properties (WVTR and OTR) on polymer films for specific application fields [10];*1 thin film in [11] [12] given with 1E-5 or 1E-4 for WVTR and OTR and *2 c-Si in [8] only WVTR is given with 1E-1 to 1E-3

In relation to PV module applications the requirements are also set related to the active semiconductor material. For example organic and/or thin-film PV modules are very sensitive to water and oxygen as the active material tends to degrade very fast in presence of water and oxygen [11]. In case of c-Si based PV modules requirements just for the WVTR were found as c-Si has a less sensitivity to water and oxygen than organic and/or thin-film PV modules [8]. An overview on OTR and WVTR properties of common polymers related to a thickness of 1 µm is shown in Figure 75. There are several possibilities to enhance the barrier properties. Every increase in thickness will lower the transmission rates. Also, as already mentioned a multilayer stack up of different polymers can be effective for moderate requirements like e.g. food packaging or even c-Si PV modules.

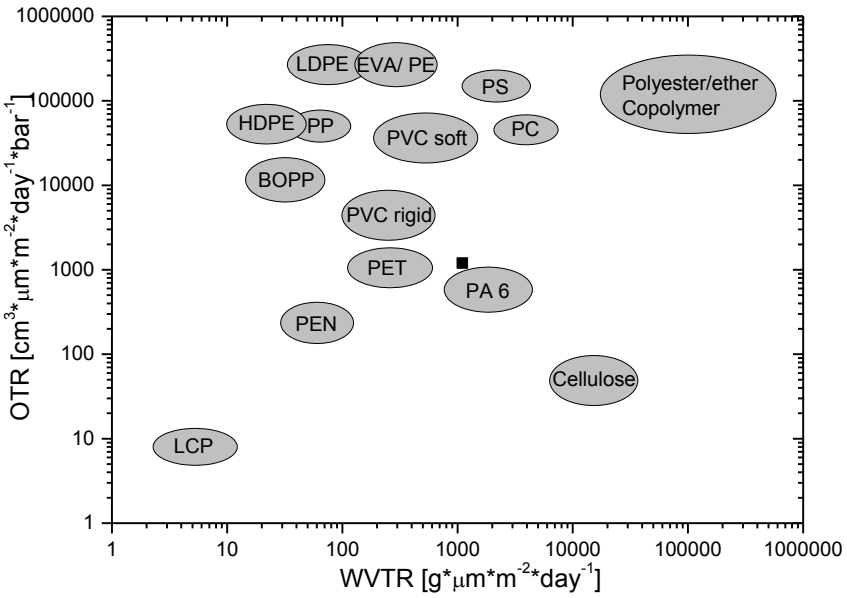

Figure 75: OTR and WVTR of some polymers related to 1 µm thickness [6]

Another approach is the use of inorganic layers, which are in principle impermeable. Permeation is possible threw defects when low thicknesses of these layers are applied, but they are still reducing the transmission rates [9] [12]. For enhancing the barrier properties within multilayers also an aluminum barrier (conducted with vapor deposition technologies) as interlayer can be used. With this aluminum layer the water vapor transmission can be reduced almost to 0 [13]. On the other hand also layers with silicon oxide (SiO_x) deposited with plasma-enhanced chemical vapor deposition (PECVD) or sputtering on the surface are used to enhance barrier properties [13]. These layers reduce the water vapor transmission by a factor of 10 [14]. For high and ultra-high barrier materials the achieved transmission rates are still too high. Two approaches are traced to get a better barrier performance: 1) deposition of almost defect-free single layers or 2) production of a barrier layer system with alternating inorganic barrier layers and polymeric inter layers. A detailed description about processing technologies for these barrier films as well as the achieved OTR and WVTR rates is given in [9] [8].

Water vapor is known to have a critical impact on various degradation phenomena of PV modules like corrosion of metal-, cell parts and solar cell surface (ARC), potential induced degradation (PID), Snail Tracks and encapsulant decomposition via hydrolysis

[15] [16] [17] [18] [19]. The metallization corrosion leads to an increased series resistance and therefore losses in module performance [20]. In Meyer et al. water vapor coming through the backsheet is claimed to dissolve silver particles which migrate into the encapsulation on top of the grid finger, where a chemical reaction within the encapsulation foil results in the typical observed coloring of Snail Tracks [17]. Lower WVTR of the used polymers showed improvements of resistance to PID effects [16]. The presence of oxygen in a PV module contributes to chemical processes like photo-oxidation and thermo-oxidation in the used polymers. Hence, it is highly relevant to choose the right combination of e.g. a backsheet with high oxygen transmission rates (OTR) with an encapsulant which tends to discoloration under UV irradiation and a backsheet with low water vapor transmission rates (WVTR) with an encapsulant susceptible to hydrolysis [20]. During aging of EVA acetic acid is formed from photo-oxidation processes. It has corrosive effects on interconnectors and cell metallization, especially copper (used in interconnectors) is very sensitive towards corrosion [15]. In [20] it is recommended to use EVA with a backsheet of high OTR values. In [21] EVA is claimed to give better results in combination with a backsheet of a high WVTR, because otherwise the water vapor will block acetic acid to escape. For PVB it is claimed to use a backsheet with low WVTR, due to its hydrolysis susceptibility. It is also discussed if for c-Si PV modules a high permeation rate for the packaging material is wanted as then the reverse process- outgassing of volatile compounds like oxygen, water vapor or even acetic acid is occurring due to the diurnal thermal cycles in application. Nevertheless, in c-Si PV modules permeation of water vapor, oxygen and acetic acid play a major role on reliability. Thus, the knowledge of the permeation rates of relevant substances through the backsheets and their sensitivity to the ageing behavior of the materials involved will allow for a better understanding of the reliability of PV systems.

The presented investigations in this chapter are the OTR and WVTR of five different backsheets in their initial state and in the course of different accelerated aging methods (chapter 4.3.1). Additional three different measurement techniques for determining the OTR and two for WVTR will be compared to give a hint to differences

when comparing permeation results of different techniques. PV modules operate at different temperatures due to diurnal and seasonal cycles, but also to operation in different climate zones. Therefore in chapter 4.3.2 the focus will be on the temperature dependence of permeation of the investigated backsheets. To allow for a better understanding of the presented results internal and external influences on permeation through polymers will be explained at first. Then the measurement principles of in this chapter used techniques will be described. Also various OTR and WVTR values for PV backsheets from literature will be summarized.

4.1.1 Influences on permeation properties of polymers

Principal permeation properties of polymers can be found in [1] [22] [23] [6] [24] and many more. Different used units as well as differing thicknesses have to be taken into account. While this can be solved by simple conversions, many internal and external impacts influence the permeation behavior of polymers. To get quantitative answers on permeation behavior, measurements have to be done on samples which are the same in application (production process, geometry...) and also in application relevant temperature/humidity levels. This is often not possible. However in the following a short overview on internal and external influences on permeation will be given to underline this statement.

4.1.1.1 Internal influences

The permeant is moving through the empty places in a polymer sample via Brownian motion. These places are provided from the free volume in polymer samples and polymer chain motion. Both are redistributed continuously as a result of the random, thermally stimulated molecular motion of the polymer segments [4].

Therefore the molecular structure of polymers has a strong influence on the permeation properties. For example, polar polymers like e.g. polyamides, polyurethanes and EVA have a higher WVTR. In contrast non-polar polymers like polyolefines have a lower WVTR. This is attributed to the polar character of water molecules [24]. In contrast to that, polar groups on or in polymer chains often increase chain rigidity, which results in lowered OTR values [4].

Increases in crystallinity of semi-crystalline polymers generally decreases gas permeability. Crystalline regions, which are much more dense and well-ordered than amorphous regions, preclude permeation [4] [1]. Additionally the crystalline parts acting as barriers to diffusion, increasing the path length for the moving permeant and in some cases also chain rigidity, which reduces diffusion [4]. Increases in cross-linking density of elastomers or thermosets also decrease the permeability due to a decreasing free volume.

Pores are larger in scale than free volume and are permanent in polymers. They are independent on molecular chain motion. Pores are built from defects which are for example occurring due to enclosed air from production processes. They enhance the permeability due to higher solubility and a higher diffusion coefficient [2].

4.1.1.2 External influences

A polymer with low permeation rates at ambient temperatures does not compulsory has a low permeation rate at all temperatures [6]. For example, an increased temperature of 20°C resulted in an approximately doubling of the oxygen transmission rate for a 12 µm PET film [6].

Two reasons can be mentioned for the temperature dependence of permeation. The Brownian motion of the permeant as well as the molecular chain motions are significantly influenced by temperature. The higher the temperature the lower kinetic energy of the permeant molecule is necessary to build interstitials to move in between the chains. Additional the polymer chain segment movement is enhanced which increases possible movements of the permeant [2]. The resulting permeation can be described with the Arrhenius equation [6]:

$$\boldsymbol{P(T) = P_0 * e^{\frac{-E_P}{R*T}}} \qquad \textbf{Equation 2}$$

or in case of water vapor permeation with

$$\boldsymbol{WVTR(T) = WVTR_0 * e^{\frac{-E_W}{R*T}}}, \qquad \textbf{Equation 3}$$

where P_0 is the temperature independent permeation coefficient, E_p the activation energy for permeation and R the gas constant. P_0 can be measured for a specific temperature, which allows with the above shown equation a calculation for not

measured temperature ranges. The temperature dependence is specific for every polymer therefore permeation results should always indicate at which temperature the measurements were accorded and in the best case (but very rare) also the temperature dependence is evaluated.

The absorption of water can increase, decrease, or have no effect on gas permeability of polymers. For example an increase of the relative humidity (RH) from 0 to 50 % increases the OTR in cellophanes by an order of magnitude. In cellophanes water acts as plasticizer and increases the free volume of the polymer. At low to moderate RH, amorphous polyamides and PET show slightly improved barrier properties with increasing humidity (until moderate RH). In this case it is explained that the water molecules not swelling the polymer, but occupying some of the polymer free volume sites instead, resulting in reduction of permeability of other gases. Polyolefines are claimed to show no effect of RH on gas permeability [4]. For these reasons also the amount of RH of permeation measurements should be given.

Also processing of polymers influences the permeability properties. The degree of curing, crystallinities and the free volume can be controlled. Also the incorporation of additives can enhance or lower permeability properties. For example plasticizer in between the polymer chains can act as spacer giving more possibilities for the permeant to move [2]. On the other hand nanoparticles can act as barrier which raises the pathways for molecules [25]. Stretching or drawing of polymer films can also improve the barrier properties. The effect is more pronounced for semi-crystalline polymers than for others [4].

4.1.2 Permeation measurement principles

There are a lot of different measurement techniques and standards for determining permeation in polymers. In [2] and [5] a description of principle measurement approaches is given. In [4] [23] [5] an overview on standards for measuring permeation properties is given. For description of different measurement techniques of WVTR and e.g. their detection limits the reader is referred to a review paper of Kempe et al. [26] or others [27] [10]. Measurement techniques used for determining

the permeation properties of backsheets described in this chapter will be discussed now.

In general, the permeation measurement techniques are distinguished between isostatic and quasi-isostatic methods. In both approaches two cavities are separated from a polymer sample. One cavity is the reservoir cavity, where the permeant is brought into. The second cavity is the receiving cavity, where the permeant is accumulated after permeating through the polymer sample. The permeant is accumulated into a carrier gas (usually nitrogen) and transported to a permeant specific detector [5]. In the isostatic methods the concentration difference between the two cavities is constant. Therein the permeant flows continuously through the reservoir cavity. Some of its molecules are permeating through the polymer sample, according to the permeation behavior of the sample. In the receiving cavity it gets accumulated from the carrier gas and continuously transported to the detector system. When the permeation equilibrium is reached, the permeant flux is constant over time and the permeation coefficient can be determined. In the quasi-isostatic methods the concentration difference decreases. Therein the permeant flows again continuously through the reservoir cavity. The permeant passing through the polymer sample accumulates in the receiving cavity. Its amount is quantified directly in the receiving cavity by the detector system. Therein the permeation occurs until the concentration in the receiving cavity reaches the concentration equilibrium; respectively the concentration of the permeant in both cavities is the same [5]. The permeation coefficient can be evaluated when the detected amount of permeant increases linear over time [2].

The measurement results discussed in chapter 4.3 are determined with four different measurement techniques. Two measurement techniques, respectively apparatus, are commercially available and produced from the company Mocon Inc., Minneapolis, USA. While the MOCON-Oxtran MH 2/20 (Oxtran) is based on a coulometric sensor specific to, the MOCON-Permatran W 3/31 (Permatran) detects the water vapor via an infrared sensor [10] [28] [29]. Both devices use the isostatic measurement methods. The schematic construction of the permeation cells of the Oxtran and Permatran are

shown in Figure 76 and Figure 77. The permeated oxygen or water vapor is transported continuously to a sensor by a flow of a carrier gas (inert gas, usually nitrogen or argon). The coulometric sensor produces an electrical current which is proportional to the amount of oxygen flowing into the detector per unit time [10]. The infrared sensor measures the water vapor concentration via specific absorption bands induced from water molecule vibrations. The restricting factors for the detection limit of these systems are the dilution of the permeant in the carrier gas and trace oxygen/water vapor impurities in the carrier gas. To overcome the impurities a catalyst bed (made from palladium-Pd) is used in the gas feed for removing residuals in case of Oxtran measurements (see also Figure 76) [10].

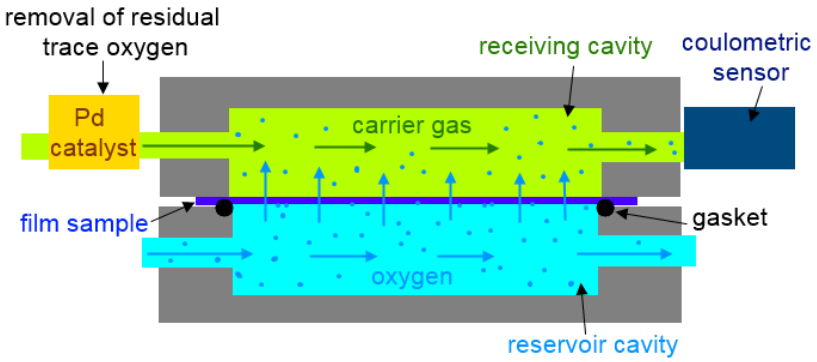

Figure 76: Schematic construction of Mocon-Oxtran permeation cell [30]

Detection limits for the Permatran models can reach values of $5*10^{-3}$ g m^{-2} day^{-1} according to the final composition of the model [29]. For the MOCON-Permatran W 3/31 the detection limit was 0.1 g m^{-2} day^{-1}. Detection limits for Oxtran models can reach values of $5*10^{-4}$ cm^3 m^{-2} day^{-1} according to the final composition of the model. For the MOCON-Oxtran MH 2/20 the detection limit was 0.1 cm^3 m^{-2} day^{-1} bar^{-1}. For further details the reader is referred to the supplier homepage of Mocon.

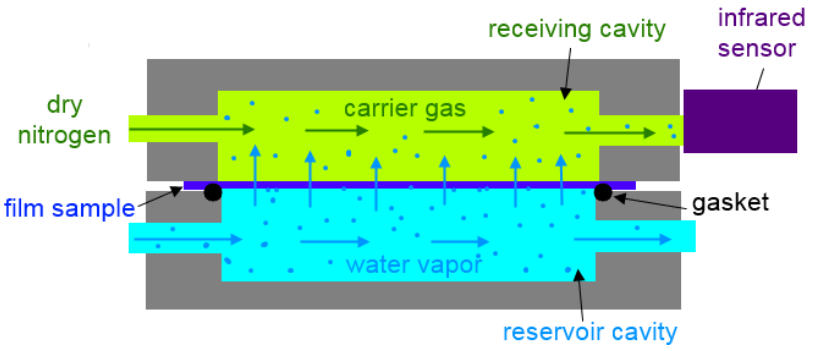

Figure 77: Schematic construction of Mocon-Permatran permeation cell [29]

The third chosen measurement technique is not a standard and not commercially available. It was newly invented at the Institute of Chemical Process Development and Control, Joanneum Research Forschungsgesellschaft mbH in Graz. The schematic construction is shown in Figure 78. This apparatus works with the quasi-isostatic method. Therefore the OTR is calculated from the rate of the resulting concentration increase. It is based on an opto-chemical detector system. Modulated light from a green light emitting diode (LED) is send to a luminescent dye [30]. The luminescent dye acts as a sensing element, via an oxygen-dependent luminescence quenching mechanism of the incoming green light (see schematically Figure 78) [10]. The light response of the luminescent dye is detected from a photo detector. The correlation of the oxygen concentration with the luminescence quenching is used for evaluation of the OTR. The advantage of this measurement system over electrochemical sensors is consumption-less oxygen detection and its extraordinary sensitivity of 10^{-5} cm^3 m^{-2} day^{-1} bar^{-1}. For further details the reader is referred to the literature [30] and [10].

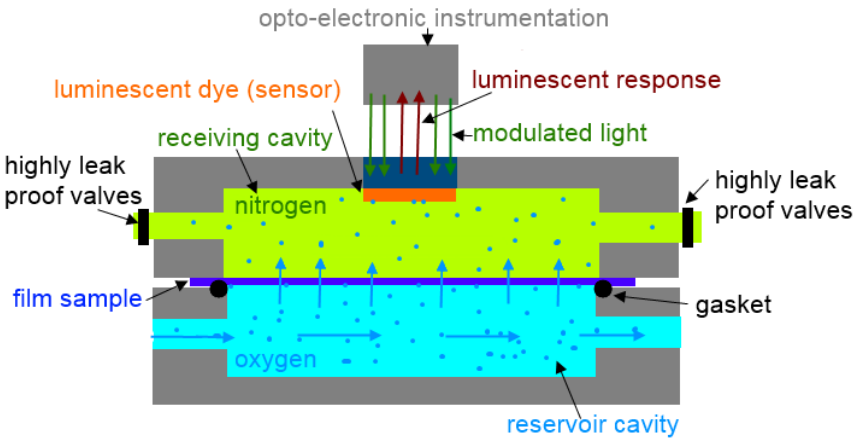

Figure 78: Schematic construction of opto-chemical permeation cell [30]

The fourth measurement technique is also not a standard and not commercially available. It was newly invented at the Fraunhofer Institute for Solar Energy Systems (ISE) in Freiburg. This technique is based on the quasi-isostatic method. Therein a mass spectrometer is used as detector. The schematic construction is shown in Figure 79. In this construction instead of a reservoir cavity filled with the permeant, the permeant loading is done via a climatic chamber. This is one of the advantages of this system as it offers application relevant conditions (temperature and humidity

adjustable for all possible climatic conditions) for determining the permeation properties of film samples. It is also highly relevant for photovoltaic backsheets as the temperature dependence of the backsheet films can have a strong influence due to different temperature conditions for PV modules.

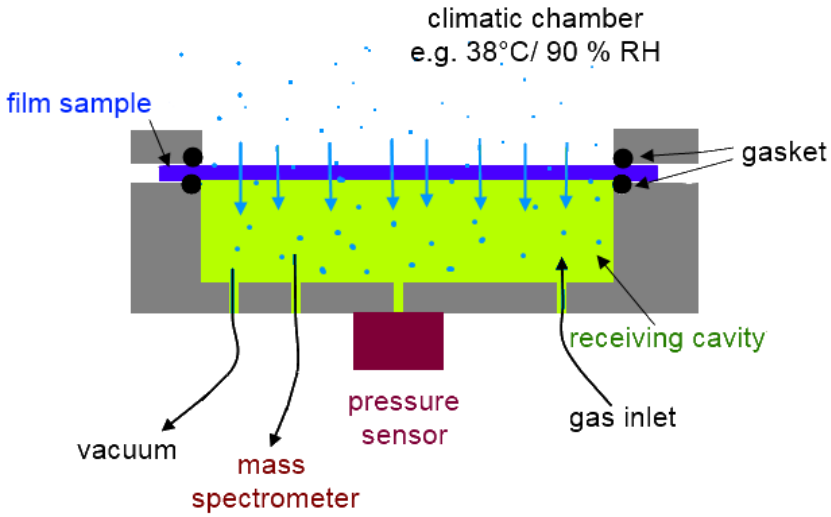

Figure 79: Schematic construction of mass spectrometer permeation cell [32]

The mass spectrometer allows recording of the partial pressure increase inside the receiving cavity of any species of interest [31]. Due to the atmosphere conditions in the climatic chamber and the detection method a simultaneous determination for single atmosphere components, especially for water vapor, oxygen and nitrogen, and interactions of the different gases is possible. The cleaning of the permeation cell before starting a measurement is done with alternate applying of vacuum and purging with argon. During measurements at different time intervals the valve between the receiving cavity and the mass spectrometer is opened and a representative amount of the gas mixture of the receiving cavity is transported to the mass spectrometer. Therefore an additional pressure sensor is applied on the receiving cavity. It allows for the compensation of the pressure decrease after the removal for the mass spectrometer. The detection limit for this system is claimed to be 10^{-6} g m^{-1} day (WVTR) and $4*10^{-3}$ cm^3 m^{-2} day^{-1} bar^{-1} (OTR). For further details the reader is referred to the literature [31] and [32].

4.1.3 Various permeation properties of polymers in PV applications

Due to the in chapter 4.1 explained impacts on permeation properties it is difficult to calculate permeation from general data given in literature or other sources. Reliable information on permeation properties of PV backsheets and/or encapsulants are also hardly to find. For example provided data from suppliers in datasheets are incomplete. In [33] [34] an overview of encapsulants and backsheets offered on the market with data provided from the suppliers are given. Therein permeation properties for encapsulants are not given, because backsheets are the limiting factor for incoming gases. For encapsulants only the water absorption at 20°C for 24 h is given for comparison. For most encapsulants a water uptake of <0.1 % was evaluated. Occasional exceptions are values of <0.01 or <1 %. For the listed backsheets only the WVTR is given, but not in all cases. Parameters like temperature and humidity for the evaluation are sometimes given or nothing was denoted. Given temperatures ranged within 23/ 38/ 40°C and the humidity level was 90 or 100 % RH. Sometimes just the standards ASTM F 1249 or ISO 15106-3 are denoted, which allow in variation of temperature and humidity levels [35] [36]. However for TPT (PVF/PET/PVF) backsheets the WVTR ranged between <0.6 and 4.8 g m^{-2} day^{-1} and for KPK (PVDF/PET/PVDF) in between <0.9 and 1.3 g m^{-2} day^{-1}, backsheets with aluminum layers in between <0.0005 and 0 g m^{-2} day^{-1}, PVF/PET/(EVA or PE) in between 2 and ≤4 g m^{-2} day^{-1} and for PET/PET/PE in between 0.5 and 2.47 g m^{-2} day^{-1}. The requirement for c-Si based PV modules with a WVTR between 0.1 and 0.001 g m^{-2} day^{-1} seems only achieved from backsheets with aluminum barriers [8].

The beneath discussed results were measured with the same measurement principle, which is based on a mass spectrometer detector and is explained in detail in chapter 4.1.2. In [20] the OTR and WVTR of encapsulants and backsheets for PV modules is given without any description of their thicknesses or the humidity level, but measured at 85°C. In [37] the OTR and WVTR of encapsulants and backsheets is given with the evaluation of their temperature dependence. Therein the values for the encapsulants were scaled to a thickness of 1 mm and the thicknesses of the backsheets are given. The humidity level at all applied temperatures for the WVTR measurements was 90 %

RH and for OTR 20 % RH. In [32] the WVTR for one EVA and two TPT type of backsheets for three different temperatures is given. Therein the humidity levels for the measurements are not given. The evaluated values from [20] [37] [32] are summarized in Table 18 for encapsulants and Table 19 for backsheets. In Table 18 values from [37] are multiplied with 2, as the values for the encapsulants were scaled to 1 mm to get values representative for a 500 µm thickness, which is in the range for common thicknesses [34]. It should also be mentioned, that the summarized data in both tables are taken from figures, as no tables with the values were given. Therefore small deviations should be taken into account. Note also that the samples were evaluated according to the polymeric type without a specification of the trade name. When looking on the data summarized in Table 18 and Table 19 the evaluated values at 23°C for most backsheets and encapsulants are in between the required range of 0.001 - 0.1 g m^{-2} day^{-1} for the WVTR [8]. The only exceptions are EVA and TPSE.

Table 18: WVTR and OTR results for different encapsulants at different temperatures

	[37] *2[32]				[20]
	23°C	38°C	60°C	80°C	85°C
WVTR	g m^{-2} day^{-1}				
PE	0.1	0.56	2.8	36	
EVA	0.24 /0.2 *2	1.8 /1 *2	14 /10 *2	50	75
TPSE	1.4	4	40	120	180
PVB	0.04	0.26	2.6	20	16
Ionomer	0.0018	0.012	0.18	1.8	4
OTR	cm^3 m^{-2} day^{-1}				
PE	200	360	700	1600	
EVA	240	440	2400	4000	3200
TPSE	14000	16000	22000	24000	16000
PVB	160	340	640	1400	5400
Ionomer	14	22	200	400	400

As most modules are produced since the early beginning with EVA as encapsulant the requirement mentioned in [8] may just be related to backsheets, or the evaluated values for EVA are above the requirement due to another measurement technique chosen for evaluation of the WVTR. However it seems reasonable to conclude the lower the WVTR the better for the PV module. All evaluated samples in both Tables

show more or less pronounced temperature dependencies. The WVTR of the investigated ionomer shows the lowest values of all encapsulants, especially at 23°C. Also the OTR values of this ionomer are significant lower in comparison to the other encapsulants. The highest WVTR and OTR values were found for TPSE. Its values are several orders of magnitude higher than those of e.g. EVA at 85°C.

Table 19: WVTR and OTR results for different backsheets at different temperatures

		[37]				[20]
	thickness (µm)	23°C	38°C	60°C	80°C	85°C
WVTR		g m^{-2} day^{-1}				
TPT 1	350	0.022	0.13	1.1	5	8
TPT 2	170	0.15	0.7	5	15	
AAA	350	0.022	0.12	2.2	11	18
PET 1	360	0.03	0.18	1.2	7	10
TPSiOx	370	0.01	0.05	0.4	2	
OTR		cm^3 m^{-2} day^{-1}				
TPT 1	350	1	2	4	11	10
TPT 2	170	0.8	4	12	28	
AAA	350	10	40	140	200	390
PET 1	360	1	2	5	12	16
TPSiOx	370	0.12	0.6	4	12	
OTR		cm^3 m^{-2} day^{-1} bar^{-1}				
TPT 1	350	5	10	20	55	50
TPT 2	170	4	20	60	140	
AAA	350	50	200	700	1000	1950
PET 1	360	5	10	25	60	80
TPSiOx	370	0.6	3	20	60	

When looking on the evaluated values for the backsheets the lowest values for the WVTR and OTR were found for TPSiOx. The constitution of this backsheet is PVF on the outer side with a silicon oxide coated PET in the middle and a PE adhesion layer on the inner side. A silicon oxide coating acts as a barrier layer within backsheets, but interestingly this backsheet shows a comparable OTR to the PET (PET/PET/PET) and TPT 1 backsheet at 60 and 80°C. It is claimed that the thickness difference between TPT 1 (350 µm) and TPT 2 (170 µm) is due to different thicknesses of the PET layer in the middle. TPT 2 is thinner than TPT 1 but shows a lower OTR value at 23°C. At all other elevated temperatures the values for TPT 2 are higher than for TPT 1 but not

only doubled in accordance to their overall thickness respectively PET thickness. These values point out the importance of the temperature dependent permeation behavior. While the AAA backsheet shows a moderate WVTR for the evaluated OTR the most significant temperature dependence with comparable high values were detected!

However to sum up: Values given for OTR and WVTR should be considered with caution because 1) there is a strong variation between different measurement technologies 2) different thicknesses of the evaluated materials are of importance 3) different temperature and humidity levels of the measurements changing the results and 4) especially in PV module applications the permeation will be faster in warmer regions than in colder regions, or on midday than in the morning and so on. Therefore the temperature dependence of permeation for materials used in PV modules is of importance and can vary strongly.

4.2 Experimental procedure

In this chapter five different types of backsheets from three different producers were investigated, all of them containing PET core layers with one exception. The outer/inner layers of the backsheets were (i) fluoropolymers (symmetric composition) or (ii) stabilized PET on the outer side and ethylene vinyl acetate (EVA)/ polyethylene (PE) as primer on the inner side. (iiii) The fifth material was a coextruded 3-layered backsheet consisting mainly of PA 12. A description of the backsheet films investigated within this study is given in Table 20.

Table 20: List of backsheets used; WVTR values from supplier information given in [34]

abbr.	inner layer	core layer	outer layer	thickness [µm]	WVTR [g m^{-2} day^{-1}]
B1	PVF *(37)*	PET *(250)*	PVF *(37)*	340	0.7
B2	PVDF *(19)*	PET *(250)*	PVDF *(19)*	325	<0.9
B3	EVA/PE *(125)*	PET *(190)* aluminum *(12)*	PET *(50)*	390	<0.01
B4	EVA/PE *(125)*	PET *(190)*	PET *(50)*	370	<1.4
AAA	PA 12 *(25)*	PA 12 *(300)*	PA 12 *(25)*	350	0.7

The OTR and WVTR of the chosen backsheets were investigated in their initial state and in the course of accelerated aging with various measurement techniques. The applied accelerated aging methods were the DH, climate and irradiation (Climate) and UV aging to see if aging effects have an influence on the permeation behavior (see Table 21). Additional the temperature dependence of the initial and aged (DH, Climate and UV) backsheets was investigated and will be discussed in chapter 4.3.2. Test conditions of the Climate as well as the DH and UV storage with the according measurement method are summarized in Table 21. All chosen measurement methods were described thoroughly in chapter 4.1.2. The three different methods coulometric sensor- Oxtran (method 1), opto-chemical sensor (method 2) and mass spectrometer (method 3) were chosen for evaluation of the OTR. For the WVTR measurements the mass spectrometer (method 3) and the coulometric sensor- Permatran (method 4)

were chosen. All measurement methods, with the applied test conditions during measurements, are summarized in Table 22.

Table 21: Test conditions of applied accelerated aging test with according permeation measurement method

name	T [°C]	irradiation [W/m²]	irradiation source	humidity [%]	duration [h]	method OTR	method WVTR
initial	-	-	-	-	-	1, 2, 3	3, 4
DH	*85*	-	-	*85*	2000	1, 2, 3	3, 4
Climate	*50*	*1000*	300-2800 nm metal halide lamp	*80*	1000	1	4
UV	*60*	*0.76*	340 nm UV lamp (8 h)	*condensation at 50°C (4 h)*	1000	3	3

The space of the test chambers for applying the Climate conditions on the backsheets did not allow for additional sets of samples to evaluate the temperature dependence with method 3. Therefore the Climate aged backsheets were just measured with method 1 (OTR) and method 4 (WVTR). The UV aging was not applied on backsheet B4, as we ran out of samples.

Table 22: Measurement methods with according test conditions for the permeation measurements

method	abbreviation	OTR	WVTR	T [°C]	RH [%]
1	Oxtran	X		23	50
2	Opto-chemical	X		23	0
3	Mass spectrometer	X	X	38, 65, 85	90; 23
4	Permatran		X	23	85

All three measurement methods had different measurement parameters. The Oxtran measures the oxygen transmission rate with parameters chosen from the ASTM F 1927:2005 with 23°C and 50 % RH. As explained, standards give a possibility in variation of the temperatures and humidity. For OTR measurements it is common to use low humidity levels. This is not applicable with the opto-chemical sensor, due to the constitution of this apparatus, respectively detection method. As it is a quasi-isostatic method with a detection of the oxygen directly in the receiving cavity, the

cleaning of the system with nitrogen does not allow for other gases. Therefore the parameters were room temperature (not further specified, but assumed as 23°C) with 0 % RH. The results from these techniques were evaluated from two sample runs to give the median and its standard deviation. With the mass spectrometer method higher temperatures (38, 65, 85°C) and humidity level (90 % RH) was chosen for two reasons. Due to the detection system, parallel measurements of OTR and WVTR are possible and for determining WVTR high humidity levels are required. The higher temperatures are application-relevant, especially for PV modules. Additional it allows for a determination of influences of water vapor transmission on the oxygen transmission. From the results of this method the temperature dependencies of the OTR and WVTR for the backsheets were calculated (see chapter 4.3.2). The temperature dependence was used to calculate the OTR and WVTR at 23°C and 90 % RH for chapter 4.3.1. To see if there is an influence of water vapor permeation on oxygen permeation the backsheet AAA was additional measured with same temperatures (38, 65, 85°C), but a lower relative humidity level (23 % RH). OTR of polyamides are claimed to be strongly influenced by water vapor in between the polymer chains. Hence, the comparison of the results should give conclusion about the humidity influence. All results from this measurement method were evaluated from just one measurement as the measurements at three different temperatures were time-consuming and sample-consuming. WVTR measurements using the Permatran were applied in accordance to ASTM F 1249:2005 with 23°C and 85 % RH.

4.3 Results and discussion

In the following the OTR and WVTR measurement results of in this work investigated backsheets will be discussed. Therein the results for the initial backsheets will be shown and those of different accelerated aged samples.

4.3.1 Permeation properties of backsheets

In general it is difficult to compare results from literature or datasheets, mainly due to not given thicknesses, measurement conditions and/or different measurement techniques for measured samples. Therefore quantities given in literature cannot be directly correlated to the presented results and so for interpretation just relations between evaluated values for polymers will be mentioned. In Figure 80 to Figure 84 the evaluated values for all three chosen OTR measurement techniques are shown.

Within permeation processes sorption and desorption plays a role, but diffusion is the limiting factor for transmission rates. For all multilayered backsheets (AAA is an exception) the thickest layer within is the PET layer with 250 µm for B1, B2 and 240 µm for B3, B4. Therefore the most reliable results have to show the same tendency in the course of aging for the PET based backsheets. The Oxtran results showed not the same tendencies within the PET based backsheets (standard deviations from 0.1 to 3.5 $cm^3\ m^{-2}\ day^{-1}\ bar^{-1}$). The decrease with the opto-chemical method results was within the standard deviations (0.3 to even 2 $cm^3\ m^{-2}\ day^{-1}\ bar^{-1}$). The determined OTR values of the mass spectrometer method are significant higher than those of the others and showed a same tendency in the course of aging. For all these reasons the further discussion on the OTR results focuses on the results measured with the mass spectrometer method.

For all other initial backsheets (B1, B2 and B4) it can be said, that B1 showed the lowest OTR value followed from B2 and B4 (see Figure 80 to Figure 83). The OTR values for commercial available PVF, PVDF and PET (outer layers of B1, B2, B3 and B4) are given in the same range [3]. The given values for PE (LDPE was taken) and EVA (with 18 % VA) were about $2*10^2$ higher in comparison to the other outer layers of the backsheets [3]. Therefore it is obviously the thickness of the PET layer in the middle

which is mainly responsible for their OTR values. This is also indicated by the differences between B4, B1 and B2. In B1 and B2 the PET middle layer is 250 µm thick, while the PET middle and outer layer of B4 is 240 µm thick. While for B1 in comparison to B2 the overall thickness (-15 µm) seems to enhance the OTR, for B4 it does not play such a significant role due to the extraordinary high OTR values for the outer layers, but still the highest OTR among all initial PET based backsheets was detected.

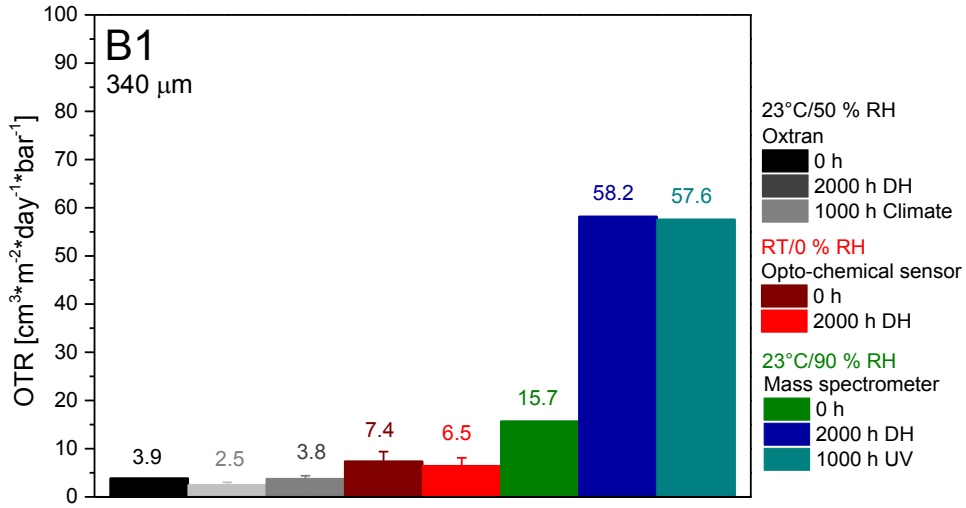

Figure 80: OTR results for the initial, 2000 h DH, 1000 h Climate and 1000 h UV aged B1 backsheet

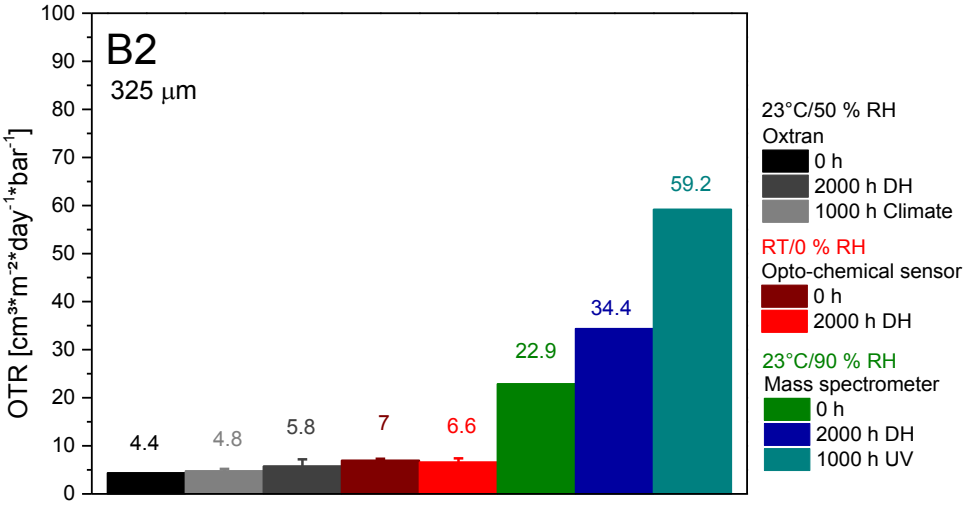

Figure 81: OTR results for the initial, 2000 h DH, 1000 h Climate and 1000 h UV aged B2 backsheet

Tendencies detected in the course of DH and UV aging showed an increase for all PET based backsheets. While B4 had the highest OTR amongst the initial PET based backsheets, it showed the lowest increase in OTR for the 2000 h DH aged samples.

Also obvious is the low OTR value for B3 (see Figure 82). In this case the upper detection limit of the Oxtran was reached. This material was not measured with the mass spectrometer method. Due to its low OTR and WVTR, the measuring times would have been too long. With the opto-chemical method a value of 0.002 cm^3 m^{-2} day^{-1} bar^{-1} (±0.0023) was detected for the initial sheet. The aluminum layer, as applied in B3, acts as barrier against oxygen and water vapor. Although metals are in general impermeable, for low thicknesses permeation is possible through small defects in such layers. Therefore a very low OTR for B3 was expected. The difference between the initial and the 2000 h DH (0.005 cm^3 m^{-2} day^{-1} bar^{-1} ±0.0063) aged sheets is difficult to interpret due to the vanishingly small values which are in the same range as the standard deviations.

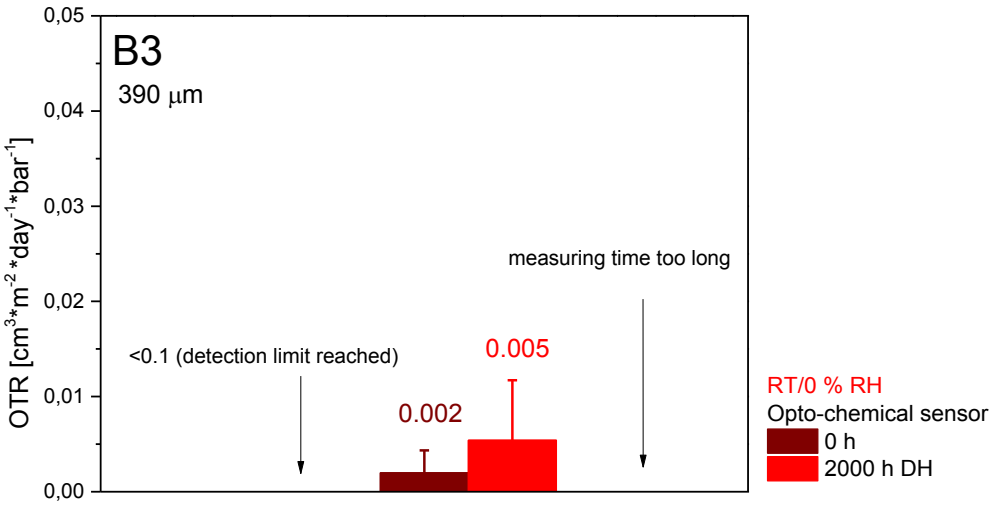

Figure 82: OTR results for the initial and 2000 h DH aged B3 backsheet

The OTR of the UV aged samples of B1 and B2 was about the same. In chapter 3.2.1 in the course of DH aging of the PET middle layers of B1, B2, B3 and B4 post-crystallization and chain scissoring due to hydrolysis was detected. Post-crystallization was also observed for the UV aged samples, but the effect (increase in PET enthalpy) was not very distinct. As explained crystalline parts in polymers are impermeable.

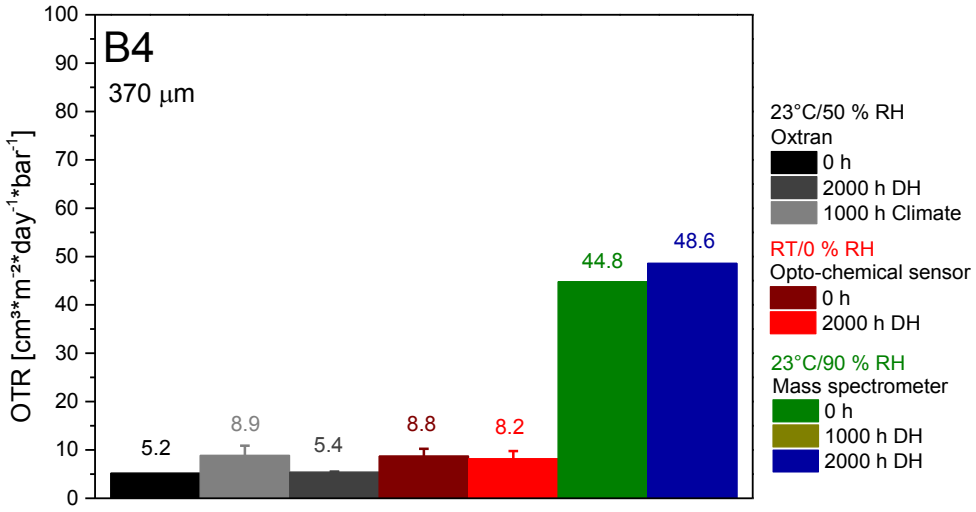

Figure 83: OTR results for the initial, 2000 h DH and 1000 h Climate aged B4 backsheet

Post-crystallization would decrease the OTR, hydrolysis seems to be more relevant for changes in the course of aging. Hydrolysis induces end-groups within the polymer chain molecules. These end-points give the permeant more possibilities to move. The evaluation of the PET crystallization temperature for the 2000 h DH and 1000 h UV aged samples, which was correlated to hydrolysis within PET in chapter 3.2.1, showed for all backsheets an increase (see Table 23).

Table 23: Increase in PET crystallization temperatures of B1, B2 and B4

	B1	**B2**	**B4**
2000 h DH	12.4	11.2	8.7
1000 h UV	1.3	1.3	2.1

The evaluated differences show conspicuous similar increases for B1 and B2, while B4 differs with lower values for the DH aged samples. As B1 and B2 had a higher increase in OTR than B4 a correlation between hydrolysis of PET layers with the increase in OTR values is assumed. But as hydrolysis was significant lower for the UV aged samples possibly surface related degradation mechanisms are involved in enhancing the OTR.

It is obviously that the PA 12 based backsheet shows a far higher OTR value (initial: 210.6 cm^3 m^{-2} day^{-1} bar^{-1}) than the PET based backsheets (see Figure 84). For the opto-chemical method the value was not determinable as the upper detection limit of 50 cm^3 m^{-2} day^{-1} bar^{-1} was reached. Semi-crystalline polyamides in general are known for

their low OTR [23] [22] [24] [3]. PA 12 is given as the polyamide with the lowest barrier against oxygen, but with no specified values [3]. PA 11 is given as slightly better barrier, but its values are not significant higher as PA 6, which is described as the best oxygen barrier material within polyamides [3] [24]. The differences can also not be explained by different thicknesses of the backsheets as the thickness of AAA with 350 µm is beneath those of B3, B4 and above those of B1 and B2.

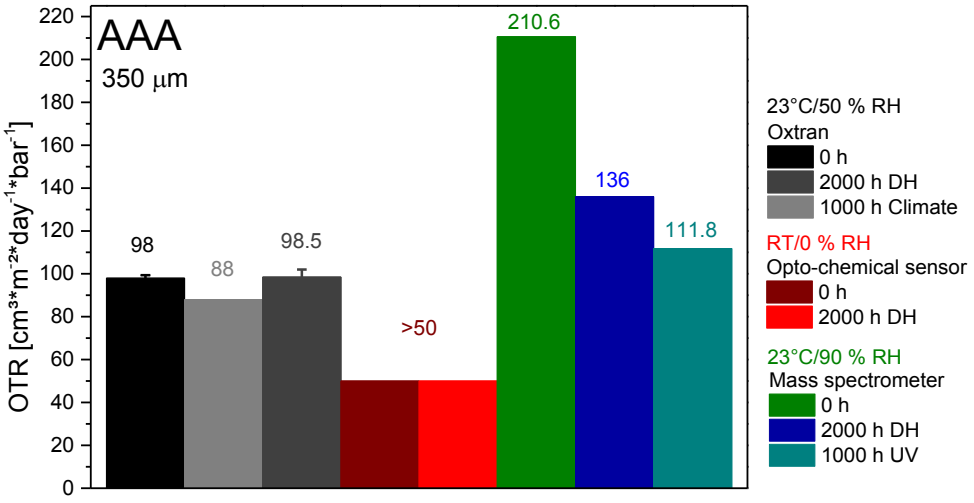

Figure 84: OTR results for the initial, 2000 h DH, 1000 h Climate and 1000 h UV aged AAA backsheet

Polyamides are claimed to get a better oxygen barrier if more water vapor is in between the polymer chains. The more CH_2 groups in relation to CONH groups are in the chains of polyamides the less water uptake can be expected due to less hydrogen bonding. As PA 12 has within semi-crystalline polyamides the highest relation of CH_2 (n=11) to CONH the high OTR can also not be explained by this effect. The decrease of the OTR in the course of DH aging (136 cm^3 m^{-2} day^{-1} bar^{-1}) was, due to the high humidity impact, expected. The only explanation which could be possible for the high OTR in general is the high load of fillers and/or polypropylene (PP) in this multilayer material [38]. The fillers may act as spacer in between the polymer chains giving more possibilities to move for the permeating oxygen. PP itself can also enhance the OTR, as its OTR is given about eight times higher than in relation to PA 11 [24]. For the UV aged sheet samples the decrease was higher than for the DH aged sheet. The general

decrease after accelerated aging can possibly attributed to more water vapor in between the polymer chains and morphological changes in the PP in the course of aging. While for the initial sheet a broad crystallization region for the PP was detected in DSC measurements, a more uniform area was obvious for the DH and UV aged samples indicating the morphological change.

In relation to the OTR the right combination of AAA (high OTR) with EVA can be regarded as a very good choice in order to meet the needs for low corrosion and less yellowing in a PV module [20]. For backsheets it can be said, that the absolute values of OTR will change in the course of aging and in some cases even a backsheet with the highest OTR for the initial sheet will have the lowest OTR in the course of aging. Therefore, when combinations in respect to the permeation behavior of oxygen are built, the changes in the course of aging should be taken into account.

In Figure 85 to Figure 88 all evaluated WVTR values for the initial and artificial aged backsheets are shown. Again the measurement parameters of both techniques differed. While the relative humidity was 90 % for the mass spectrometer, it was 85 % for the Permatran method. The backsheet B3 was not measurable with the Permatran method (detection limit reached) and for the mass spectrometer method the detection time (about 1-2 weeks) was too long.

In contrast to the OTR values, the values for the mass spectrometer method are significant lower than the ones determined with the Permatran method. As the relative humidity conditions for both techniques are comparable (only 5 % difference) and the temperature (23°C) is the same, an influence of the oxygen permeation is assumed. Possibly the permeating oxygen within the mass spectrometer measurements occupies free volume in the polymeric layers and hinders the water vapor to use them for diffusion. Additional, a mass spectrometer detects every molecule due to its general detection principle. This supports the assumption and as oxygen is one component of air (~21 %) it gives more practice relevant results. But the WVTR results detected with the mass spectrometer method show no uniform tendencies for the PET based backsheets in the course of aging. This possibly gives a hint to too low values, with too high standard deviations. As the determined values

are low also inhomogeneity and deviating thicknesses among the samples can have a more significant influence. Unfortunately we have only one sample run within these measurements and cannot give a proof of that. One other aspect is the calculation of the given results from the evaluated values of the temperature dependence. Not in all cases a perfect coefficient of determination for evaluation of the results were found. It gives another uncertainty. However, the results for all backsheets ranged between 0.002 and 0.042 and will not further be discussed, as in chapter 4.3.2 the evaluated temperature dependence will give further details.

However the Permatran is mostly used in the PV industry for determining the WVTR. Therefore, the WVTR results of the Permatran for the used backsheets are similar to those listed in Table 8 (chapter 4.1.3). Additional, the Permatran results show about the same tendencies for the PET based backsheets in the course of aging. For this reason the WVTR results will at first be discussed for this technique.

The backsheets B1 and B2 showed similar WVTR values, just enhanced for the DH aged samples but also with a high standard deviation. B4 showed values general beneath those of B1 and B2. This is in contrast to the results of the OTR measurements, where B4 showed slightly enhanced values. Also the given WVTR values in the supplier information, listed in Table 8, claims a higher WVTR than for B1 and B2. The overall thickness for B1 (340 µm) and B2 (325 µm) is beneath those of B4 (370 µm), while the thicknesses of the PET layer of B1 and B2 (250 µm) is slightly above those of B4 (240 µm for middle + outer layer). PE is generally claimed to be a good barrier against water vapor [23] [22]. Listed values for LDPE were similar to those of PET but lower than for PVF [4]. For B4 it is assumed that on the one hand the higher thickness of the whole layer and on the other hand the better barrier properties of PE decreasing the WVTR. It seems that the OTR values are more influenced by the barrier properties of PET as otherwise the values for B4, B1 and B2 would be in the same range also for the WVTR. In chapter 3.2.1 the DH aging behavior of the PET middle layers of B1, B2, B3 and B4 indicated little post-crystallization and significant chain scission due to hydrolysis. Crystalline parts in polymers are generally impermeable, but imperfections introduced due to hydrolysis can enhance

permeation. Consequently the WVTR values increased for the DH aged samples. This is supported by similar WVTR values for the initial and the Climate aged samples. The investigated Climate aged backsheets (chapter 3.2.2) showed significant lower hydrolysis than the DH aged samples. But one has to keep in mind the high standard deviations of the Permatran method. The increase in WVTR values for the 2000 h DH aged samples is possibly just due to low reproducibility.

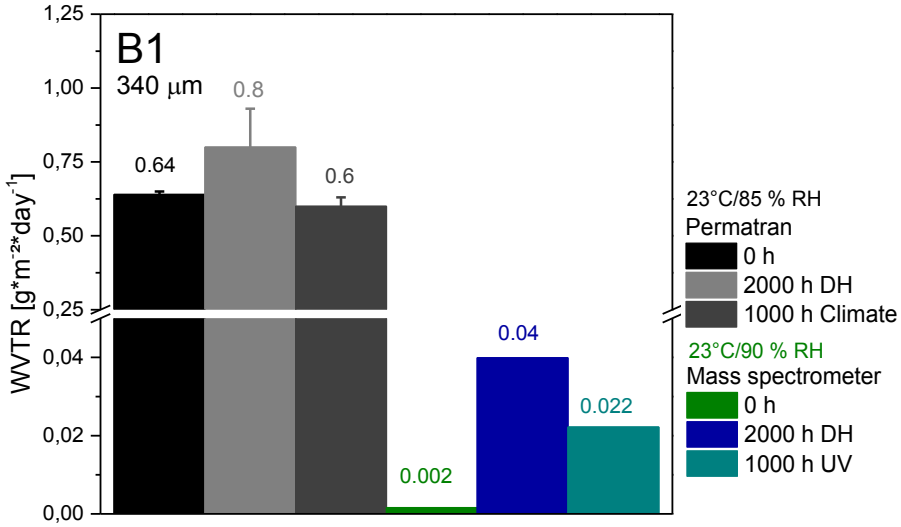

Figure 85: WVTR results for the initial, 2000 h DH, 1000 h CIimate and 1000 h UV aged B1 backsheet

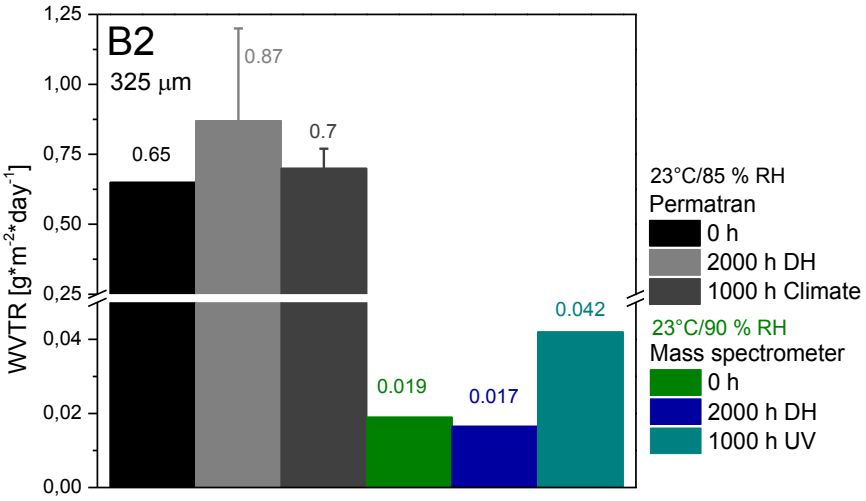

Figure 86: WVTR results for the initial, 2000 h DH, 1000 h CIimate and 1000 h UV aged B2 backsheet

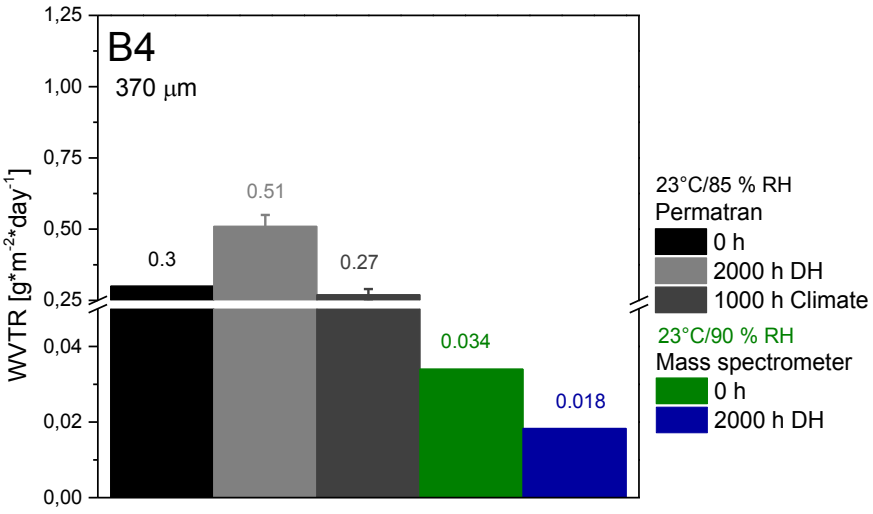

Figure 87: WVTR results for the initial, 2000 h DH, 1000 h CIimate aged B4 backsheet

The initial median value (0.66 g m^{-2} day^{-1}) for AAA is slightly beneath the supplier given value of 0.7 g m^{-2} day^{-1} (see Figure 88 and also Table 8) [34]. Although the OTR values of AAA are significant higher in comparison to the other backsheets, there is no significant difference in the WVTR values in comparison to the others (also for the mass spectrometer method results). When looking on the values of WVTR given for PP, PA 6 (which are comparable to PA 12) and PET in Figure 75 it seems that the barrier properties of AAA are significantly influenced by the in the middle layer incorporated PP, as also assumed for the OTR. Therein PP is given as a much better water vapor barrier as PA 6. For AAA vanishingly small changes in the course of both aging methods were detected. It seems that the aging related changes in AAA don`t have a significant influence on the water vapor permeation. As shown in chapter 2.2.2 and 3.2.2 this material exhibits a re-crystallization with a vanishingly small increase in crystallinity. No other aging effects were found under these accelerated aging conditions. This supports the assumption of the permeation behavior mainly driven by the permeation properties of PP. But for the OTR values a correlation of the morphology of the PP layer with its changes in the course of aging was assumed. Within the WVTR values these discussed changes seems to have no influence on the results. Another possibility is that the permeating oxygen hinders the water vapor diffusing path.

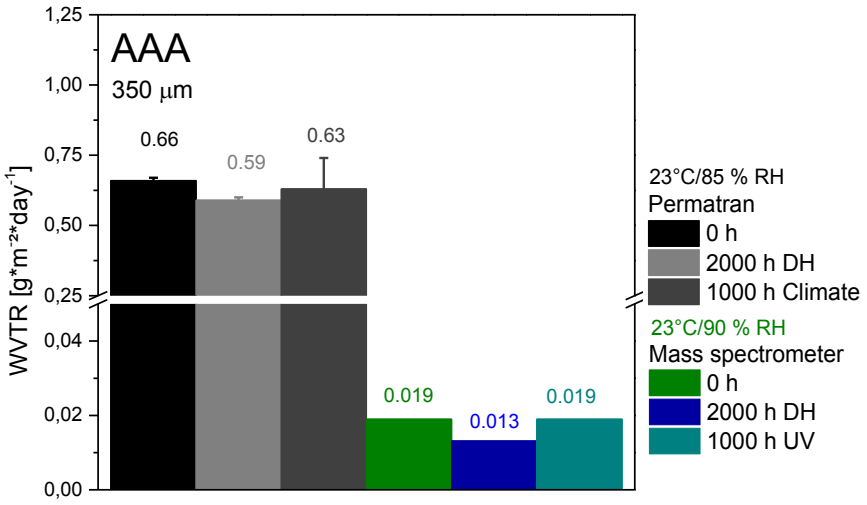

Figure 88: WVTR results for the initial, 2000 h DH, 1000 h Climate and 1000 h UV aged AAA backsheet

With respect to the WVTR results it can be said, that all backsheets had comparable results. A much lower susceptibility to degradation of encapsulants and corrosion of the PV module is expected, when B3 is used as backsheet. This backsheet had by far the lowest OTR and WVTR, but one has to keep in mind the wanted permeation of acetic acid when EVA is used. With such tight backsheet unwanted effects like enhanced corrosion due to acetic acid and also possibly an enhancement of PID can be expected. Additional the aluminum layer in between the multilayered backsheet can inhibit security issues.

4.3.2 Temperature dependent permeation properties of backsheets

The temperature dependent oxygen and water vapor transmission rates for the investigated backsheets are shown from Figure 89 to Figure 98. The permeation process is strongly temperature controlled and can be described with the Arrhenius-model (see also Equation 1 and 2). Therefore a logarithmic scaling of the results over the inverse temperature (1/K) was chosen to allow for the linear evaluation. With the linear adjustments, respectively gradients, the calculation of the activation energy via Arrhenius approach was done. The activation energy is the energy necessary for triggering a reaction [39]. Therefore according values of OTR and WVTR with the evaluated activation energies are depicted in Table 24 to Table 32.

The evaluated temperature dependent OTR and WVTR of B1, B2, B4 and AAA clearly indicating an increase in transmission rates with temperature, resulting in different gradients as well as activation energies. The coefficients of determination for the OTR results were among 0.78 and 1 and the WVTR results among 0.98 and 1. The activation energies for the PET based backsheets of the OTR were significant lower (2.3- 9.5 kJ mol^{-1} K^{-1}; for AAA 14.7- 20.1 kJ mol^{-1} K^{-1}) as those of the WVTR (32.4- 39.1 kJ mol^{-1} K^{-1}; for AAA 40.8- 42.5 kJ mol^{-1} K^{-1}). At elevated humidity levels water molecules can act as spacer in between polymer chains which are increasing the free volume and possibly allow for an easier formation of interstitials for the permeating oxygen. Polyolefines are claimed to show no effect of RH on gas permeability [4]. This may also lower the general activation energies for oxygen permeation as the conditions during measurements had a high humidity level (90 % RH).

The OTR results for B1 are shown in Figure 89 and Table 24. The initial values increased significant from 22.8 (38°C) to 57.8 (85°C) cm^3 m^{-2} day^{-1} bar^{-1} with an activation energy of 8 kJ mol^{-1} K^{-1}. The OTR in the course of aging ranged among 63.8 (38°C 2000 h DH) and 98.1 (1000 h UV) cm^3 m^{-2} day^{-1} bar^{-1}. The OTR values of the 1000 h UV aged sheets are in general higher than those of the 2000 h DH aged ones, but with similar activation energy. The difference between the activation energies can possibly attributed to a coefficient of determination of 0.95 for the UV aged samples.

Interestingly, for all aged samples a change in the gradient of the OTR results was detected, also obvious in the lowered activation energies (see Table 24).

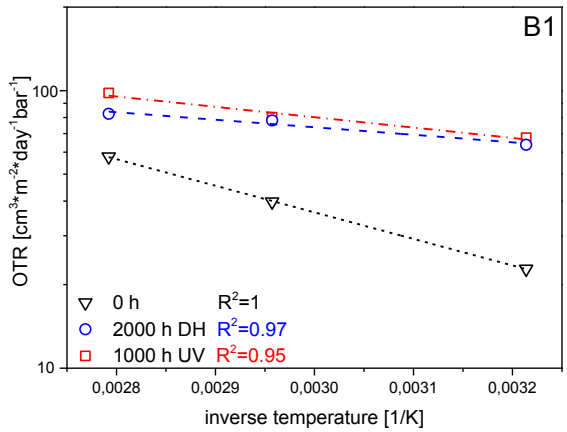

Table 24: OTR results of B1 with calculated activation energies (Ea) in its initial, 2000 h DH and UV aged state

B1	38°C	65°C	85°C	*Ea*
0 h	22.8	39.8	57.8	*8.0*
2000 h DH	63.8	78.1	82.5	*2.3*
1000 h UV	67.7	80.2	98.1	*3.1*

Figure 89: Temperature dependent OTR of backsheet B1 in its initial, 2000 h DH and 1000 h UV aged state

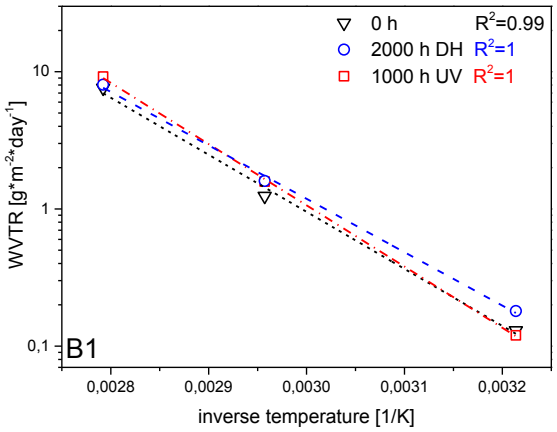

Table 25: WVTR results of B1 with calculated activation energies (Ea) in its initial, 2000 h DH and UV aged state

B1	38°C	65°C	85°C	*Ea*
0 h	0.13	1.24	7.61	*37.6*
2000 h DH	0.18	1.6	8.04	*32.4*
1000 h UV	0.12	1.58	9.22	*37.1*

Figure 90: Temperature dependent WVTR of backsheet B1 in its initial, 2000 h DH and 1000 h UV aged state

This was not detected within the WVTR results shown in Figure 90 and Table 25. For the 2000 h DH aged sheets significant hydrolysis effects and little post-crystallization was observed in chapter 3.2.1. For the UV aged sheets a combination of post-crystallization and initial chemical aging effects were observed, similar to the Climate aged sheets in chapter 3.2.2 (see also Table 23). Possibly the resulting chain depletion of chemical aging mechanisms in between the polymer film induces more interstitials making the movement of the permeant easier. At higher temperatures these imperfections possibly rearrange via e.g. chemo-crystallization and as a result the determined values at 65 and 85°C converge to the ones of the initial sample.

The WVTR results of the B1 initial samples increased with temperature from 0.13 (38°C) to 7.61 (85°C) g m^{-2} day^{-1}. The WVTR increased slightly in the course of both aging methods. The activation energies did not change significant in the course of aging, but are significant higher than those of the OTR.

For B2 the initial samples showed also a significant increase of OTR with temperature from 33.8 (38 °C) to 99.5 (85°C) cm^3 m^{-2} day^{-1} bar^{-1} (see Figure 91 and Table 26). All initial values of B2 are slightly above those for B1. All other OTR in the course of aging ranged among 39.8 (38°C 2000 h DH) and 88.5 (1000 h UV) cm^3 m^{-2} day^{-1} bar^{-1} and showed therefore lower OTR values in the course of aging than B1. While the activation energies for the 2000 h DH and 1000 h UV aged sheets were similar for B1, for B2 the activation energy for the 2000 h DH aged sheet of 5.7 kJ mol^{-1} K^{-1} was enhanced in comparison to the UV aged one (2.8 kJ mol^{-1} K^{-1}). But when looking on the coefficient of determination this can possibly be attributed to an outlier of the determined OTR at 85°C for the UV aged sample. However, also for this sheet a decrease in activation energy in the course of aging was detected with general higher values of the 1000 h UV aged samples.

For B2 the initial values of WVTR with temperature are about in the same range as those of B1 (see Figure 92 and Table 27). For B2 also an increase in WVTR results was detected in the course of aging, which is again more significant for the UV aged samples than for the DH aged ones.

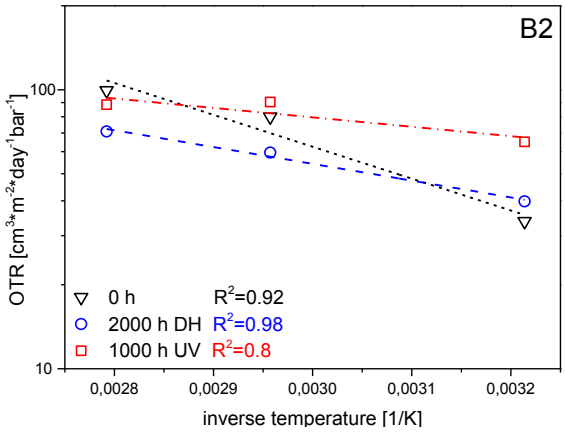

Figure 91: Temperature dependent OTR of backsheet B2 in its initial, 2000 h DH and 1000 h UV aged state

Table 26: OTR results of B2 with calculated activation energies (Ea) in its initial, 2000 h DH and UV aged state

B2	38°C	65°C	85°C	*Ea*
0 h	33.8	80	99.5	*9.5*
2000 h DH	39.8	59.5	70.9	*5.7*
1000 h UV	65.0	90.4	88.5	*2.8*

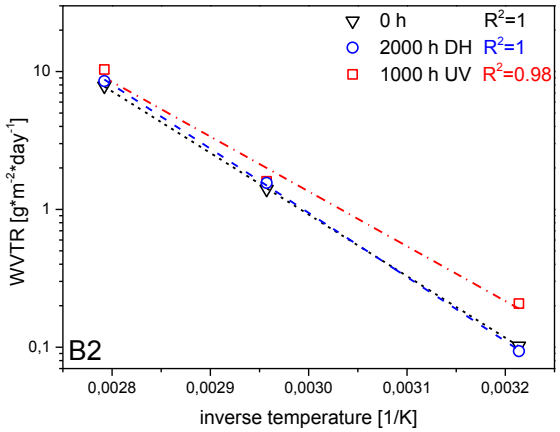

Figure 92: Temperature dependent WVTR of backsheet B2 in its initial, 2000 h DH and 1000 h UV aged state

Table 27: WVTR results of B2 with calculated activation energies (Ea) in its initial, 2000 h DH and UV aged state

B2	38°C	65°C	85°C	*Ea*
0 h	0.1	1.4	7.86	*37.2*
2000 h DH	0.09	1.56	8.53	*38.7*
1000 h UV	0.21	1.6	10.36	*33.1*

For B4 the OTR values for the initial samples ranged between 54.2 (38°C) and 89.3 (85°C) cm^3 m^{-2} day^{-1} bar^{-1} (see Figure 93 and Table 28). The 2000 h DH aged sample showed similar values to the ones of B1 and B2 with values between 44.7 (38°C) and 87.4 (85 °C) cm^3 m^{-2} day^{-1} bar^{-1}. The OTR values in the course of aging decreased. For B4 the lowest change in activation energy was detected. It increased from 4.3 to 5.7 kJ mol^{-1} K^{-1}. This backsheet showed also the lowest increase in melting enthalpies in the course of DH aging for all PET based backsheets. Possibly this explains the almost similar inclination of the initial to the 2000 h DH aged backsheet (activation energy: 4.3 and 5.7 kJ mol^{-1} K^{-1}). Polyolefines are claimed to show no effect of RH on gas permeability [4]. This possibly explains the vanishingly small change in the gradient for the aged samples.

For B4 the WVTR values for the initial samples ranged between 0.47 (38°C) and 10.63 (85°C) g m^{-2} day^{-1} (see Figure 94 and Table 29). The WVTR results decreased for the 2000 h DH aged samples and showed therefore the same tendency as for the OTR results. B4 had the highest WVTR for the initial samples with, in contrast to B1 and B2, lower values for the 2000 h DH aged samples than for the initial ones.

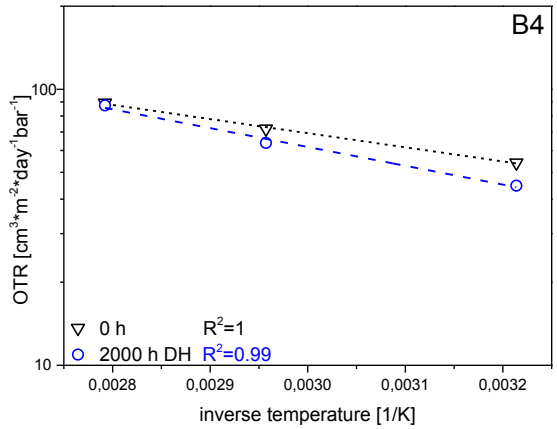

Figure 93: Temperature dependent OTR of backsheet B4 in its initial and 2000 h DH aged state

Table 28: OTR results of B4 with calculated activation energies (Ea) in its initial and 2000 h DH aged state

B4	38°C	65°C	85°C	*Ea*
0 h	54.2	71.9	89.3	*4.3*
2000 h DH	44.7	63.9	87.4	*5.7*

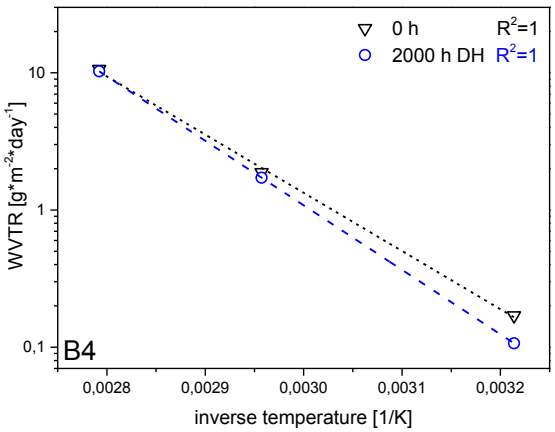

Figure 94: Temperature dependent WVTR of backsheet B4 in its initial, 2000 h DH and 1000 h UV aged state

Table 29: WVTR results of B4 with calculated activation energies (Ea) in its initial and 2000 h DH state

B4	38°C	65°C	85°C	*Ea*
0 h	0.47	1.88	10.63	*35.3*
2000 h DH	0.11	1.7	10.26	*39.1*

For AAA a wide spread of the OTR values for the initial sheet samples were detected, resulting in a low coefficient of determination, therefore the linear adjustment is not shown (R^2=0.78; see Figure 95 and Table 30). The initial values are in general significant higher than those of the PET based backsheets B1, B2 and B4. At 38°C the OTR was 386 cm^3 m^{-2} day^{-1} bar^{-1} and at 85°C significant enhanced with 2642 cm^3 m^{-2} day^{-1} bar^{-1}. In contrast to the PET based backsheets, AAA showed distinct decreases in OTR for the aged samples. The OTR values for the 2000 h DH aged samples at all temperatures are the lowest among all results of AAA. In contrast to the results for the PET based backsheets OTR values diverge with increase in temperature.

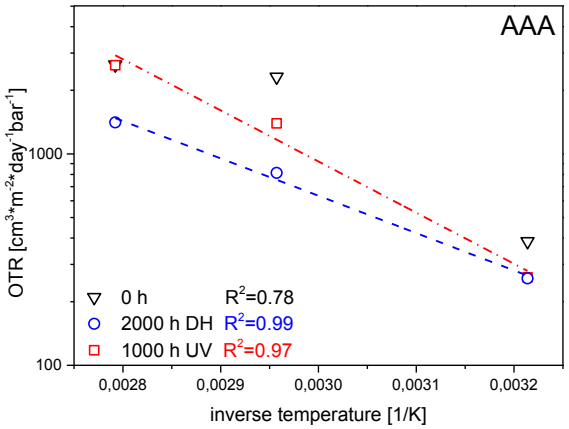

Figure 95: Temperature dependent OTR of backsheet AAA in its initial, 2000 h DH and 1000 h UV aged state

Table 30: OTR results of AAA with calculated activation energies (Ea) in its initial, 2000 h DH and UV aged state

AAA	38°C	65°C	85°C	*Ea*
0 h	386	2315	2642	*17.2*
2000 h DH	258	813	1410	*14.7*
1000 h UV	261	1395	2629	*20.1*

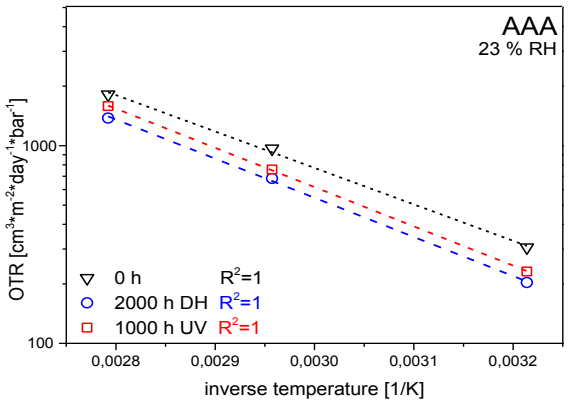

Figure 96: Temperature dependent OTR of backsheet AAA in its initial, 2000 h DH and 1000 h UV aged state measured at 23 % RH

Table 31: OTR results of AAA with calculated activation energies (Ea) in its initial, 2000 h DH and UV aged state

AAA	38°C	65°C	85°C	*Ea*
0 h	306	967	1814	15.3
2000 h DH	203	683	1380	16.5
1000 h UV	231	758	1585	16.5

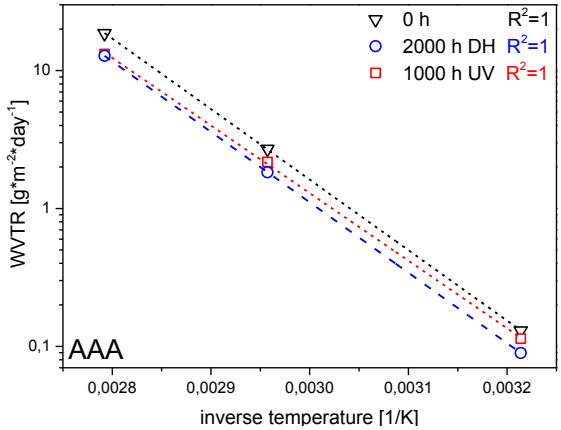

Figure 97: Temperature dependent WVTR of backsheet AAA in its initial, 2000 h DH and 1000 h UV aged state

Table 32: WVTR results of AAA with calculated activation energies (Ea) in its initial, 2000 h DH and UV aged state

AAA	38°C	65°C	85°C	*Ea*
0 h	0.13	2.7	18.63	*42.5*
2000 h DH	0.09	1.83	12.8	*42.5*
1000 h UV	0.11	2.17	13.18	*40.8*

OTR of polyamides are claimed to be strongly influenced by water vapor in between the polymer chains. To see if there is an influence of the humidity level on the OTR of AAA additional the measurement results of the same temperatures but with lower

relative humidity (23 % RH) is shown in Figure 96. The comparison of the results shown in Figure 95 (90 % RH) and Figure 96 (23 % RH) clearly indicates a significant humidity influence on the oxygen permeation behavior of AAA. The measurement results for the 23 % RH showed significant lower OTR for all initial and aged samples. Also, in contrast to the 90 % RH measurements, no changes in the gradient in the course of aging were detected.

The initial WVTR results for AAA at 38°C with 0.13 g m^{-2} day^{-1} was the same as for B1 and comparable to B2. At the elevated temperatures of 65 and 85°C significant higher WVTR were detected than for B1, B2 and even B4. The WVTR values in the course of aging decreased for this backsheet, as also detected for the OTR.

In Figure 98 all WVTR (left side) and OTR (right side) results for the initial backsheets for a better comparison are shown. All investigated backsheets point out the importance of knowing the temperature dependence to give application relevant OTR and WVTR to according temperatures. Again, it is obvious, that in OTR there are larger differences in between the backsheets. Especially AAA showed in comparison to the PET based backsheets significant enhanced OTR, which was more distinct for measurements at higher humidity level (90 % RH). Comparison of both measurements at 90 % RH and 23 % RH of AAA reveals possibly an outlier at 65°C and 90 % RH. However, it is still obvious that the lower humidity level of 23 % induces lower OTR for AAA. Interestingly, the backsheet AAA showed similar or same values of WVTR to the other backsheets, but at elevated temperatures higher WVTR results were detected. AAA seems to be a good choice for combination with EVA as encapsulant due to its high OTR. The higher WVTR in contrast to the PET based backsheets can enhance PID effects, but it also indicates a higher acetic acid transmission rate than for backsheets with low WVTR.

B1 and B2 showed approximately the same inclinations in WVTR and OTR results. B2 (325 µm) is thinner than B1 (340 µm), but if the thickness would be the only driving factor, also approximately same values in OTR would have been detected for these materials. The outer layers of B1 (PVF) are given as slightly better oxygen barrier than those of B2 (PVDF) [3]. This possibly is the reason for the difference in OTR values. B4

showed a differing behavior with a slightly different inclination of WVTR and significant other inclination of OTR results. Remarkable differences between B1 and B2 to B4 are the higher overall thickness of B4 (370 µm), but lower thickness of PET (240 µm) and different outer layers (inner layer: PE, EVA). The different results can possibly be attributed to other outer layers.

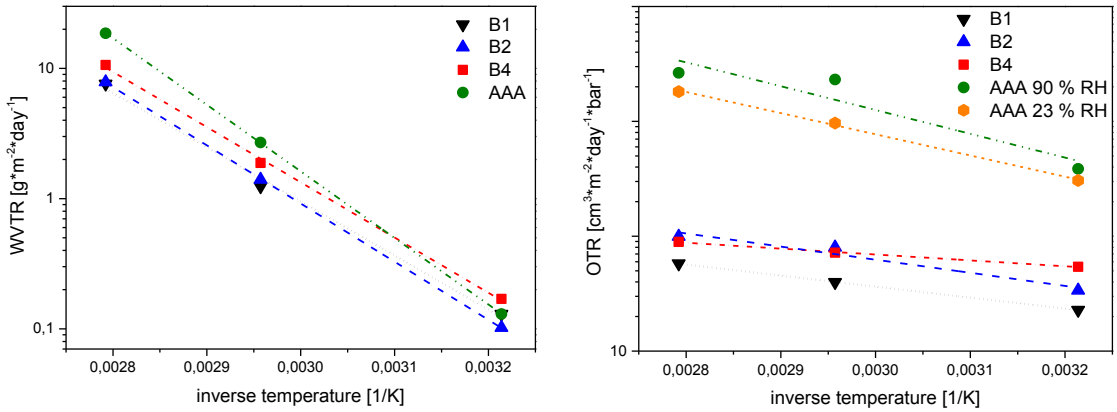

Figure 98: Temperature dependent WVTR (left side) and OTR (right side) of all initial backsheets

The results revealed that changes in the course of aging should also be investigated. Changes of the OTR with temperature are more significant than those for the WVTR. Tendencies (increase or decrease) in the course of aging were different among the PET based backsheets. But the same tendencies were detected for OTR and WVTR within one backsheet.

4.4 Summary and conclusions

In c-Si PV modules permeation of water vapor and oxygen play a major role on reliability. Thus, the knowledge of the permeation rates of relevant substances through the backsheets and their sensitivity to the ageing behavior of the materials involved is of prime importance.

Therefore in chapter 4.3.1 the OTR and WVTR of five different backsheets in their initial state and in the course of different accelerated aging methods were discussed. Additional different measurement techniques for determination of OTR and WVTR were compared. It clearly pointed out the difficulties when permeation results of different techniques are compared. As most relevant influences different measurement parameters were indicated, but also the detection methods. The results of OTR and WVTR gave an overview on the general permeation properties of the investigated backsheets. Changes in the course of aging are not negligible and revealed increases in OTR.

As PV modules operating at different temperatures due to diurnal and seasonal cycles, but also to operation in different climate zones, in chapter 4.3.2 the focus was on the temperature dependence of OTR and WVTR of four backsheets. Therein the activation energies were calculated to allow calculation of the results for other temperatures. They revealed general lower energies necessary for inducing oxygen permeation. In the course of aging lower activation energies for oxygen permeation were found for two backsheets. The WVTR decreased in the course of aging with no significant change in activation energies. The Arrhenius concept proved to be applicable for describing the aging effects of the structural changes on permeation rates.

A correlation between water molecules acting as spacer in polymer chains and the enhancement of oxygen permeation was assumed. The influence of the humidity level on oxygen permeation of a polyamide based backsheet was found to have a significant role on resulting OTR values.

4.5 References

[1] J. Comyn, Polymer Permeability, Elsevier Applied Science Publishers Ltd, Essex, 1985.

[2] M. Knausz, Praxisnahe Charakterisierung von Kunststoffen fluidischer Systeme von Analysatoren hinsichtlich Sauerstoffaustauschvorgängen. Diploma thesis, Montanuniversitaet Leoben, 2010.

[3] L.K. Massey, Permeability Properties of Plastics and Elastomers. A Guide to Packaging and Barrier Materials, Plastics Design Library, 2003.

[4] H.F. Mark, "Barrier Polymers". In: Encyclopedia of Polymer Science and Technology, 5th ed., John Wiley and Sons Inc., New York, 2002.

[5] B. Duncan, J. Urquhart, S. Roberts, Review of Measurement and Modelling of Permeation and Diffusion in Polymers, NPL Report DEPC MPR 012 (2005).

[6] G. Menges, E. Haberstroh, W. Michaeli, E. Schmachtenberg, Werkstoffkunde Kunststoffe, 5th ed., Carl Hanser Verlag, Munich, 2002.

[7] A. Naranjo, M.d.P. Noriega, T.A. Osswald, A. Roldán-Alzate, J.D. Sierra, Testing and Characterization of Plastics: Permeability Properties, Carl Hanser Verlag, Munich, 2007.

[8] J. Fahlteich, Transparente Hochbarriereschichten auf flexiblen Substraten. Doctor thesis, Technical University Chemnitz, 2010.

[9] J. Fahlteich, M. Fahland, W. Schönberger, N. Schiller, Permeation barrier properties of thin oxide films on flexible polymer substrates, Thin Solid Films 517 (2009) 3075–3080.

[10] M. Tscherner, C. Konrad, A. Bizzarri, M. Suppan, M. Cajlakovic, V. Ribitsch, F. Stelzer, Opto-chemical Method for Ultra-Low Oxygen Transmission Rate Measurement, in: IEEE Sensors, Christchurch, New Zealand, 2009.

[11] J. Spanring, A. Droisner, B. Erler, M. Kraxner, W. Krumlacher, A. Plessing, A. Ruplitsch, High Performance Barrier Films for Flexible Photovoltaic Module Encapsulation, in: 24th European Photovoltaic Solar Energy Conference and Exhibition, Hamburg, 2009.

[12] W. Krumlacher, H. Muckenhuber, A.K. Plessing, C. Schinagl, E. Url, A. Nigg, Flexible Encapsulation with Backsheets and Frontsheets for PV Applications, in: 27th European Photovoltaic Solar Energy Conference and Exhibition, Paris, France, 2013.

[13] G. Oreski, Untersuchung des Delaminationsverhaltens von Folienverbunden für die Einkapselung von PV-Modulen. Diploma thesis, Montanuniversitaet Leoben, 2004.

[14] G.D. Barber, G.J. Jorgensen, K. Terwilliger, S.H. Glick, J. Pern, T.J. McMahon, New Barrier Coating Materials for PV Module Backsheets: Preprint, in: 29th IEEE Photovoltaic Specialists Conference, New Orleans, USA, 2002.

[15] G. Stollwerck, W. Schoeppel, A. Graichen, C. Jaeger, Polyolefin Backsheet and New Encapsulant Supress Cell Degradation in the Module, in: 28th European Photovoltaic Solar Energy Conference and Exhibition, Paris, France, 2013.

[16] C. Reid, S.A. Ferrigan, J.I. Martinez, J.T. Woods, Contribution of PV Encapsulant Composition to Reduction of Potential Induced Degradation (PID) of Crystalline Silicon PV Cells, in: 28th European Photovoltaic Solar Energy Conference and Exhibition, Paris, France, 2013.

[17] S. Meyer, S. Timmel, U. Braun, C. Hagendorf, Polymer Foil Additives Trigger the Formation of Snail Trails in Photovoltaic Modules, Energy Procedia 55 (2014) 494–497.

[18] G.J. Jorgensen, K. M. Terwilliger, J. A. DelCueto, S. H. Glick, M. D. Kempe, J. W. Pankow, F. J. Pern, T. J. McMahon, Moisture transport, adhesion, and corrosion protection of PV module packaging materials, Solar Energy Materials & Solar Cells 90 (2006) 2739–2775.

[19] P. Hülsmann, K.-A. Weiß, M. Köhl, Temperature-dependent water vapour and oxygen permeation through different polymeric materials used in photovoltaic-modules, Progress in Photovoltaics: Research and Applications 22 (2012) 415–421.

[20] C. Peike, P. Hülsmann, M. Blüml, P. Schmid, K.-A. Weiß, M. Köhl, Impact of Permeation Properties and Backsheet-Encapsulant Interactions on the Reliability of PV Modules, ISRN Renewable Energy 2012 (2012) 1–5.

[21] H. Gong, G. Wang, M. Gao, Degradation mechanism analysis of damp heat aged PV modules, in: 27th European Photovoltaic Solar Energy Conference and Exhibition, Frankfurt, Germany, 2012.

[22] H. Dominghaus, P. Eyerer, P. Elsner, T. Hirth, Kunststoffe: Eigenschaften und Anwendungen, Springer Berlin Heidelberg, Heidelberg, 2007.

[23] E. Baur, J.G. Brinkman, T.A. Osswald, E. Schmachtenberg, Saechtling Kunststoff Taschenbuch, 30th ed., Carl Hanser Verlag, Munich, 2007.

[24] M. D. Kempe, M. O. Reese, A. A. Dameron, Evaluation of the sensitivity limits of water vapor transmission rate measurements using electrical calcium test, Review of Scientific Instruments 84 (2013) 025109-1–10.

[25] M. Stevens, S. Tuomela, D. Mayer, Water Vapor Permeation Testing of Ultra-Barriers: Limitations of current methods and advancements resulting in increased sensitivity, in: 48th Ann. Tech. Conf. Proc. Society of Vacuum Coaters, Denver, USA, 2005.

[26] Mocon Inc., Minneapolis, USA, 05.03.2015, OX-TRAN Model 2/21.

[27] Mocon Inc., Minneapolis, USA, 05.03.2015, PERMATRAN-W Model 3/33. The Standard for Water Vapor Transmission Rate Testing.

[28] M. Tscherner, C. Konrad, A. Bizzarri, M. Suppan, M. Cajlakovic, V. Ribitsch, S. Stelzer, Opto-chemical Method for Ultra-Low Oxygen Transmission Rate Measurement, lecture in: 8th IEEE Conference on Sensors, Christchurch, New Zealand, 2009.

[29] P. Hülsmann, D. Phillipp, M. Köhl, Measuring temperature-dependent water vapor and gas permeation through high barrier films, Review of Scientific Instruments 80 (2009) 113901-1-6.

[30] P. Hülsmann, M. Jäger, K. A. Weiss, M. Köhl, Measuring and simulation of water vapour permeation into PV-modules under different climatic conditions, in:

SPIE 7773; Reliability of Photovoltaic Cells, Modules, Components and Systems III, Bellingham, USA, 2010.

[31] D. Richard, EVA and Tedlar still dominate: Market survey on encapsulation materials, Photon International, August 2010, 236–259.

[32] C. Warren, Foiled again: Market survey on encapsulation materials, Photon International, September 2009, 292–309.

[33] American Society for Testing and Materials, ASTM F 1249, Standard Test Method for Water Vapor Transmission Rate Through Plastic Film and Sheeting Using a Modulated Infrared Sensor, 2006.

[34] International Organisation for Standardisation, ISO 15106-3, Plastics - Film and sheeting - Determination of water vapour transmission rate Part 3: Electrolytic detection sensor method, 2003.

[35] P. Hülsmann, K.-A. Weiß, M. Köhl, Temperature-dependent water vapour and oxygen permeation through different polymeric materials used in photovoltaic-modules, Progress in Photovoltaics: Research and Applications 22 (2014) 415–421.

[36] P. Eyerer, Thomas Hirth, P. Elsner, Polymer Engineering- Eigenschaften von Kunststoffen in Bauteilen, Springer Berlin Heidelberg, Heidelberg, 2008.

[37] G. Mikats (ISOVOLTAIC GMBH) WO 2011/066595 A1, 2010.

[38] G.W. Ehrenstein, S. Pongratz, Beständigkeit von Kunststoffen, 1st ed., Carl Hanser Verlag, Munich, 2007.

CHAPTER V:

SUMMARY

5 Summary

The results presented in this work were separated into three parts. In the first part (chapter II) investigations in short-term aging processes on polymeric encapsulation materials were done. Special emphasis was given on physical aging mechanisms playing a substantial role for PV module lamination and its end-product. In the second part (chapter III) the focus was on the long-term aging processes on polymeric encapsulation materials. The accelerated aging conditions were applied on single and module laminated backsheets. The influence of material-interactions and micro-climate on aging processes of polymeric backsheets for PV modules in the course of accelerated aging was evaluated. The third part (chapter IV) concerned about the permeation behavior of backsheets and its changes in the course of accelerated aging. Special emphasis was given on the temperature dependent permeation behavior.

Chapter II revealed highly relevant influences of the thermal expansion behavior of polymeric encapsulants on PV module lamination processes. Therein Thermo-Mechanical Analysis (TMA) proved to be a suitable method for ability but also quality control of solar encapsulation films. As so far, no data on the thermal expansion behavior and material anisotropy of solar cell encapsulants is published in scientific literature it also gives for first time an overview on the thermal expansion behavior of several encapsulation materials.

The aging behavior of a co-extruded polyamide based backsheet under several accelerated aging and PV module lamination conditions was investigated. It was indicated, that the lamination temperature can have a significant influence on physical aging processes, respectively mechanical behavior, of this backsheet. The detected drop in mechanical behavior was more significant in transversal direction of the films, but stayed for all directions above the critical 18 % tensile strain. However, as permanent temperatures above 65°C are rare even for hot climates zones under standard operating conditions without clouding, not only after lamination but also in case of hot climates only limited influence of weathering induced polyamide re-

crystallization on the mechanical stability of the backsheet and consequently PV module reliability is expected.

In Chapter III for first time investigations on single and simultaneous module laminated backsheets under two different accelerated aging conditions were investigated. It gave an understanding of comparableness for reliability testing. It revealed significant chemical aging processes (hydrolysis) of the PET core layer of backsheets under extended DH conditions. No significant differences between single and module aged sheets were found. For this reason, reliability testing of PET based backsheets can be deduced from the aging related changes in the core layer, PET. Exceptions are backsheets with barrier layers. This allows simplified sample preparation, lower costs and offers more testing options for the characterization of the DH aging induced changes of the polymeric backsheets.

If the aging conditions include irradiation the microclimate was found to play a substantial role in enhancing aging effects as it induces higher temperature loads on module sheets. Hence, while for reliability testing of PET based backsheets under DH conditions testing of single sheets yield meaningful results which can be directly correlated to the behavior of backsheets within modules, for aging of backsheets combined with irradiation the module warming has to be taken into account. As irradiation is always a part of external impacts on PV modules in application it is highly relevant for validation of aging induced changes.

Chapter IV demonstrates the criticalness and incomparableness of OTR and WVTR results of different measurement techniques. Different measurement parameters were indicated as the most influencing factor. The results of the investigated initial and aged backsheets, measured with the technique evaluated best for the relevant conditions, revealed little differences in WVTR and significant differences in OTR values can be expected in the course of aging. For PET based backsheets a similar behavior was found. The permeation behavior of a backsheet with an aluminum barrier layer and a polyamide based backsheet revealed differing behavior. While the barrier backsheet showed vanishingly low OTR and WVTR results, the polyamide based backsheet had significant higher OTR values.

Special emphasis was also given in the temperature dependent permeation behavior, which revealed its importance for relation to application relevant conditions. The evaluated results allow for a calculation of OTR and WVTR results for different temperatures and revealed general lower energies necessary for inducing oxygen permeation. While changes in activation energies for OTR in the course of aging were found for all backsheets, the WVTR showed no significant changes in activation energies. A correlation of polymer morphological changes in the course of aging with the resulting permeation behavior was found and the Arrhenius concept proved to be applicable for describing the effects of the structural changes on permeation rates.